UNIVERSIDADE FEDERAL DO RIO GRANDE DO NORTE
CENTRO DE CIÊNCIAS EXATAS E DA TERRA
PROGRAMA DE PÓS-GRADUAÇÃO EM GEODINÂMICA E GEOFÍSICA

TESE DE DOUTORADO

MORFOESTRUTURA DA CORDILHEIRA MESO-OCEÂNICA ENTRE AS ZONAS DE FRATURAS MARATHON E 8°48'N

Autor:

PATRÍCIA REIS ALENCAR OLIVEIRA

Orientador:

PROF. DR. MOAB PRAXEDES GOMES

Tese nº 91/PPGG

Janeiro de 2025

Natal/RN, Brasil

UNIVERSIDADE FEDERAL DO RIO GRANDE DO NORTE
CENTRO DE CIÊNCIAS EXATAS E DA TERRA
PROGRAMA DE PÓS-GRADUAÇÃO EM GEODINÂMICA E GEOFÍSICA

TESE DE DOUTORADO

MORFOESTRUTURA DA CORDILHEIRA MESO-OCEÂNICA ENTRE AS ZONAS DE FRATURAS MARATHON E 8°48'N

Autor:

PATRÍCIA REIS ALENCAR OLIVEIRA

Tese apresentada em 08 de janeiro de 2025 ao Programa de Pós-Graduação em Geodinâmica e Geofísica (PPGG) da Universidade Federal do Rio Grande do Norte (UFRN) como requisito à obtenção do Título de Doutor em Geodinâmica e Geofísica, Área de Concentração Geodinâmica.

BANCA EXAMINADORA:

PROF. DR. MOAB PRAXEDES GOMES - *Presidente e orientador (PPGG-UFRN)*
PROF. DR. DAVID LINO VASCONCELOS - *Membro externo (UFPB)*
PROFA. DRA. MARY LUCIA DA SILVA NOGUEIRA - *Membro externo (UFOP)*
PROFA. DRA. NARELLE MAIA DE ALMEIDA - *Membro externo (UFPE)*
PROFA. DRA. TEREZA CRISTINA MEDEIROS DE ARAUJO - *Membro externo (UFPE)*

Janeiro de 2025
Natal/RN, Brasil

Universidade Federal do Rio Grande do Norte - UFRN
Sistema de Bibliotecas - SISBI
Catalogação de Publicação na Fonte. UFRN - Biblioteca Central Zila Mamede

Oliveira, Patricia Reis Alencar.
Morfoestrutura da Cordilheira Meso-Oceânica entre as Zonas de Fraturas Marathon E 8°48'N / Patricia Reis Alencar Oliveira. - 2025.
111f.: il.

Tese (doutorado) - Universidade Federal do Rio Grande do Norte, Centro de Ciências Exatas e da Terra, Programa de Pós-Graduação em Geodinâmica e Geofísica, Natal, 2025.
Orientação: Prof. Dr. Moab Praxedes Gomes.

1. Dorsal Mesoatlântica - Tese. 2. Descontinuidades não transformantes - Tese. 3. Falhas de descolamento - Tese. I. Gomes, Moab Praxedes. II. Título.

RN/UF/BCZM CDU 551

Elaborado por Jackeline dos Santos Pinheiro da Silva Maia Cavalcanti - CRB-15/317

Dedico todo meu esforço a minha filha querida que vivenciou intensamente todo o processo, ao meu pai amado, em memória, que foi o grande propulsor e meu admirador, a minha mãe, irmãos e amigos mais próximos que me apoiaram e acreditaram em mim.

"Não andeis ansiosos de coisa alguma; em tudo, porém, sejam conhecidas, diante de Deus, as vossas petições, pela oração e pela súplica, com ações de graças".

Filipenses 4:6

RESUMO

A Cordilheira Mesoatlântica é uma região geotectônica de alta complexidade, essencial para compreender a evolução das crostas oceânicas e os processos associados à tectônica de placas divergentes. Este estudo analisou aproximadamente 400 km de eixo axial da dorsal, entre as Zonas de Fratura Marathon e 8°48’N, com profundidades variando entre 1.600 m e 6.000 m, utilizando dados multifeixe, gravimétricos e de sismicidade. O objetivo foi investigar a interação entre magmatismo e tectonismo na formação do relevo oceânico, com ênfase nas interseções cordilheira-transformantes (RTIs) e não-transformantes (NTDs). A porção norte da área, localizada acima da Zona de Fratura de Vema, foi compartimentada em dois supersegmentos,12°N e 11°N, sendo o último subdividido nos segmentos 11°55'N e 11°20'N. Já a porção sul apresentou os supersegmentos 9°N e 10°N, segmentados por descontinuidades de segunda ordem. Os resultados indicam que essas segmentações apresentam características morfológicas e geofísicas peculiares, mas compartilham processos de formação e evolução semelhantes, evidenciado como a interação entre magmatismo e tectonismo influencia diretamente a configuração morfotectônica da Dorsal Mesoatlântica. Estruturas como falhas de descolamento em cantos internos elevados desempenham um papel crucial na geração de assimetrias, refletindo o impacto do desacoplamento litosférico em regiões de expansão lenta, com evidências de redução do fluxo magmático. Adicionalmente, as descontinuidades NTDs favorecem a redução e/ou ausência do magmatismo, expondo maciços e rochas de reologia alteradas, distintas das observadas nas colinas abissais dos supersegmentos. Estas feições, em particular, são regiões propícias para à percolação de fluidos e à formação de sistemas hidrotermais, destacando-se como áreas prioritárias para investigações, especialmente na interseção do segmento 11°20’N com a falha transformante de Vema.

Palavras-chave: Dorsal Mesoatlântica; falhas transformantes; descontinuidades não transformantes; falhas de descolamento, morfotectônica.

ABSTRACT

The Mid-Atlantic Ridge is a highly complex geotectonic region, essential for understanding the evolution of oceanic crust and the processes associated with divergent plate tectonics. This study analyzed approximately 400 km of the ridge's axial segment, between the Marathon Fractures Zone and 8°48'N, with depths ranging from 1,600 m to 6,000 m, using bathymetric, gravimetric, and seismicity data. The objective was to investigate the interaction between magmatism and tectonism in shaping the oceanic relief, with an emphasis on ridge-transform intersections (RTIs) and non-transform discontinuities (NTDs). The northern portion of the area, located above the Vema Fracture Zone, was divided into two supersegments, 12°N and 11°N, the latter further subdivided into the 11°55'N and 11°20'N segments. The southern portion presented the 9°N and 10°N supersegments, segmented by second-order discontinuities. The results indicate that these segmentations exhibit peculiar morphological and geophysical characteristics but share similar formation and evolution processes, highlighting how the interaction between magmatism and tectonism directly influences the morphotectonic configuration of the Mid-Atlantic Ridge. Structures such as detachment faults in elevated inside corners play a crucial role in generating asymmetries, reflecting the impact of lithospheric decoupling in slow-spreading regions with evidence of reduced magmatic flow. Additionally, NTDs promote reduced or absent magmatism, exposing massifs and rocks with altered rheology, distinct from those observed in the abyssal hills of the supersegments. These features, in particular, are favorable for fluid percolation and the formation of hydrothermal systems, standing out as priority areas for future investigations, especially at the intersection of the 11°20'N segment with the Vema transform fault.

Keywords: Mid-Atlantic Ridge; transform faults, non-transform discontinuities; detachment faults; morphotectonics.

AGRADECIMENTO

Primeiramente, agradeço a Deus por abrir caminhos e me fortalecer diante dos desafios mais difíceis desta jornada.

Ao Serviço Geológico do Brasil (SGB), expresso minha profunda gratidão pela infraestrutura e concessão dos dados essenciais para o desenvolvimento desta tese, bem como pelo apoio financeiro e logístico que viabilizou minha experiência no doutorado sanduíche.

À Université de Bretagne Occidentale (UBO) em Brest, França, e ao L'Institut Universitaire Européen de la Mer (IUEM), agradeço pelo acolhimento durante o estágio de doutorado sanduíche realizado entre 1º de dezembro de 2023 e 31 de maio de 2024.

Um agradecimento especial à professora Márcia Maia pela oportunidade e pela experiência enriquecedora desse período, bem como pelo tempo dedicado em inúmeras reuniões. Seu apoio, orientação e expertise foram fundamentais para o avanço dos artigos.

Ao amigo e orientador Mob Praxedes Gomes, sou imensamente grata por sua orientação, paciência e incentivo constantes. Sua dedicação e conhecimento foram indispensáveis para a realização deste trabalho.

Aos demais membros da banca e colaboradores, agradeço pelas discussões enriquecedoras, pelas sugestões valiosas e pelo olhar crítico, que contribuíram significativamente para o aprimoramento deste estudo.

Ao chefe da Divisão de Geologia Marinha, Valter Rodrigues Sobrinho e chefia anterior Hortencia de Assis, agradeço pelo suporte e pela prontidão no atendimento às minhas demandas, sempre com dedicação e acreditando no meu trabalho.

Aos colegas Heliasio Simões, Vadim Harlamov, Hugo Leonardo Rocha (DGM), Oderson Filho (CEDES) e Maurício da Silva (DIG - DIINFO) do SGB, agradeço pela troca de conhecimentos, pelo apoio técnico e pelas conversas que tornaram este percurso mais seguro e produtivo. O ambiente de colaboração e amizade que encontrei foi essencial

Sou profundamente grata à minha família e amigos, que sempre esteve ao meu lado, oferecendo amor, compreensão e apoio incondicional em cada etapa desta caminhada. Em especial, ao meu irmão, Rafael Reis, por suas palavras de encorajamento, e à minha filha, Beatriz Reis, que, mesmo sem compreender totalmente a importância desta tese, foi uma fonte constante de motivação e alegria, materializada em pequenos gestos simbólicos, como os lanchinhos deixados silenciosamente ao lado do computador. Te amo filha!

SUMÁRIO

LISTA DE FIGURAS

LISTA DE ABREVIATURAS E SIGLAS

AF	Africana
CIRM	Comissão Interministerial para os Recursos do Mar
CNUDM	Convenção das Nações Unidas sobre o Direito do Mar
CTD	Conductivity, Temperature and Depth
CUBE	Combined Uncertainty and Bathymetry Estimator
FTs	Falhas Transformantes
GEBCO	Carta Batimétrica Geral dos Oceanos
Geo-Ocean	Laboratório de Áreas Oceânicas
IBGE	Instituto Brasileiro de Geografia e Estatística
ICR	Índice de Concentração da Rugosidade
ICR	Índice de Concentração de Rugosidade
Ifremer	Instituto Francês de Pesquisa para a Exploração do Mar
IGRF	Campo Magnético Internacional de Referência
ISA	International Seabed Authority
ITR12	Interseção Transformante Marathon - Cordilheira 12º N
IUMER	Institut Universitaire Europeen de La Mer
KHz	Kilohertz
LDMA	Leste da Dorsal Mesoatlântica
NA	Norte-Americana
NOAA	National Oceanic and Atmospheric Administration
NTD	Non-transform discontinuit
OCCs	Ocen Core Complex
PNRM	Política Nacional para os Recursos do Mar
PPGG	Programa de Pós-Graduação em Geodinâmica e Geofísica
PROCORD	Projeto de Prospecção e Exploração de Sulfetos Polimetálicos da Cordilheira Mesoatlântica
RMBA	Bouguer Residual do Manto
RTI	Ridge-transform intersection
SA	Sul-Americana
SGB	Serviço Geológico do Brasil
SIG	Sistema de Informações Geográficas
TPU	Total Propagated Uncertainty

UBO	Universidade da Bretanha Ocidental
UFRN	Universidade Federal do Rio Grande do Norte
XBT	Expendable BathyThermograph
ZF	Zona de Fratura
ZPD	Zona Principal de Deslocamento

CAPÍTULO I
INTRODUÇÃO

1. INTRODUÇÃO

1.1. Apresentação

A presente tese, intitulada "*Morfoestrutura da Cordilheira Meso-oceânica entre as Zonas de Fraturas Marathon e 8º48'N*", foi elaborada como parte dos requisitos necessários para a obtenção do grau de Doutora junto ao Programa de Pós-Graduação em Geodinâmica e Geofísica (PPGG) da Universidade Federal do Rio Grande do Norte (UFRN). O desenvolvimento desta pesquisa está alinhado à linha de pesquisa prioritária do Plano estratégico 2019-2023 do Serviço Geológico do Brasil (SGB), inserido no contexto do Projeto de Prospecção e Exploração de Sulfetos Polimetálicos da Cordilheira Mesoatlântica (PROCORD).

A autora, vinculada ao SGB, contou com o apoio financeiro dessa instituição para realizar um estágio de pesquisa doutorado sanduíche de 6 meses na Universidade da Bretanha Ocidental (UBO), localizada em Plouzane, Brest, França. Durante esse período, foi acolhida no Institut Universitaire Européen de La Mer (IUMER), sendo orientada pela professora Márcia Maia, membro do IUMER, do Laboratório de Áreas Oceânicas (Geo-Ocean) da UBO e do Instituto Francês de Pesquisa para a Exploração do Mar (Ifremer).

1.2. Justificativa

A presente tese insere-se no contexto do projeto de pesquisa desenvolvido pelo SGB e foi elaborada com a intenção de dar suporte a questões fundamentais sobre a importância geológica e econômica das dorsais oceânicas. Esas estruturas desempenham um papel fundamental na geração da litosfera oceânica e na redistribuição de material do manto.

As dorsais oceânicas, predominantemente localizadas na *Area* do Oceano Atlântico, conforme definido no Artigo XI da Convenção das Nações Unidas sobre o Direito do Mar (CNUDM), são reconhecidas como patrimônio comum da humanidade e reguladas pela Autoridade Internacional dos Fundos Marinhos (ISA) (SOUZA, 2007). Além de sua importância geotectônica, essas regiões apresentam grande potencial mineral, com depósitos de sulfetos polimetálicos associados a sistemas hidrotermais ativos e extintos, contendo metais estratégicos como cobre, ouro, prata, zinco e chumbo.

Apesar do avanço no conhecimento sobre dorsais oceânicas, ainda há lacunas significativas na compreensão dos mecanismos que influenciam sua segmentação e evolução. Em particular, a interação entre falhas transformantes, descontinuidades não transformantes (NTDs) e falhas de descolamento ainda é um tema amplamente debatido. A presente pesquisa busca suprir essa lacuna ao analisar como o magmatismo e o tectonismo controlam a morfologia e a estruturação de segmentos da DMA situados entre as Transformantes Marathon e Vema**.** A tese emprega um conjunto de dados geofísicos, incluindo batimetria multifeixe, anomalias gravimétricas e informações sobre sismicidade, permitindo uma abordagem integrada da geodinâmica dessa região.

Além de contribuir para o avanço do conhecimento científico sobre os processos de segmentação de dorsais de espalhamento lento, os resultados desta pesquisa possuem implicações aplicadas, auxiliando na avaliação do potencial mineral da região. A identificação e caracterização de descontinuidades estruturais podem otimizar a seleção de áreas promissoras para depósitos de sulfetos polimetálicos, reduzindo custos exploratórios e fornecendo subsídios estratégicos para futuras requisições brasileiras junto à ISA.

Dessa forma, esta tese não apenas contribuirá para o aprofundamento da compreensão científica sobre a segmentação e evolução das dorsais meso-oceânicas, como também fornecerá uma base técnica e metodológica para a tomada de decisões no âmbito da prospecção mineral e da gestão dos recursos do oceano profundo.

1.3. Localização da área de estudo e objetivo

Este estudo propõe realizar uma análise detalhada dos diferentes estilos estruturais presentes na Dorsal Meso-oceânica, localizada entre as Zonas de Fratura Marathon (ZFM) e 8°48'N, abrangendo as latitudes de 12°42'N a 8°48'N (Fig. 1.1). Essa área é caracterizada por distintas interseções cordilheira-transformantes (RTI, na sigla em inglês para ridge-transform intersection) e não-transformantes (NTD, na sigla em inglês non-transform discontinuit), sendo ideal para investigar a interação entre magmatismo e tectonismo na formação e evolução do relevo oceânico em sistema de dorsais oceânicas.

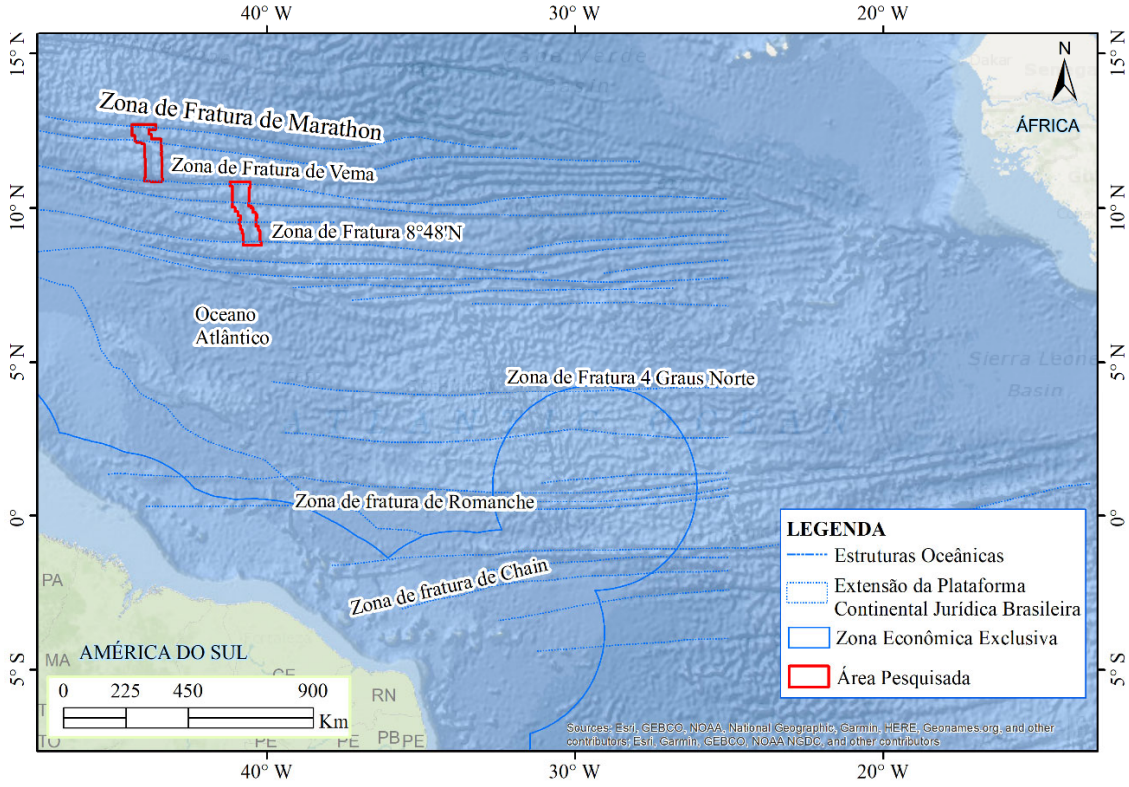

Figura 1.1 - Mapa de localização do trecho da Cordilheira Meso-oceânica analisada, destacando a área de estudo do Projeto PROCORD e área de jurisdição brasileira. O traçado das zonas de fraturas foi obtido a partir do GEBCO BATHYMETRIC COMPILATION GROUP 2022 (2022), enquanto os limites marítimos foram fornecidos pela Marinha do Brasil (BRASIL, 2024).

CAPÍTULO II
CONTEXTO GEOLÓGICO E TEÓRICO

2. CONTEXTO GEOLÓGICO E TEÓRICO

2.1. Dorsais oceânicas

As Dorsais Mesoatlânticas (MARs, na sigla em inglês Mid-Atlantic Ridges) são feições morfológicas submarinas de grande amplitude (- 4.000 m a -2.500 m), caracterizadas por um declive baixo que se eleva acima da planície abissal (POMEROL *et al*., 2013). Essas estruturas ocorrem em centros de expansão, refletindo os processos mecânicos e térmicos que regem a formação de novas crostas oceânicas e manto litosférico (ESTEP *et al*., 2021; LIGI *et al*., 2022; MACDONALD *et al*., 1988; MACDONALD & FOX, 1988). A acomodação das crostas oceânicas recém-formadas resulta de uma combinação entre os tipos de acreção magmática (vulcanismo extrusivo e intrusões) e os mecanismos de movimentação das falhas extensionais (BUCK *et al*., 2005).

2.1.1. Taxa de espalhamento

A morfologia geral do eixo da dorsal pode mostrar uma variabilidade morfológica significativa ao redor do globo em decorrência da mudança na taxa de expansão, velocidade com que as placas tectônicas se afastam, uma em relação a outra, sobre uma dorsal (MACDONALD, 2001; PÜTHE & GERYA, 2014; SMALL, 1994). Podendo estas serem classificadas como sendo rápida (taxas acima de 8 cm/ano), intermediária a (5,5 a 8,0 cm/ano) e lenta (menores que 4cm/ano) (Figs. 2.1 e 2.2) (MACDONALD, 1982).

As MARs (Fig. 2.3 a) são consideradas dorsais típicas de crista de expansão lenta, onde as taxas de propagação são menores que 4cm/ano (MACDONALD, 1982) (Fig. 2.1). Tais morfologias apresentam um eixo axial caracterizado pela presença de um vale central estreito e profundo (SMALL, 1994), com vulcões alongados de baixa amplitude gerado a partir do efeito combinado de erupção fissural de magmas, geralmente de baixa viscosidade, e o constante transporte (*rafting*) de depósitos de erupção devido à separação de placas (RUBIN, 2014). Essas dorsais apresentam vales de rifte axial medianos, com profundidades variando entre 1,5 a 3,0 km, que marcam o eixo da dorsal e ao longo do vale axial, vulcões ativos, de cerca de 2 a 3 km de diâmetros extravasam magma e dão

origem à formação de nova crosta oceânica (MACDONALD, 2001; MCKENZIE & BOWIN, 1976).

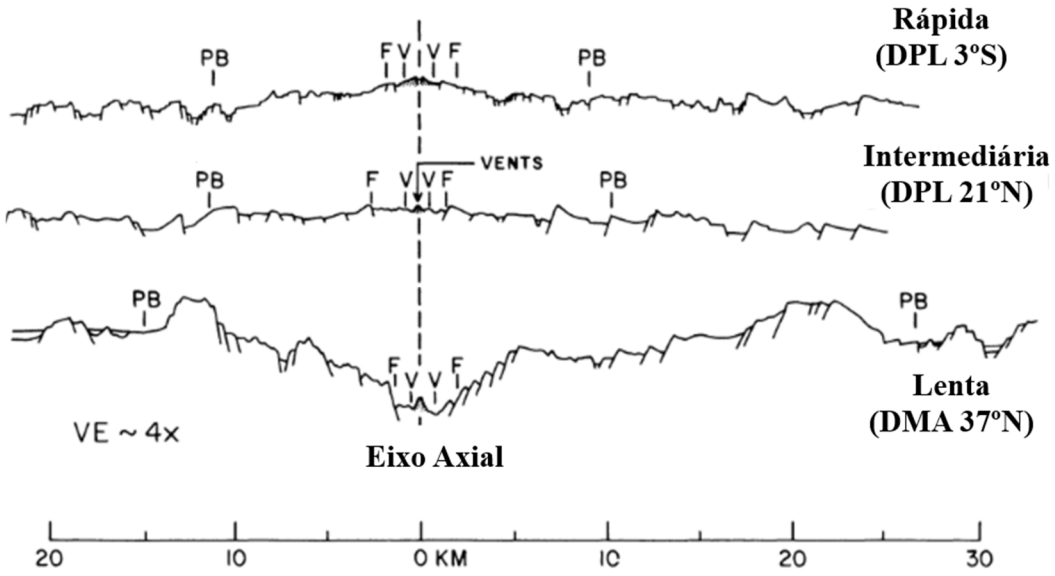

Figura 2.1 - Variação topográfica do eixo axial em função da taxa de propagação. DPL (Dorsal do Pacífico Leste), DMA (Dorsal Mesoatlântico), F (Zona de fissura), V (Zona neovulcânica) e PB (Zona de borda de placa). Adaptado de MACDONALD (1982).

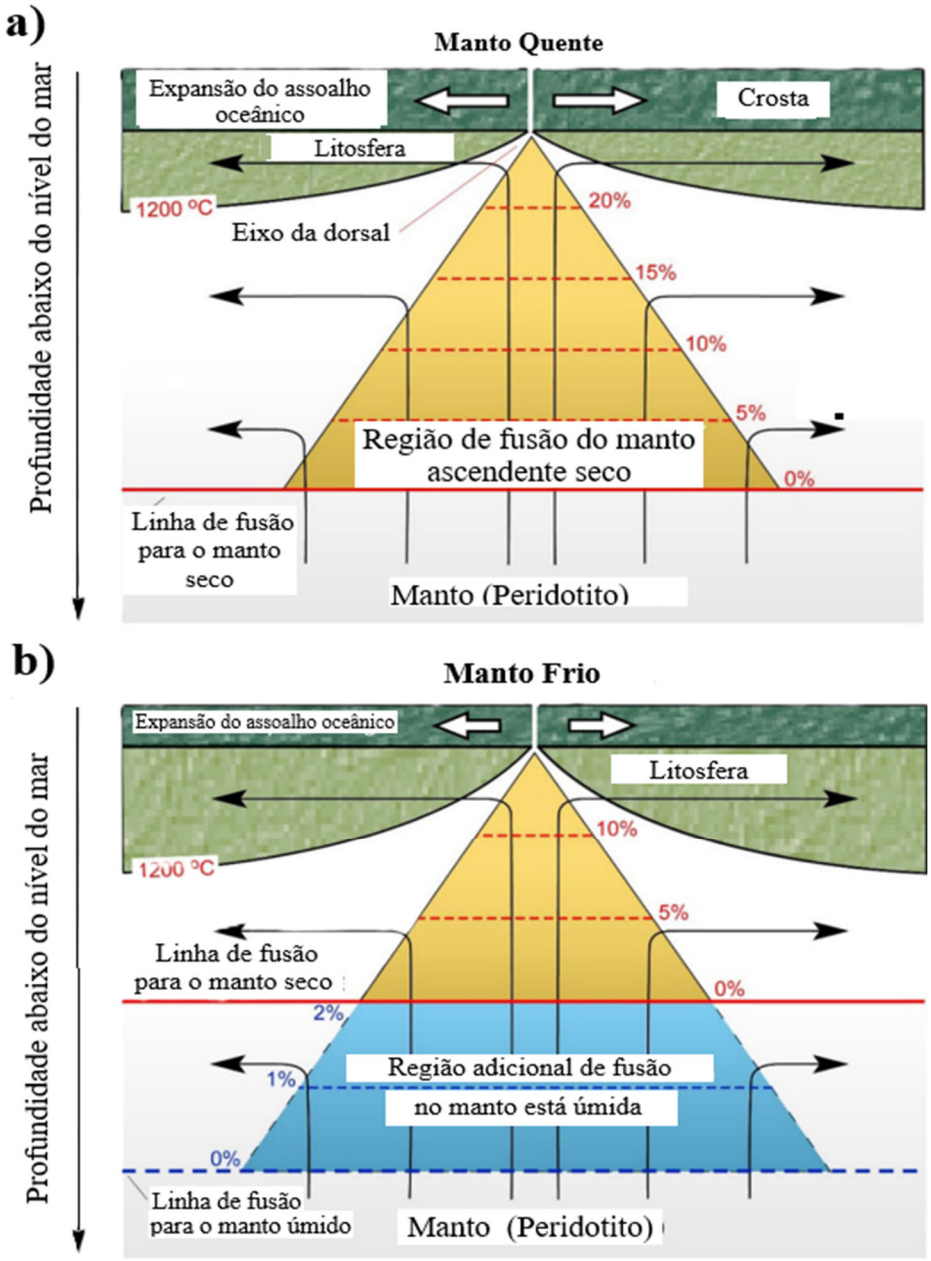

Figura 2.2 - Relação entre a formação de cristas oceânicas e taxa de propagação. O grau de fusão do manto ascendente varia conforme a velocidade de separação das placas, classificada como (a) lenta ou (B) rápida. Linhas esquemáticas representam o fluxo passivo na astenosfera, enquanto triângulos sombreados indicam a fração de fusão ao longo do eixo, influenciada pela presença de água no peridotito sólido. Em mantos com baixo teor de H2O, a fusão ocorre em uma região mais ampla e profunda. Uma ascensão mais rápida do manto reduz a profundidade de fusão, aumentando a geração de magma e resultando em uma crosta basáltica mais espessa. Adaptado de LIGI *et al*. (2022).

Em contraste, dorsais de expansão rápida (taxas acima de 8 cm/ano – PÜTHE & GERYA (2014), como as dorsais do Leste do Oceano Pacífico (Fig. 2.3 b), possuem morfologias mais suaves, caracterizadas por eixos axiais alto e topografia de até 400 m de altitude. Essas dorsais apresentam vales estreitos (1-2 km de largura), escarpas de falhas com desníveis de dezenas de metros e planos de falhas que mergulham em ambas as direções do eixo, associadas a altos suprimentos magmáticos (KEAREY *et al*., 2009).

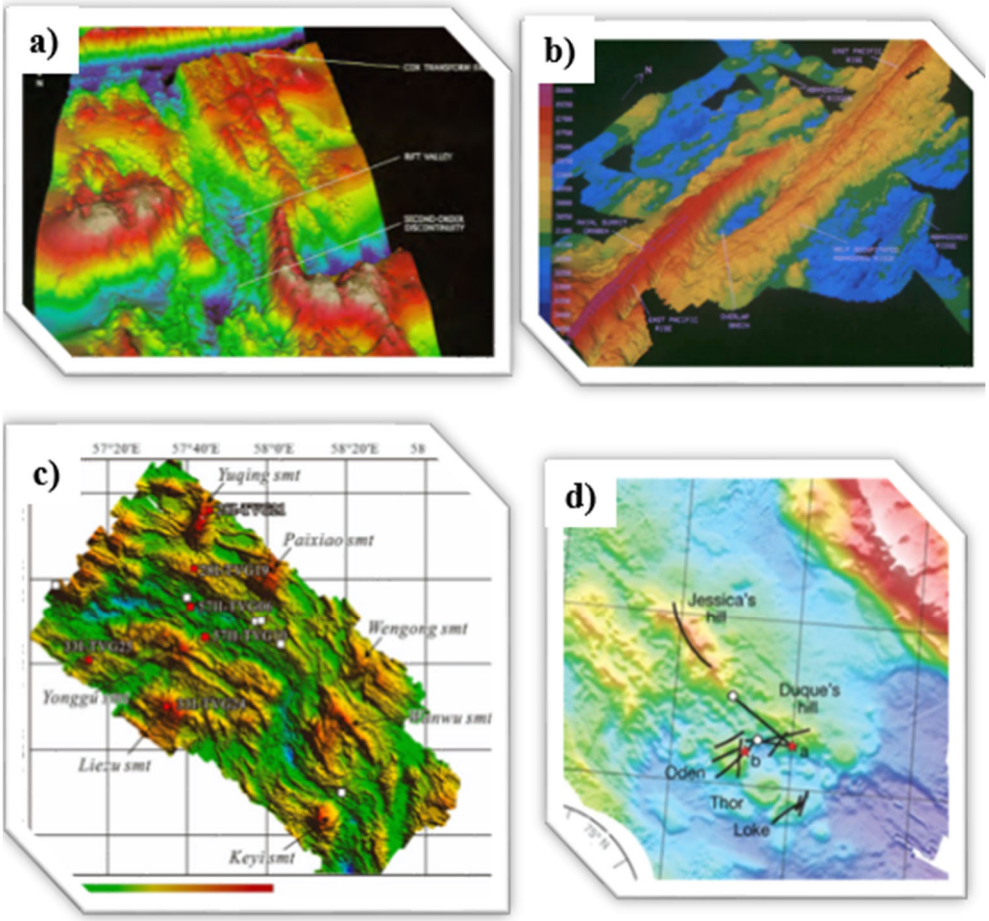

Figura 2.3 - Exemplos de dorsais: Lenta - DMA (a), rápida – Dorsal do Pacífico Leste (b), intermediária – Sistema de Dorsal do Oceano Índico (c) e ultralenta - Dorsal de Gakkel a 85°6'E no oceano Ártico (d). Imagens obtidas a partir de PERRAM & MACDONALD (1990), MACDONALD & FOX (1988); HU *et al*. (2023); and SOHN *et al*. (2008), respectivamente.

As dorsais de expansão intermediária (5,5 a 8,0 cm/ano), como a Dorsal do Sudoeste do Oceano Índico (Fig. 2.3 c), apresentam elevações axiais (MACDONALD & FOX, 1988), enquanto dorsais ultralentas (taxa inferiores a 2 cm/ano) (Fig. 2.3 d), como a Dorsal Gakkel (SOHN *et al.*, 2008), possuem topografia acidentada, alternando entre segmentos magmáticos e amagmáticos, e ausência de FTs (DICK *et al.*, 2003).

2.1.2. Magmatismo

As variações morfológicas do eixo axial das dorsais oceânicas não dependem apenas de taxa de expansão do fundo oceânico, mas também de fatores espaciais e temporais (GRINDLAY *et al*., 1991). Quando o suprimento de magma é relativamente baixo em relação à taxa de expansão, os eixos de rifte tendem a ser estreitos e alongados. Em contrapartida, um suprimento de magma elevado em relação à taxa de expansão resulta em eixos de rifte mais contínuos e com formas mais arredondadas (MORGAN *et al*., 1993; BUCK *et al*., 1998).

Entretanto, existem exceções, como a cordilheira Reykjanes (BENEDIKTSDÓTTIR *et al*., 2012), localizada no Atlântico Norte, nas proximidades da Islância. Embora classificada como uma dorsal lenta, com taxas de espalhamento em torno de 1 a 2 cm/ano (MORGAN *et al*., 1993; BENEDIKTSDÓTTIR *et al*., 2012), a Reykjanes apresenta um alto axial elevado devido ao suprimento significativo (MACDONALD, 2001). Outra exceção é a região anômala da Zona Discordante Australia-Antartica, onde a influência da taxa de expansão pode ser anulada por controle de escala maior, como fluxo do manto e estrutura térmica (SMALL, 1994). A proximidade de pontos quentes, ou mesmo sua ocorrência sob a dorsal, pode intensificar o magmatismo na região, gerando morfologias anômalas.

KLEIN & LANGMUIR (1987) sugerem que a profundidade regional do eixo das cordilheiras e sua espessura crustal são indicadores importantes para aferir variações no suplemento magmático ao longo das dorsais meso-oceânicas. Além disso, a variação na química dos basaltos das cristas oceânicas, na profundidade axial e na espessura crustal está relacionada às diferenças de temperatura do manto. Nos chamados "pontos quentes", regiões associadas a temperaturas mais altas no manto, ocorre maior volume de magmatismo, menor profundidade axial e maior espessura crustal. Já os "pontos frios", caracterizados por temperaturas mais baixas no manto, apresentam magmatismo menos intenso, profundidades maiores e crosta mais finas.

2.1.3. Tectonismo

A teoria das placas tectônicas afirma que, à medida que a litosfera oceânica se afasta de uma margem de placa de acreção, ela esfria e se contrai, resultando em uma

subsidência progressiva. Esse processo estabelece uma relação consistente entre profundidade e a idade do embasamento oceânico, excetuando áreas anomalamente elevadas, como ilhas vulcânicas e cordilheiras assimétricas. Essas exceções estão associadas a anomalias térmicas do manto (pontos quentes) e a maior atividade magmática (BONATTI, 1978).

Na área de estudo deste trabalho, localizada no Atlântico Equatorial, a região é marcada por uma história tectônica complexa. Essa complexidade está relacionada ao movimento da junção tripla entre as placas litosféricas Norte-Americana (NA), Sul-Americana (AS) e Africana (AF), além da abertura do Oceano Atlântico (por exemplo, BONATTI *et al*. (1996); SMITH *et al*. (2008) e referências contidas). Estudos indicam que a junção tripla NA-SA-AF migrou de uma posição próxima a 10º N para a região entre 14º e 16º N, durante o intervalo entre 72,5 e 35,5 Ma (SMITH *et al*., 2008), e que ainda podem ocorrer movimentos entre as placas NA e SA (SELLA *et al*., 2002).

Embora o limite entre essas placas seja frequentemente associado à zona de fratura Fifteen-Twenty, ele não é claramente definido por atividade sísmica ou por características tectônicas inequívocas. As posições atuais da junção tríplice NA-SA-AF e da NA-SA-Caribe permanecem incertas e são objeto de debate por exemplo, (ESCARTÍN *et al*., 2003). O eixo da dorsal próximo à Zona de Fratura Fifteen-Twenty tem sido objeto de diversas investigações geofísicas (ESCARTÍN *et al*., 2008; ESCARTÍN & CANNAT, 1999; FUJIWARA *et al*., 2003). Processos tectônicos compressivos e transicionais ocorrem ao longo das margens dessas grandes zonas de fratura, sendo influenciados pela geometria do movimento de transformação. Isso é particularmente evidenciado em área onde ocorrem mudanças na direção do espalhamento ou no polo de rotação (BONATTI, 1978).

2.2. Descontinuidades

As dorsais não são estruturas contínuas, sendo segmentadas em trechos discretos de comprimentos variados, separadas por descontinuidades com *offsets* distintos. Essas descontinuidades incluem falhas transformantes (primeira ordem), descontinuidades não-transformantes (segunda ordem) e outras de menor escala, como as de terceira e quarta ordem (FOX *et al*., 1991; MACDONALD, 1983; MACDONALD & FOX, 1983).

Essas descontinuidades não apenas delimitam novos segmentos de cristas e modificam seu comprimento, mas também compartimentam o terreno em unidades tectônicas distintas. Essa segmentação reflete variações na atividade vulcânica e tectônica ao longo do eixo das dorsais (MACDONALD, 2001). Embora não seja completamente esclarecido se a segmentação é governada principalmente pela história tectônica regional ou pela dinâmica da ressurgência do manto, sabe-se que os deslocamentos migratórios ocasionados a essas descontinuidades influenciam diretamente a profundidade axial e o relevo das dorsais (SMALL, 1994).

2.2.1. Falhas

Ao longo do tempo geológico, uma parte significativa da tensão de extensão no eixo das cristas oceânicas é absorvida pela acreção magmática de nova crosta e litosfera. A tensão remanescente, por sua vez, é acomodada por falhas normais de grande escala (BUCK *et al*., 2005; ESCARTÍN & CANNAT, 1999; MACDONALD *et al*., 1996). A taxa de espalhamento influência diretamente a expansão tectônica por falhas, sendo que o papel dessas estruturas aumenta à medida que a taxa de espalhamento diminui. Além disso, a taxa de espalhamento' também modifica o estilo das falhas tectônicas (BEHN *et al*., 2002).

De maneira geral, falhas formadas em dorsais de expansão lenta tendem a ser mais longas, com maior rejeito (*throw*) e espaçamento maior em comparação às falhas em dorsais de expansão rápida (BEHN *et al*., 2002; MACDONALD, 1982). Contudo, variações sistemáticas podem ocorrer ao longo de segmentos individuais, como na DMA. Nessa região, falhas próximas aos centros de segmentos apresentam menor espaçamento e rejeito, possivelmente devido à presença de uma crosta mais espessa, o que também concentra terremotos e tensão tectônica (BUCK *et al*., 2005).

As falhas normais nas cordilheiras oceânicas tornam-se mais ortogonais à medida que aumenta o espaçamento entre elas e o rejeito individual (BEHN *et al*., 2002). Estudos sugerem que essa ortogonalidade entre falhas transformantes e os centros de espalhamento é influenciada pelo estresse térmico em placas oceânicas em resfriamento, assim como por diferenças reológicas nas zonas de margem de placas (GERYA, 2012). Além disso, a orientação dessas falhas está associada à dissipação de energia em canais

verticais sob as dorsais, sugerindo uma relação entre dinâmica térmica e tectônica na formação dessas estruturas.

2.2.1.1. Falhas de Descolamento

As falhas de descolamento são falhas normais de baixo ângulo e longa duração, capazes de cortar a litosfera até profundidades de 7-8 km. Essas estruturas permitem a penetração de água do mar em grandes profundidades e expõem crosta oceânicas e rochas do manto no fundo marinho (ESCARTÍN *et al*., 2008). Comuns em dorsais de expansão lenta, essas falhas acomodam extensão significativas, da ordem de 1-3 Ma, estando frequentemente associadas a dois modos principais de acreção (ver item 2.3) (ESCARTÍN *et al*., 2008).

2.2.1.1.1. Complexo de núcleo oceânico

Os Complexos de Núcleo Oceânicos (OCCs) são maciços em forma de domos formados em dorsais oceânicas, diretamente associados a falhas de descolamento oceânicas. Geologicamente, são análogos aos complexos metamórficos de núcleo encontrados em ambiente continentais, embora apresentem características específicas em regiões marinhas marinhas Clique ou toque aqui para inserir o texto.(BLACKMAN *et al.*, 1998; CANN *et al.*, 1997; TUCHOLKE *et al.*, 1998). Essas estruturas resultam da exumação de rochas da crosta inferior e do manto superior no leito marinho (BLACKMAN *et al*., 1998; CANN *et al*., 1997; TUCHOLKE *et al*., 1998), causada pelo desdobramento tectônico em paredes de grandes falhas de descolamento que se enraízam abaixo do eixo axial das dorsais. Essas estruturas estão associadas com uma contínua fusão de um *footwall* dúctil, influenciada por irregularidades em um *hanging wall* rúptil. Além disso, os OCCs estão frequentemente vinculados a sistemas hidrotermais ativos (MORRIS *et al*., 2009), o que reforça sua relevância na dinâmica tectônica e magmática do fundo marinho.

Estudos litológicos de OCCs revelam a presença de uma diversidade de rochas, incluindo materiais eruptivos, plutônicos e ultramáficos do manto, que frequentemente apresentam sinais de intensa alteração e deformação (ESCARTÍN *et al.*, 2003, 2017; MACLEOD *et al.*, 2002; PEIRCE *et al.*, 2019). Esses diferentes tipos padrões litológicos

e estruturais indicam que os OCCs são regiões favoráveis à ocorrência de intensa circulação de fluidos, concentrada ao longo de descolamento. SMITH *et al*. (2006 and 2008) discutem estágios e morfologias associadas ao deslizamento em falhas de descolamento, apresentando dois modelos principais para a formação de complexos centrais (Fig. 2.4). Esses modelos ilustram como a interação entre tectônica, magmatismo e circulação hidrotermal molda essas feições únicas.

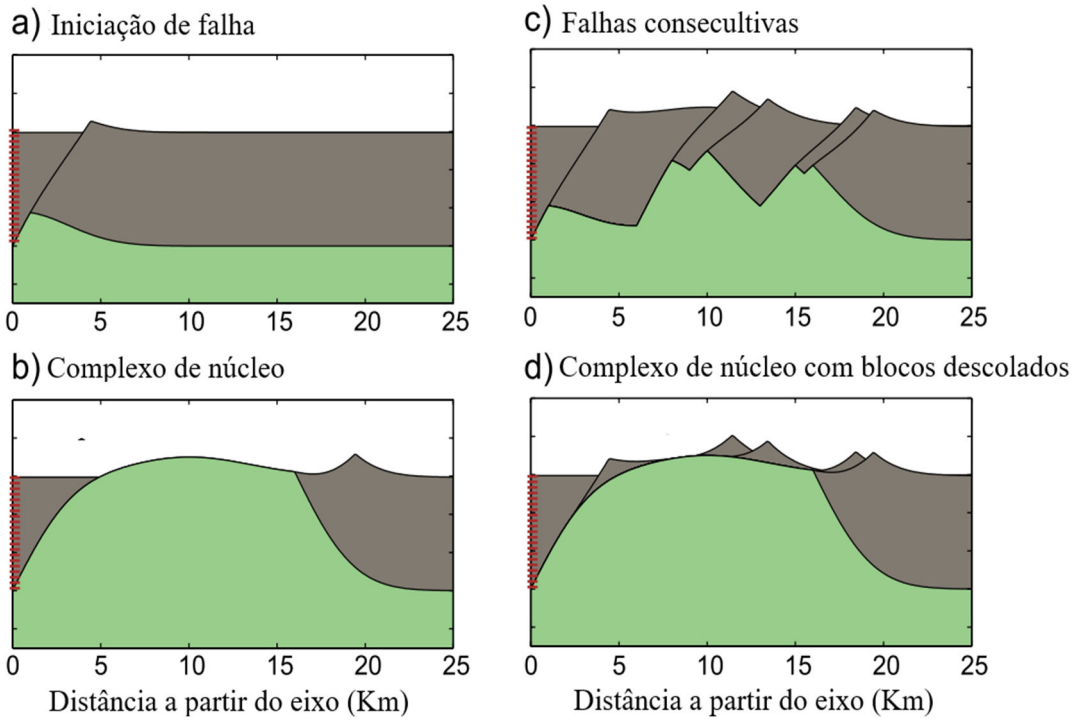

Figura 2.4 - Evolução de uma falha de descolamento. (a) Falha normal no eixo axial: no estágio inicial, uma falha normal no eixo axial sofre rotação flexural, resultando na formação de uma cordilheira linear e de uma bacia adjacente. O deslocamento é de 1 km, com uma rotação de 18°. (b) Extensão contínua e rotação da falha: à medida que a extensão continua, a rotação da falha aumenta, expondo rochas da crosta inferior e gerando um footwall corrugado. O deslocamento da falha neste estágio atinge 16 km, com rotação de 36°. (c) Falhas consecutivas: Falhas adicionais se desenvolvem consecutivamente. Nessa fase, a maior parte da litosfera é formada por processos magmáticos típicos de dorsais de expansão lenta. (d) Falha de descolamento contínua: novas falhas são formadas no eixo axial que se conectam à falha principal de descolamento. Seções triangulares do fundo do vale axial são transferidas do hanging wall para o footwall e transportadas para fora do eixo. Espaços entre os blocos transportados podem expor a superfície principal de descolamento, que frequentemente apresenta corrugações. A crosta anterior ao início da falha é representada em cinza, enquanto o material proveniente de profundidades maiores, exposto durante o movimento da falha, está em verde. Adaptado de SMITH *et al*. (2008).

Uma hipótese avançada sugere que a transição do OCC para um descolamento sob o fundo oceânico, oculto por blocos transportados, é impulsionada pelo aumento do preenchimento vulcânico e pela diminuição da hidratação enfraquecedora da superfície de deslizamento à medida que se afasta da extremidade do segmento (PEIRCE *et al*., 2019). Essa dinâmica sugere que o descolamento pode se estender por todo o segmento

ou terminar lateralmente conforme os centros magmáticos são abandonados (PEIRCE *et al*., 2019). Caso os descolamentos, em escala de segmento, influenciem significativamente a propagação e a ressurgência do manto ao longo dos segmentos inteiros, é possível que eles também desempenhem um papel no padrão de segmentação das cordilheiras oceânicas, podendo persistir por períodos excepcionalmente longos (PEIRCE *et al*., 2019).

Por outro lado, MORRIS *et al*. (2009) apresentam uma abordagem distinta, considerando os OCCs como características geológicas de curta duração, espacialmente limitadas e estruturalmente isoladas. De acordo com essa visão, a presença dos OCCs depende diretamente de flutuações na distribuição local de magma. O deslizamento, nessa perspectiva, persiste apenas quando o suprimento de magma é reduzido abaixo de um limiar crítico, insuficiente para formar uma crosta ígnea contínua capaz de suportar a expansão tectônica. Tais interpretações contrastantes ilustram a complexidade dos processos que regulam a formação, evolução e persistência dos OCCs, evidenciando a interação dinâmica entre tectônica, magmatismo e segmentação das dorsais oceânicas.

2.2.2. Falhas transformantes e zonas de fraturas

As falhas transformantes oceânicas deslocam os eixos axiais das dorsais (zonas transformantes), enquanto que as Zonas de Fraturas registram a história tectônica das placas até os limites continentais (BUCK *et al*., 2005; PEIRCE *et al*., 2019). Ambas estruturas estão relacionadas a regiões com temperaturas anômalas (BONATTI, 1978). Neste trabalho, será feita uma distinção entre essas duas feições, apesar de, em algumas abordagens, ambas serem englobadas sob o termo “zona de fratura”.

Uma zona transformante segue um pequeno círculo sobre o polo de rotação específico para as placas tectônicas envolvidas. Alterações na posição desse polo ou na direção de propagação das placas em um ou ambos os lados da transformante podem resultar em ajustes geométricos, buscando limites mais estáveis para a transformante (BONATTI, 1978). Esses ajustes podem provocar o desaparecimento de antigas zonas transformantes e o surgimento de novas, como as falhas transformantes menores do tipo dorsal-dorsal, que ocorrem em litosfera jovem, relativamente fina, quente e plástica, como observada no Atlântico Norte (BONATTI, 1978). Em zonas de fratura com deslocamentos extensos, o ajuste da geométrico encontra maior resistência devido à maior

rigidez da litosfera mais antiga e mais espessa. Isso pode resultar na formação de bandas de alta tensão, gerando tensões compressivas ou distensivas ao longo dessas zonas (LIGI *et al*., 2022) (Fig. 2.5). Essas descontinuidades apresentam tamanhos variados (*offset*), com muitas delas sendo pequenas (< 20 km), enquanto outras são maiores e frequentemente interceptadas por zonas de fraturas transformantes.

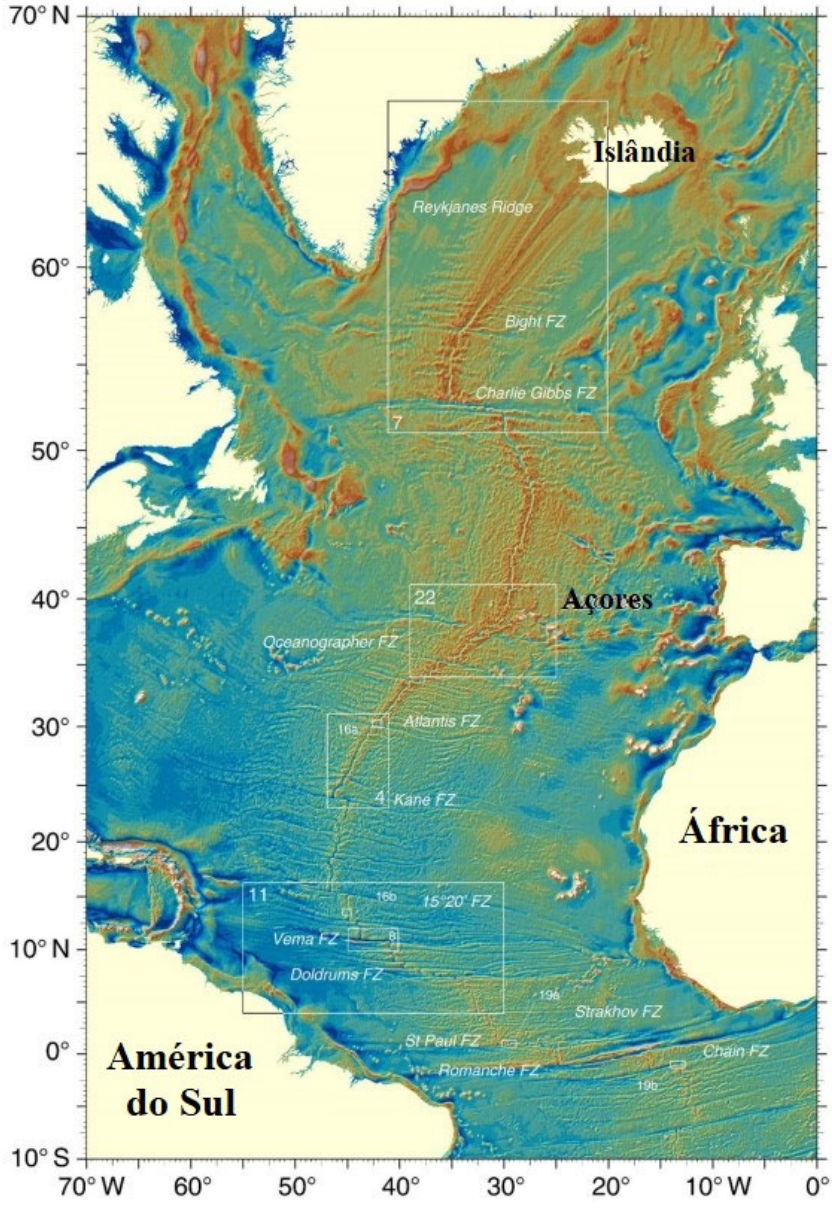

Figura 2.5 - Imagem de gravidade por satélite, obtida a partir dos dados dos satélites CryoSat-2 e Jason-1, abrangendo o Atlântico Central e Norte. Os dados de gravidade de ar livre foram derivados de altimetria por satélite, utilizando a grade global versão 30. Destacam-se na imagem as elevações da Islândia e dos Açores, separadas pela significativa Transformante Charlie-Gibbs. Além disso, são visíveis os traços das transformantes equatoriais de grande deslocamento que se estendem da América do Sul até a África. Os retângulos brancos numerados indicam áreas de estudo detalhadas em outras figuras do trabalho de LIGI *et al.*, 2022.

2.2.2.1. Zona de Fratura Marathon e Mercurius

Zona de Fratura Marathon (ZFM) é caracterizada por uma estrutura crustal complexa e por processos geológicos ativos, como magmatismo e serpentinização. Similar à Zona de Fratura Mercurius (ZFMe), a ZFM desempenha um papel significativo na evolução das estruturas oceânicas profundas, incluindo OCCs (PEIRCE *et al*., 2020).

De acordo com LAGABRIELLE *et al*. (1992), a ZFM apresenta um pequeno fragmento do embasamento ou crista transversal em sua porção sul, bastante semelhante àquelas observadas na Zona de Fratura Vema (ZFV). Os intra-sedimentos presentes evidenciam uma rotação relativa em torno de um eixo leste-oeste e elevação ao norte. Esse movimento ascendente é acomodado na borda lateral norte da depressão batimétrica, em vez de ocorrer em seu centro. Além disso, a ZFM desloca crostas mais jovem (1 Ma contra 8 Ma) em comparação à ZFMe. O terreno é coberto por sedimentos plano e amplos (> 10 km), deslocando crostas de cerca de 8 Ma contra outra de 11 Ma.

Nas proximidades do vale batimétrico da ZFM, observa-se um afinamento crustal destacado por modelagens sísmicas e gravimétricas. Essa característica resulta de uma região de baixa densidade, interpretada como reflexo da serpentinização do manto superior. Tal processo importantes caminhos para o fluxo de fluidos em direção à crosta profunda e ao manto superior. A flutuabilidade causada pela redução de densidade contribui para a elevação da região, promovendo metamorfismo da crosta inferior e serpentinização do manto (BONATTI, 1976, 1978), promovendo metamorfismo da crosta inferior **e** serpentinização do manto superior (PEIRCE *et al*., 2020). POCKALNY *et al*. (1996) sugerem que a configuração flexural observada é resultado da extensão transtensional. A batimetria rasa dos cantos internos das intersecções de um *ridge-transform* é dinamicamente sustentada, consequência do desacoplamento da placa oposta através da transformação.

A crosta ao sul de ZFMe possui 5 km de espessura, constituída de uma crosta superior e média de aproximadamente 2 km de espessura (velocidade sísmica entre 3,0 a 4,5 km s-1), e uma crosta inferior de 3 km de espessura que atinte 7,5 km s-1 na descontinuidade de Moho. Se o contorno de velocidade de 7,5 km s-1 é usado para denotar a base da crosta, a velocidade do manto superior também é relativamente.

Na ZFMe (Fig. 2.2 c), a disposição em camadas intra-sedimentares sugere movimentos relativos entre os lados norte e sul da ZF. As camadas mais profundas no lado norte apresentam uma configuração arqueada, indicando que houve um

levantamento relativo da litosfera mais jovem, embora esse processo pareça não ter persistido até o presente (PEIRCE *et al*., 2019).

2.2.2.2. Zona de Fratura Vema

A ZFV é marcada por um deslocamento significativa que desvia a DMA em aproximadamente 320 km na direção leste-oeste, entre 10° e 11°N (BONATTI *et al*., 2005; FABRETTI *et al*., 1998; VAN ANDEL *et al*., 1971). O vale transformante de Vema exibe uma forte assimetria entre suas porções norte e sul (LIGI *et al*., 2022), com largura variando de 15 a 22 km (FABRETTI *et al*., 1998). A parede sul mergulha sob os depósitos turbidíticos que preenchem o vale, alcançando espessura de cerca de 1 km (BONATTI *et al*., 2005; LIGI *et al*., 2022). Esses sedimentos, predominantemente de origem turbidítica, foram depositados durante o Pleistoceno e refletem processos sedimentares complexos (LIGI *et al.*, 2022 e referências), com contribuições de material detrítico e biogênico proveniente das paredes do vale (CHAMOV *et al*., 2020)

A cerca de 140 km a oeste da interseção sul da transformante com a dorsal encontra-se a *Vema Transverse Ridge* (VTR), uma elevação topográfica proeminente que se estende paralelamente à Transformante de Vema e se eleva mais de 3 km acima do nível previsto de contração térmica (BONATTI *et al*., 2005; LIGI *et al*., 2022). Estudos recentes sugerem que a VTR representa a borda exposta de uma placa de litosfera oceânica flexionada e elevada, que, em determinado momento, emergiu acima do nível do mar. Posteriormente, esta área foi erodida e recoberta por carbonatos de águas rasas, principalmente durante o Mioceno e Plioceno, enquanto passava por subsidência (BONATTI *et al*., 2005; BONATTI et at., 1983; LIGI *et al*., 2022; PALMIOTTO *et al*., 2013).

Os carbonatos sobrepõem uma sequência de peridotitos com cerca de 1 km de espessura, seguidos por uma unidade de gabro com espessura variável, um complexo de diques bem desenvolvido e uma camada superior de basaltos maciços. Juntas, essas unidades compõem a Seção Litosférica de Vema. A VTR delimita a porção norte do segmento axial de 10°N, também conhecida como Leste da Dorsal Mesoatlântica (LDMA), cujo desenvolvimento teve início há cerca de 40 milhões de anos (FABRETTI *et al*., 1998; LIGI *et al*., 2022).

A extremidade leste da falha transformante de Vema é interpretada como sendo marcada por uma zona principal de deslocamento (ZPD), que representa o início do

segmento LMAR (BONATTI *et al*., 1994; EITTREIM & EWING, 1975), denominado neste trabalho como segmento de 10° N. Neste segmento, a crosta manteve uma espessura constante de 26 a 20 Ma, apresentando um espessamento gradualmente até o presente (LIGI *et al*., 2022). Oscilações na espessura crustal, com períodos de 3 a 4 milhões de anos, foram atribuídas à convecção secundária no manto subjacente à dorsal (LIGI *et al*., 2022). Este manto, rico em H_2O e de baixa viscosidade, está situada abaixo de um manto residual pobre em H_2O e de alta viscosidade (BONATTI *et al*., 2003). Tal configuração pode estar relacionada a mudanças na geometria da fronteira de placas tectônicas, resultando em regimes de transpressão ou transtensão no domínio transformante. Este domínio transformante é coberto por depósitos sedimentares compostos por brechas polimíticas, arenitos e siltitos, contendo clastos basálticos, doleríticos e gabroicos. Esses depósitos sedimentares passaram por metamorfismo em fácies xisto-verde antes de serem desagregados e depositados (LAGABRIELLE *et al*., 1992; LIGI *et al*., 2022).

Desde aproximadamente 16 milhões de anos atrás, o grau de fusão do manto sob a DMA tem aumentado, embora de forma oscilatória. Estudos indicam que o manto astenosférico sob a dorsal, especialmente próximo a 11° N, apresenta um gradiente de resfriamento e/ou perda de fertilidade à medida que se migra da Islândia em direção ao equador. "Ondas" de manto quente e fértil, possivelmente originadas das plumes da Islândia e dos Açores, tem migrado para o sul, contribuindo para o aumento da fusão observado na região nos últimos 16 milhões de anos (BONATTI *et al*., 2003; LIGI *et al*., 2022).

Adicionalmente, foram identificadas reorientações anti-horária no eixo da dorsal e mudanças na direção de expansão da litosfera próximas à falha tranformante, combinadas com alterações na posição do polo de rotação de Euler. Essas mudanças, ocorridas em placas com mais de 10 milhões de anos, culminaram na flexura e no soerguimento de uma porção da placa litosférica. Movimentos verticais ao longo de zonas de fratura podem estar relacionados a numerosos fatores, como condução de calor horizontal através de uma ZF; forças viscodinâmicas; diapirismo gravitacional serpentinita; e tensões horizontais de compressão ou tração (BONATTI, 1978).

2.2.2.3. Zona de Fratura Lema

A Zona de Fratura Lema (ZFL) delimita o segmento LDMA em sua porção sul. Segundo (BONATTI *et al*., 2005), a ZFL foi reativada devido à presença de uma grande

falha de mergulho, do tipo descolamento, localizada na porção norte dessa estrutura. A borda sul da placa flexionada da ZFV encontra-se com o escarpamento da ZFV, que possui cerca de 1 km de altura. Essa grande falha de mergulho, associada à reativalçao da ZFL, corresponde a um antigo deslocamento transformante do eixo da DMA. A ZFL atua como uma estrutura de desacoplamento, separa a placa flexionada ao norte da litosfera "normal' ao sul. Como resultado, a placa litosférica inclinada e flexionada apresenta uma extensão aproximada de 300 km de na direção leste-oeste e 80 km na direção norte-sul.

2.3. Modo de acreção em dorsais oceânicas

OLIVE & ESCARTÍN (2016) documentaram a existência de dois modos principais de formação do fundo marinho (simétrico e assimétrico), que refletem a heterogeneidades ao longo do eixo da dorsal na quantidade de massa fundida fornecida à litosfera axial, resultando em morfologias distintas.

2.3.1. Simétrico-suportada por colinas abissais (Abyssal hill bearing)

Segundo OLIVE & ESCARTÍN (2016), aproximadamente 50% do fundo oceânico é formado dentro dos vales axiais, as quais são delimitados por falhas normais voltadas para o centro, regularmente espaçadas entre 5 e 10 km. Essas falhas resultam em colinas abissais alongadas e contínuas ao longo do eixo, com configuração aproximadamente simétrica e regular.

Esse tipo de acreção é dominado por processos magmáticos, nos quais falhas secundárias de alto ângulo contribuem para a formação das colinas abissais em ambos os flancos. Essas acomodações são acompanhadas por baixa sismicidade, concentrada principalmente nas extremidades dos segmentos (ESCARTÍN *et al*., 2008; OLIVE &; ESCARTÍN, 2016).

2.3.2. Assimétrico-suportada por descolamento (Termed Detachment bearing)

Regiões da dorsal onde a acomodação tectônica ocorre por meio de falhas de baixo ângulo e grande compensação, incluindo descolamentos oceânicos, apresentam uma

morfologia assimétrica, frequentemente localizada em apenas um dos lados do eixo axial (ESCARTÍN *et al*., 2008; OLIVE & ESCARTÍN, 2016). Nessas regiões, as colinas abissais resultam de terrenos de acreção assimétrica, definidos por falhas normais íngremes e de longa duração, que se iniciam abaixo do fundo do vale do rifte e giram para ângulos mais baixos à medida que os blocos do *footwall* são expostos. Os flancos conjugados exibem uma forte assimetria (SMITH *et al*., 2008). Elevações estreitas e distintivas, com encostas íngremes voltadas para o exterior e frequentemente curvadas em vista plana, são comumente observadas próximas aos descolamentos expostos no fundo marinho. Essas elevações delimitam oscilações profundas e resultam na formação de terrenos caóticos e fragmentados (SMITH *et al*., 2008).

Porções da dorsal associadas a esse modo de acresção apresentam maior atividade sísmica, provavelmente relacionada à acomodação de uma porção significativa da separação total entre as placas tectônicas (SMITH *et al*., 2008). Evidências sísmicas e geoquímicas corroboram a ideia de que esses segmentos de dorsal possuem uma litosfera axial mais espessa e fria em comparação com regiões de acreção simétrica. Essa característica pode ser explicada pela maior penetração da circulação hidrotérmica em profundidades significativas ou pela presença de um manto ascendente mais frio (ESCARTÍN *et al*., 2008).

Os terrenos relacionados ao descolamento **(***detachment-related terrain***)** apresentam cristas estreitas distintas, com encostas íngremes voltadas para o exterior. Essas cristas são frequentemente curvas em vista plana, desenvolvem-se próximas a descolamento expostos no fundo do mar, e delimitam oscilações profundas, resultando em terrenos caóticos e fragmentados **(***blocky and chaotic terrain*) (SMITH *et al*., 2008).

Um exemplo clássico desse modo de acreção assimétrica é a Cordilheira de espalhamento ultralento do Suldoeste do Índico. A morfologia nessa região é amplamente controlada por grandes campos de superfícies de descolamento, que se estendem por uma porção significativa da litosfera oceânica. Nessa região, as morfologias associadas à acreção das colinas abissais são controladas por falhas de alto ângulo paralelas ao eixo axial, contrastando com os terrenos onde falhas normais de longa duração, iniciadas abaixo do vale do rifte, giram para ângulos mais baixos à medida que são expostas (SMITH *et al*., 2008).

2.3. Tipo de fundo marinho em dorsais oceânicas

Conforme trabalho de CANNAT *et al*. (2006), a morfologia do fundo marinho em dorsais oceânicas pode ser classificada em três tipos principais (fundo oceânico vulcânico, fundo oceânico corrugado e fundo oceânico liso), com base em suas características estruturais e morfológicas (Fig. 2.6).

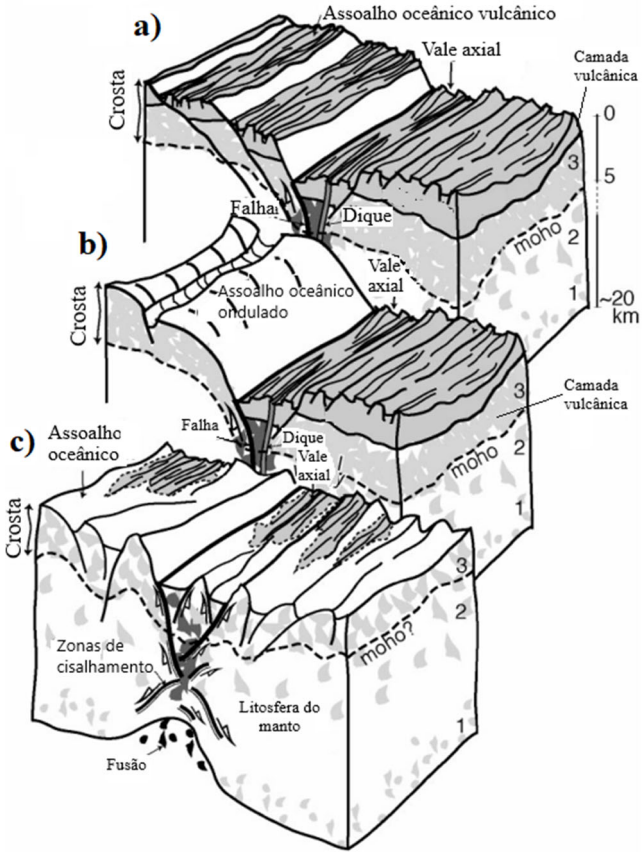

Figura 2.6 - Esboço em escala litosférica da região axial, ilustrando três modos propostos de espalhamento ultralento pobre em fusão, organizados de acordo com a redução no suprimento de fusão. O modo A (vulcânico-vulcânico) e o modo B (corrugado-vulcânico) também ocorrem em cordilheiras de propagação mais rápidas da dorsal mesoatlântica e em regiões magmaticamente mais robustas de dorsais ultralentas. Por outro lado, o modo C (suave-suave ou suave-vulcânico), caracterizado por vulcanismo axial muito limitado ou inexistente, parece ser exclusivo de cristas ultralentas pobres em fusão. As dimensões horizontais das estruturas representadas são de aproximadamente 80 km transversalmente e 40 km ao longo delas. As concentrações de fusão são indicadas em preto (na astenosfera) ou cinza escuro (na litosfera), enquanto as rochas magmáticas cristalizadas são representadas em cinza mais claro. A abundância de rochas magmáticas em diferentes níveis de crosta e da litosfera do manto (1, 2 e 3) é influenciada tanto pela quantidade de fusão cristalizada em cada profundidade quanto pela extensão em que esse material cristalizado foi transportado tectonicamente para níveis superiores. (Compilado de CANNAT *et al*., 2006).

Os fundos oceânicos vulcânicos (*volcanic seafloor*) são caracterizados pela presença de numerosos cones vulcânicos, incluindo, ocasionalmente vulcões de topo plano. As escarpas de falhas nessas regiões são estreitas e podem se estender de 2 a 20

km ao longo do eixo, com deslocamento que variam de menos que 50 m a até 500 m (Fig. 2.6 a).

O fundo oceânico corrugado (*corrugated seafloor*) ocorre na forma de domos, ou áreas sub-horizontais livres de cones vulcânicos. Essas regiões apresentam ondulações paralelas à superfície do fundo marinho, gerando uma textura característica (Fig. 2.6 b).

Por outro lado, o fundo oceânico liso (*smooth seafloor*) é composto por cristas amplas, com topografia suave e arredondada, sem cones vulcânicos ou escarpas. Essas cristas apresentam comprimentos de 15 a 30 km, altura entre 500 e 2000 m, e seguem a orientação local da crista no momento de sua formação. Algumas dessas estruturas são simétricas, enquanto outras exibem inclinações mais íngremes voltadas para o exterior (Fig. 2.6 c).

CAPÍTULO III
MATERIAIS E MÉTODOS

3. MATERIAIS E MÉTODO

3.1. Batimetria Multifeixe

No âmbito do PROCORD, o SGB realizou campanhas geofísicas na Cordilheira Mesoatlântica Equatorial, mapeando uma área de 27.730 km² entre as ZFM e 18°48'N. Durante essas campanhas, foram coletados dados batimétricos em perfis orientados na direção leste-oeste, com espaçamento entre 6 e 7 km e extensão variando de 40 a 60 km. A batimetria foi adquirida por meio do ecobatímetro multifeixe Reson 7150-F, operando em dupla frequência, com 12 kHz.

O processamento dos dados constou com ajustes de posicionamento, offsets, maré e velocidade do som da água, utilizando perfis contínuos de CTD/XBT. Posteriormente, o processamento foi realizado no software CARIS HIPS & SIPS, onde os dados foram corrigidos para incertezas totais propagadas (TPU, na sigla em inglês *Total Propagated Uncertainty*), remoção de ruídos extremos e minimização de artefatos de borda. A superfície batimétrica final, com resolução de 100 m/pixel, foi gerada utilizando o algoritmo CUBE (*Combined Uncertainty and Bathymetry Estimator*), que estima múltiplas hipóteses para valores batimétricos e suas incertezas, representando variações potenciais do fundo marinho.

Subprodutos derivados dessa superfície (Fig. 3.1) foram gerados em ambiente SIG utilizando a ferramenta Spatial Analyst do ArcGIS, incluindo: mapa de isolinhas batimétricas, com equidistância de 100 m; carta de declividade, classificada em intervalos conforme IBGE (2007) em plano (0°-3°), suavemente ondulado (3°-8°), ondulado (8°-20°), fortemente ondulado (20°-45°), montanhoso (45°-75°) e escarpado (>75°); carta de rugosidade, calculada pelo Índice de Concentração de Rugosidade (ICR), que possibilita a compartimentação e quantificação do relevo, bem como a identificação de estruturas geológicas; carta de aspecto, que indica a direção preferencial das declividades, medida no sentido horário, onde as áreas planas receberam valor de -1; carta de backscatter, gerada com resolução de 50 m por meio do algoritmo SIPS Backscatter do CARIS HIPS & SIPS, com refinamento posterior no software ArcGIS; e perfis batimétricos, extraídos perpendicular e ortogonalmente ao eixo da cordilheira, com espaçamento de 1 km.

Para uma visualização mais detalhada das estruturas geológicas, foi aplicado um sombreamento do relevo, utilizando iluminação com 45° de altitude e azimute de 315°, sobreposto a todos os subprodutos, para realçar e enfatizar as feições morfotectônicas.

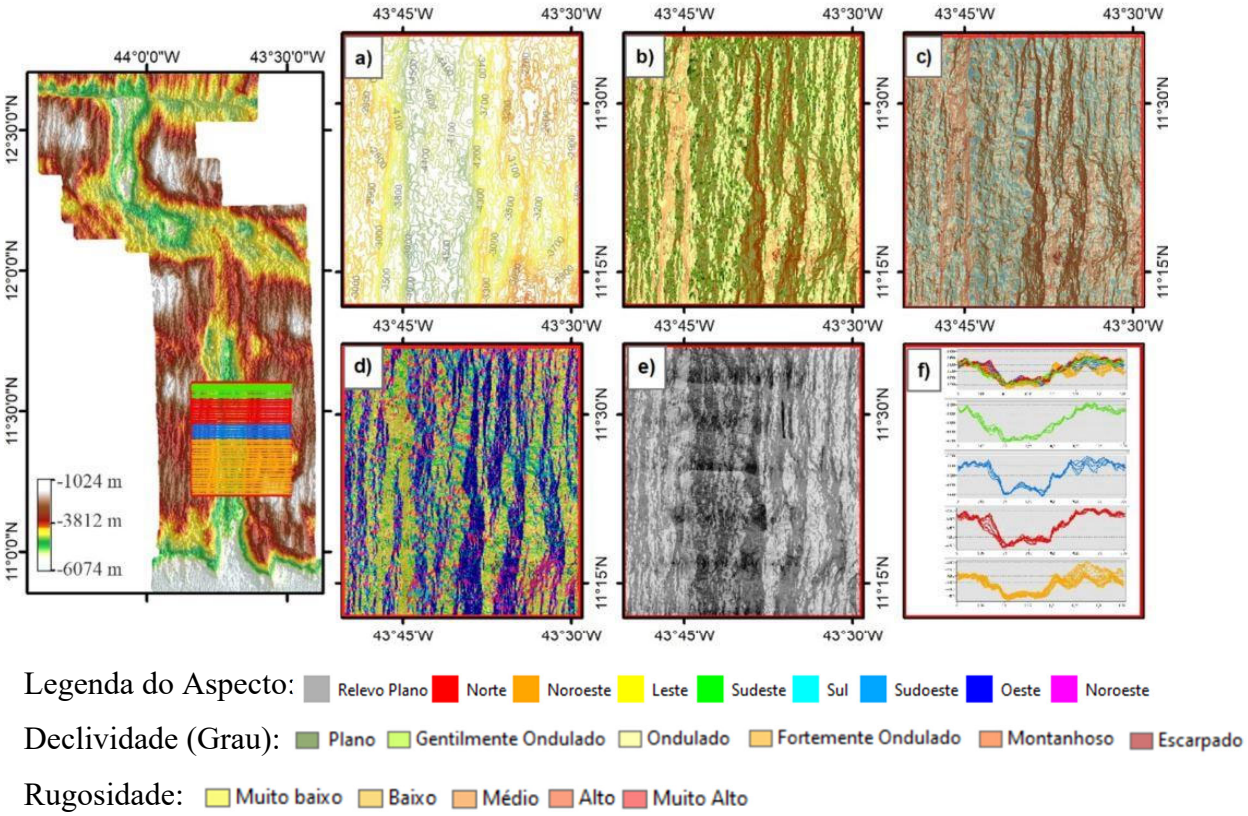

Figura 3.1 - Subprodutos derivados da superfície batimétrica porção norte de Vema: (a) isóbatas com equidistância de 100 m; (b) carta de declividade (Plano 0-3%, Suavemente Ondulado 3-8%, Ondulado 8-20%, Fortemente Ondulado 20-36%, Montanhoso 36-75% e Escarpado > 75%); (c) carta de rugosidade; (d) carta de aspecto; (e) carta de backscatter; e (f) perfis batimétricos E/W a cada 1 km, agrupados por cor conforme similaridade de fundo. Área de zoom delimitado pelo polígono vermelho e a carta de sombreamento do relevo encontra-se sobre todos as demais cartas para efeito tridimensional e realce das estruturas geológicas.

3.2. Dados complementares

Adicionalmente, foram integrados dados regionais de altimetria de satélite (Fig. 3.2), anomalia do ar livre (*free air anomaly*), traços das zonas de fraturas, e registros de sismicidade (Fig. 3.2) do General Bathymetric Chart of the Oceans (GEBCO) (MAIA & ARKANI-HAMED, 2002).

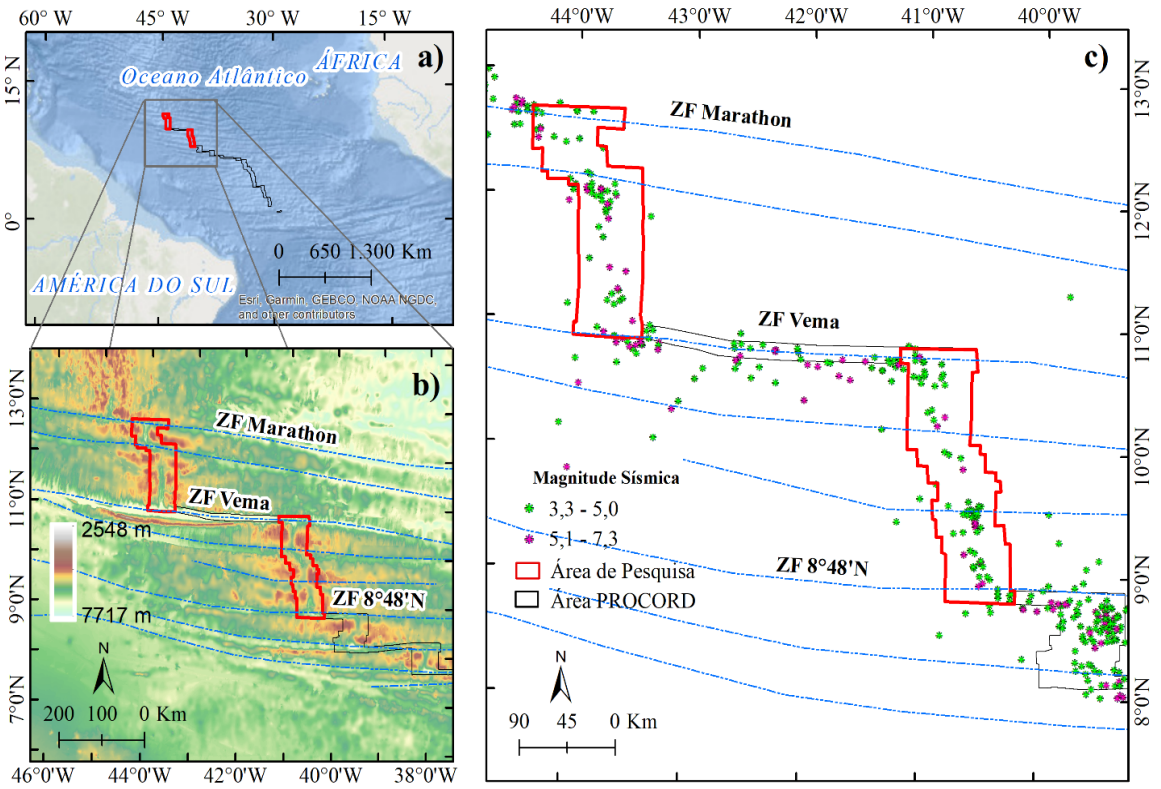

Figura 3.2 - Mapa da localização da área de estudo. a) Oceano Atlântico Equatorial e margens equatoriais da América do Sul e África, com a área de levantamento do Projeto de Prospecção e Exploração de Recursos Minerais no Atlântico Sul e região Equatorial Internacional (PROCORD) delimitada por um polígono preto; b) Área de levantamento do PROCORD (polígono preto), incluindo a área específica de estudo (polígono vermelho), zonas de fratura (linhas azuis pontilhadas) e dados de altimetria por satélite obtidos do (GEBCO BATHYMETRIC COMPILATION GROUP 2022, 2022); c) Mapa de sismicidade obtido do (GEBCO BATHYMETRIC COMPILATION GROUP 2022, 2022).

3.3. Dados Gravimétricos

Para análise gravimétrica (Fig. 3.3), inicialmente foi construída uma grade regional utilizando dados de anomaliasde gravidade de ar livre (GEBCO BATHYMETRIC COMPILATION GROUP 2022, 2022) integrando a dados de altimetrias de satélite, conforme o método descrito em (MAIA & ARKANI-HAMED, 2002). Esse método consiste no cálculo do efeito gravitacional de uma camada de espessura constante e densidades lateralmente variáveis. Os cálculos foram realizados no domínio da Transformada de Fourier, adotando densidades médias de 2800 kg/m³ para a crosta oceânica, 3300 kg/m³ para o manto superior e 1030 kg/m³ para a água do mar.

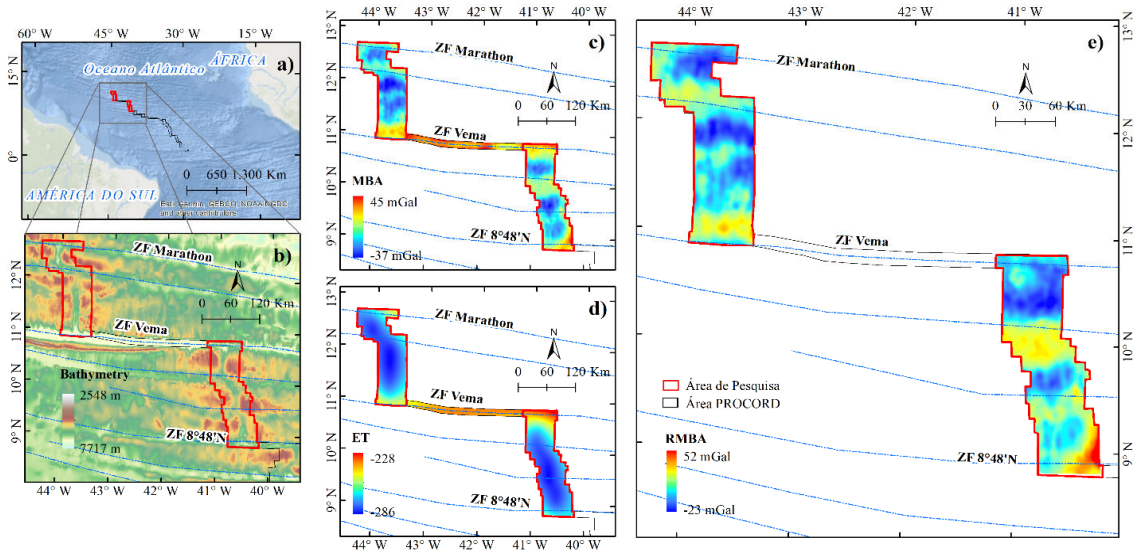

Figura 3.3 – Dados gravimétricos. a) Mapa de localização da área de estudo. b) Dados de altimetria por satélite obtidos do (GEBCO BATHYMETRIC COMPILATION GROUP 2022, 2022). c) Mapa anomalia Bouguer do manto (MBA). d) Mapa do efeito térmico (ET) global das idades. e) Mapa de Anomalia Residual do Manto. Todos os mapas acompanham levantamento do PROCORD (polígono preto) e a área específica de estudo (polígono vermelho).

Para calcular a **anomalia de Bouguer do manto** (MBA, na sigla em ingês *Mantle Bouguer Anomaly*), foram removidos os efeitos da topografia e da interface teórica crosta-manto (Moho), assumindo uma espessura média crustal de 6 km. O efeito gravimétrico da Moho teórico foi somado ao efeito da topografia, resultando no efeito gravimétrico do modelo. Esse efeito foi subtraído das anomalias do ar livre, obtendo-se assim a MBA.

O efeito do resfriamento da litosfera foi modelado com base em um modelo de meio-espaço dependente da idade da litosfera, representando sua evolução térmica. Nesse modelo, assume-se que a litosfera esfria e se torna mais densa à medida que se afasta do eixo da dorsal oceânica. Primeiramente, foi calculado a base da litosfera, considerando o contraste de densidade entre astenosfera e litosfera de -60 kg/m³. O efeito gravimétrico desse modelo foi determinado conforme descrito por MAIA & ARKANI-HAMED (2002). Posteriormente, o efeito do resfriamento foi subtraído da MBA para se obter a Anomalia de Bouguer do Manto Residual (RMBA, na sigla em inglês *Residual Mantle Bouguer Anomaly*).

A RMBA foi invertida para interpretar variações de espessura da crosta em relação ao modelo assumido de 6 km, com contraste de densidade de 500 kg/m³. A espessura total da crosta foi calculada somando-se 6 km às variações resultantes da inversão, conforme método de (CHEN, 1992).

A RMBA reflete variações na espessura crustal e possibilita interpretações detalhadas das estruturas tectônicas e processos de formação crustal. Valores baixos de RMBA indicam uma crosta mais espessa (até 8 km) no modelo de densidade constante ou a presença de materiais menos densos na crosta ou no manto superior (CANNAT *et al*., 2006). Valores altos de RMBA refletem uma crosta mais fina (até 0,5 km) e estão associados a materiais crustais ou mantélicos mais densos.

3.4. Extração das feições morfotectônicas

A análise de dados batimétricos, gravimétricos e de sismicidade permitiu a delimitação de diversas estruturas, como vales axiais, escarpas, lineamentos e montanhas submarinas, em diferentes escalas nas dorsais oceânicas. O vale do rifte da dorsal (*rift valley*), localizado na porção mais profunda, estreita e central do relevo da dorsal, é delineado em perfis batimétricos e gravimétricos. Ele é marcado por escarpas quase retilíneas e descontínuas, associadas a planos de falhas normais nos flancos. O piso do vale (*rift valley floor*) corresponde à área entre as primeiras grandes falhas em cada lado do eixo. É caracterizando por bacias ou topografias positivas de baixa amplitude, frequentemente alinhadas ortogonalmente ao eixo de expansão. Essas elevações apresentam morfologia típica de acreção vulcânica extrusiva em ambientes submersos (THAMMINIDI, 2022), servindo como referências para a definição estimada do eixo de crista vulcânica axial (neste trabalho denominado em inglês de *axial volcanic ridge axis, ridge axis or spreading axial*), também corroborado por anomalias gravimétricas. Sendo esses eixos considera o topo vulcânico fissural e as profundidades máximas locais nos centros de expansão.

De acordo com SMALL (1994), o eixo do vale (*axial valley*) pode ser determinado pela presença de cristas axiais (montes submarinos ou colinas) ou por vale axial no centro de expansão. Embora sua forma varie consideravelmente, ela mantém uma consistência morfológica. A região onde as cristas axiais se concentram são denominadas de zona neovulcânicas (*neovulcanic zone*), uma estreita faixa no centro da dorsal oceânica de lento espalhamento, que se afasta progressivamente do eixo axial (FOX *et al*., 1991). Essa zona, marcada como a mais profunda, é delimitada por falhas normais em ambos os flancos. Em dorsais de lento espalhamento, as profundidades típicas variam entre 1 a 2 km, com larguras de 20 e 30 km (BONATTI *et al*., 2005).

Os terrenos extensionais (*extensional terrain*) das dorsais oceânicas são delimitados por escarpas íngremes e lineares e definidas por depressões retangulares (grabens) e cânios estreitos em forma de caixa (FOX *et al*., 1991). As descontinuidades, como falhas, juntas e fraturas, foram agrupadas sob o termo "lineamentos" (*structure lineation*) e identificadas com base em critérios como mudanças abruptas nas isóbatas nos mapas batimétricos, que indicam deslocamentos nos padrões morfológicos. Exemplos incluem o desalinhamento e interrupções abruptas de cristas abissais (*abissal hill*), além da formação de depressões ou altos topográficos em margens opostas. As escarpas destacaram-se como marcadores importantes, sendo identificadas por sua linearidade paralela ao *strike*, associadas a assimetrias e nitidez em perfis transversais. Depósitos de tálus, descritos por (MACDONALD & ATWATER, 1978), estão frequentemente associados a essas escarpas. A utilização da Carta de Declividade, com critérios do IBGE (2007), foi fundamental para identificar escarpas com inclinações superiores a 70° (*major fault scarp*) e suas variações.

As montanhas submarinas foram descritas como estruturas predominantemente planares, com simetria em perfis transversais e, em alguns casos, cumes colapsados (YESSON *et al*., 2011). Além disso maciços (*massifs*) correspondem a domos de forma irregular desconectados do padrão de falhas paralelas à dorsal dos flancos dos segmentos adjacentes (GRÀCIA *et al*., 2000).

CAPÍTULO IV
ARTIGO CIENTÍFICO

The magmatic and tectonic role on spreading styles at ridge-transform intersection between Marathon and Vema Transform faults

Este documento consiste em um artigo submetido à revista Marine Geology. Para garantir a conformidade com os critérios de originalidade informamos o código de submissão: MARGO-D-25-0000.

4. ARTIGO CIENTÍFICO: THE MAGMATIC AND TECTONIC ROLE ON SPREADING STYLES AT RIDGE-TRANSFORM INTERSECTION BETWEEN MARATHON AND VEMA TRANSFORM FAULTS

The magmatic and tectonic role on spreading styles at ridge-transform intersection between Marathon and Vema Transform faults

Patrícia Reis Alencar Oliveira[a,b], Marcia Maia[c], Moab Paxedes Gomes[b], Heliásio Augusto Simões[a]

[a] *Geological Survey of Brazil, 840 Rodrigues Junior, Fortaleza, CE, 60.060-000, Brazil*
[b] *Federal University of Rio Grande do Norte, Lagoa Nova University Campus, 59078-970, Natal, RN, Brazil*
[c] *Geo-Ocean, UMR 6528 CNRS-IFREMER-UBO-UBS, IUEM Plouzané, France*

E-mail adresses: patricia.alencar@sgb.gov.br (P.R.A. Oliveira), marcia.maia@univ-brest.fr (M. Maia), moab.gomes@ufrn.br (M.P. Gomes), heliasio.simoes@sgb.gov.br (H.A. Simões)

ABSTRACT

The Mid-Atlantic Ridge (MAR) exhibits tectonic and magmatic characteristics shaped by transform faults, non-transform discontinuities, and detachment faults, which expose mantle and lower crustal rocks, forming oceanic core complexes and massifs. This study examines the 11°N and 12°N MAR supersegments, located between the Marathon and Vema Fracture Zones, focusing on transform ridge intersections and the Mercurius non-transform discontinuity. Multibeam bathymetry and gravity data were utilized to characterize morphology, tectonics, and crustal thickness, assessing the impacts of magmatism and tectonism. The results reveal distinct morphotectonic domains between the supersegments. In the 11°N supersegment, subdivided into 11°55'N and 11°20'N, higher magmatic activity, seafloor roughness, and axial uplift were observed, associated with initial-stage detachment faults. Conversely, the 12°N supersegment showed reduced magmatic supply, favoring the development of detachment faults. The Vema Transform Fault exhibited intense cooling and hydrothermal activity, with its inside corner characterized by long-lived faults and prominent massifs. The Marathon Transform Fault displayed less evolved tectonic features, with no significant corrugations. These results suggest that MAR segmentation is strongly influenced by the interplay between magmatism and tectonics, with variations in crustal thickness playing a crucial role in structural evolution. The asymmetries between inside and outside corners reflect lithospheric decoupling, particularly at offsets such as Mercurius and Vema. This study highlights the integration of geophysical and morphological data as essential to understanding slow-spreading ridges, contributing to hypotheses on lithospheric coupling and the formation of oceanic segments.

KEYWORDS: Mid-Atlantic Ridge, non-transform discontinuities, transform fault, ridge-transform intersection and crustal thickness.

1. Introduction

The Mid-Atlantic Ridge (MAR) exhibits a series of volcanic and tectonic features, such as first-order transform faults (TFs), higher-order non-transform discontinuities (NTDs) and detachment faults, that are significant tectonic discontinuities shaping the ridge morphology (MACDONALD, 1982; SEMPÉRÉ *et al*., 1993). These structures affect the axial magma budget and distribution and drive the exhumation of lower crust and mantle rocks (ESCARTÍN *et al*., 2017). In particular, detachment faults are responsible for exhuming in their footwall crustal sections that typically take the form of non-corrugated blocky massifs, and in the domal OCCs (oceanic core complexes), mantle rocks intruded by plutonic gabbros are observed (BLACKMAN; CANALES; HARDING, 2009; MACLEOD *et al*., 2009; TUCHOLKE; LIN; KLEINROCK, 1998; WHITNEY *et al*., 2013).

Detachment faults formation are related to thermal changes in the upper mantle and lower crust, as well as with the hydrothermal activity within the newly developed lithosphere (e.g., BUCK *et al*., 2005; CARBOTTE & MACDONALD, 1994; MACDONALD *et al*., 1996; MACLEOD *et al*., 2011; TUCHOLKE & LIN, 1994). These structures provide insights into the distribution and rates of spreading-induced stresses, mantle upwelling, seismicity, and hydrothermal activity (DANNOWSKI *et al*., 2018; MACDONALD *et al*., 1996; MACLEOD *et al*., 2011; TUCHOLKE & LIN, 1994).

Alternating magmatic and tectonic dominant phases accommodate the expansion of the MAR (CANALES *et al*., 2005; CARBOTTE & MACDONALD, 1994; ESCARTÍN *et al*., 1999; ESCARTÍN & CANNAT, 1999; HOWELL *et al*., 2016; OLIVE & DUBLANCHET, 2020). The accommodation of extension through magmatism, represented by the M factor, is a fundamental parameter that governs the formation and evolution of faults. This factor regulates the rate at which an active fault, formed in the axial lithosphere, migrates away from the axis, encountering progressively thicker and stronger lithosphere (BUCK *et al*., 2005; ITO & BEHN, 2008; OLIVE & DUBLANCHET, 2020; SCLATER *et al*., 1970; TUCHOLKE & LIN, 1994). The formation of new faults is more efficient than maintaining slip on an existing fault as it moves away from the axis (OLIVE & DUBLANCHET, 2020), considering that as the magmatic supply decreases, faults migrate more slowly and remain active for longer periods (BUCK *et al*., 2005). ESCARTÍN *et al*., 1999) found that magmatic supply is typically higher at the axial center of mid-ocean ridges, while at the ends, it decreases and

the tectonic influence dominates. The balance between magmatic heat injected during crustal accretion and heat loss to the seafloor by hydrothermal circulation strongly influences the axial ridge morphologies (SHAW & LIN, 1996). Furthermore, magma supply, faulting, crustal composition, and lithospheric thickness all play a role in shaping the final morphological configuration along the axis (ESCARTÍN *et al*., 1999).

The MAR is classified as a slow-spreading ridge. In the segment between the Marathon an Vema Fracture Zone, the total spreading velocity (Speed) is 11.76 mm/yr, (DEMETS *et al*., 2010). More than 50% of the new ocean crust is created in segments with a well-defined axial valley bordered by axial parallel normal faults regularly spaced at intervals of 5 to 10 km (CANN *et al*., 2015; OLIVE & ESCARTÍN, 2016). These faults delimitat abyssal hills that extend along the ridge axis and are approximately symmetrical to the neo-volcanic zones (CANN *et al*., 2015; OLIVE & ESCARTÍN, 2016).

Spreading rates are directly related to the thickness of the crust and lithosphere, playing a crucial role in shaping faulting patterns (HOWELL *et al*., 2016; ITO & BEHN, 2008; LIN & MORGAN, 1992; YONGSHUN CHEN & MORGAN, 1990). At slower spreading rates, the oceanic crust becomes cooler, more brittle, and thinner due to reduced thermal flux and crustal heating (ITO & BEHN, 2008).SHAW & LIN (1996) suggest that a 50% decrease in crustal thickness can lead to a two- to threefold increase in fault spacing and height.

Offset length between adjacent segments also critically influences fault formation. When the offset is sufficiently small, thermal interaction between the segments may occur, altering fault behavior. This thermal interaction often causes the fault axis to curve toward the crust located in the inside corner. In this region, faults tend to exhibit greater size and complexity. Such asymmetry, characteristic of slow-spreading ridges, is often amplified by the structural weakness associated with TF, contributing to the development of topographic highs in the inside corners.

Lithospheric thickness is another key factor in fault zone development and the interaction between the brittle plate and viscous mantle flow. In slow-spreading ridges, the relatively narrow decoupling region promotes strong coupling between the brittle plate and the mantle, leading to the formation of axial rift valleys with rugged topography, as well as lithospheric thinning (CHEN & MORGAN, 1990; HOWELL *et al*., 2016; ITO & BEHN, 2008; MORGAN *et al*., 1993).

The lithosphere formed at the inside corner (IC) of a ridge-transform intersection is transported along the transform fault (TF) and initially subjected to extensional stresses,

which promote the formation of a deeper valley in the active transform compared to the adjacent fracture zones. Subsequently, magmatic addition of new crust occurs as the lithosphere passes through the opposite ridge-transform intersections.

The tectonic stress changes observed at ridge-transform intersections, where normal faults from the spreading axis transition to strike-slip faults, result in significant bathymetric differences. These differences are not caused by flexural adjustments or differential subsidence associated with crustal age but rather by tectonic processes such as lithospheric extension and thinning, along with magmatic addition. This contradicts thermal subsidence predictions based on plate cooling, as the older ocean floor at the intersections becomes shallower. The magnitude of this depth difference does not have a direct relationship with the spreading rate, although slower slip systems tend to exhibit greater differences. Instead, the depth of transform valleys appears to be a combined function of the spreading rate and the age offset at ridge-transform intersections.

Studies demonstrate that these changes favor asymmetry between the inside corners (ICs) and outside corners (OCs) of ridge-transform intersections. ICs are characterized by thinner crust, greater lithospheric thinning, outcrops of serpentinized peridotites, and larger, more irregular faults compared to OCs. Previous studies support these patterns (BEHN & ITO, 2008; ESCARTÍN & CANNAT, 1999; ITO & BEHN, 2008; SEVERINGHAUS & MACDONALD, 1988).

Moreover, the increase in obliquity with depth below the seafloor within the shear zone promotes an extensional component that results in significant lithospheric thinning. This process contributes to the formation of deeper valleys in active transforms and to the uplift of the ocean floor in adjacent zones.

The present study conducts an analysis of the main structural features in the 11°N and 12°N supersegments of the MAR between the Marathon and Vema transform faults, with a primary focus on the Marathon Ridge-Transform Intersection (MRTI) and Vema Ridge-Transform Intersection (VRTI), as well as the intersections of the Mercurius Non-Transform Discontinuity (MeNTD) with supersegments 11 (11RNTD) and 12 (12RNTD) (Fig. 4.1). The aim of this study is to investigate how variations in magmatism and tectonics influence the morphological and structural characteristics of the seafloor in this part of the MAR. Specifically, the study evaluates the role of NTDs and TFs in shapping these segments along the ridge axis.

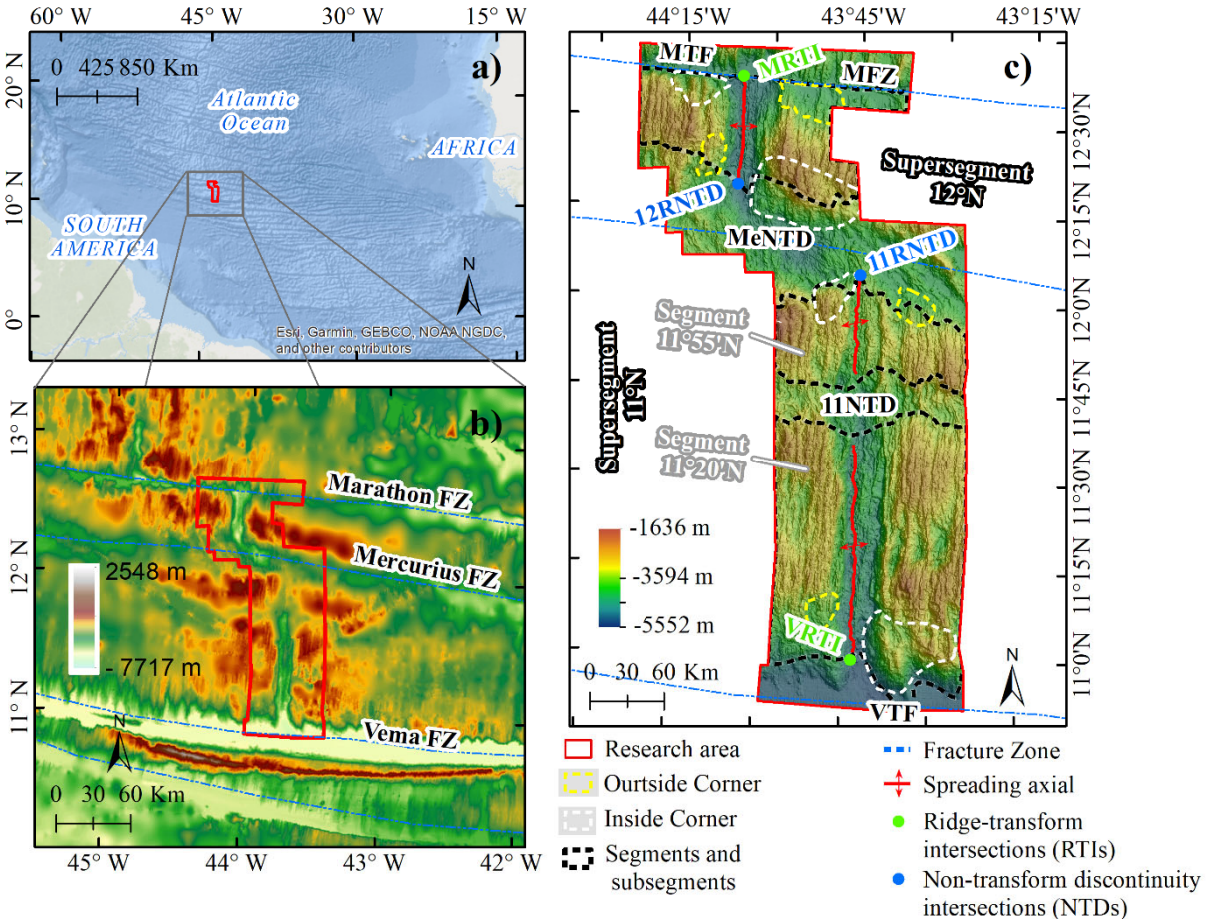

Figure 4.1 – Map showing the location of the study area. a) Equatorial Atlantic Ocean and South America and Africa Equatorial Margins. The specific study area is highlighted in the red polygon; b) Specific survey area (red polygon), including the fracture zones (blue dotted lines) and satellite altimetry data sourced from (GEBCO BATHYMETRIC COMPILATION GROUP 2022, 2022); c) Division of supersegments and segments of the MAR axis. MTF – Marathon Transform Fault, MFZ – Marathon Fracture Zone, MRTI – Marathon Ridge-transform Intersection, MeNTD – Mercurius Non-Transform Discontinuity, 12RNTD – 12°N Supersegment - Mercurius Non-Transform Discontinuity, 11RNTD – 11°N Supersegment - Mercuius Non-Transform Discontinuity, 11NTD – 11°N Non-Transform Discontinuity, VTF – Vema Ridge-Transform Intersection, and VRTI - Vema Ridge-Transform Intersection.

2. Study Area

Oceanic transform faults play a crucial role in displacing the axial ridges of mid-ocean ridges, while FZ record the tectonic history of plates up to the continental margins (BUCK *et al*., 2005; PEIRCE *et al*., 2019). Both structures are associated with regions of anomalous temperatures (BONATTI, 1978).

A transform zone follows a small circle around the specific pole of rotation for the tectonic plates involved. Changes in the position of this pole or the propagation direction of the plates on one or both sides of the transform fault may lead to geometric adjustments in search of more stable boundaries (BONATTI, 1978). These adjustments may result in

the disappearance of old transform zones and the emergence of new ones, such as smaller ridge-ridge transform faults formed in young, relatively thin, hot, and plastic lithosphere, as observed in the North Atlantic (BONATTI, 1978). On the other hand, in FZs with extensive offsets, the greater rigidity of the older and thicker lithosphere resists geometric adjustments, often leading to the formation of high-stress bands and generating compressive or extensional stresses along these zones extensional component that results in significant lithospheric thinning. This process contributes to the formation of deeper valleys in active transform and to the uplift of the ocean floor in adjacent zones.

2.1. Marathon and Mercurius Fracture Zone

Marathon Fracture Zone (MFZ) is a significant geographical area characterized by a complex crustal structure and active geological processes, such as magmatism and serpentinization. Similar to the Mercurius Fracture Zone (MeFZ), the MFZ plays a critical role in the evolution of deep oceanic structures, including oceanic core complexes (OCCs) (PEIRCE *et al*., 2020).

According to LAGABRIELLE *et al*. (1992), the MFZ features a small basement fragment or transverse ridge in its southern portion, quite similar to those observed in the Vema Fracture Zone. The present intra-sediments reveal relative rotation around an east-west axis and elevation to the north. This upward movement is accommodated along the northern lateral edge of the bathymetric depression rather than at its center. Additionally, the MFZ offsets younger crusts (1 Ma compared to 8 Ma) in relation to the MeFZ. The MFZ terrain is covered by flat and wide sediments (>10 km), displacing crusts of approximately 8 Ma against others of 11 Ma.

In the vicinity of the bathymetric valley of the MFZ, a crustal thinning is highlighted by seismic and gravity modeling. This feature results from a low-density region, interpreted as a reflection of serpentinization of the upper mantle. This process represents important pathways for fluid flow toward the deep crust and upper mantle. The buoyancy caused by density reduction contributes to the elevation of the region, promoting lower crust metamorphism and upper mantle serpentinization (BONATTI, 1976; PEIRCE *et al*., 2020).

Although less constrained by seismic modeling, the crust south of the MeFZ has an approximate thickness of 5 km. This crust consists of an upper and middle crust about

2 km thick (3.0–4.5 km/s) and a lower crust 3 km thick, reaching 7.5 km/s at the Moho. If the 7.5 km/s velocity contour is used to denote the base of the crust, the upper mantle velocity is also relatively high (PEIRCE *et al*., 2019).

In the MeFZ, the arrangement of intra-sedimentary layers suggests relative movement between the northern and southern sides of the fracture zone. The deeper layers on the northern side display an arched configuration, indicating a relative uplift of the younger lithosphere, although this process appears not to have persisted to the present (PEIRCE *et al*., 2019).

POCKALNY *et al*. (1996)suggest that the observed flexural configuration results from transtensional extension. The shallow bathymetry of the inside corners of RTI is dynamically supported, as a consequence of the opposite plate decoupling through the transform fault.

2.2. Vema Fracture Zone

The Vema Fracture Zone (VFZ) is characterized by a significant offset that shifts the MAR approximately 320 km in an east-west direction between 10° and 11°N (BONATTI *et al*., 2005; FABRETTI *et al*., 1998; VAN ANDEL *et al*., 1971). The Vema transform valley exhibits strong asymmetry between its northern and southern sections (LIGI *et al*., 2022), with widths ranging from 15 to 22 km (FABRETTI *et al*., 1998). The southern wall dips beneath the turbiditic deposits filling the valley, reaching a thickness of about 1 km (BONATTI *et al*., 2005; LIGI *et al*., 2022). These sediments, predominantly of turbiditic origin, were deposited during the Pleistocene and reflect complex sedimentary processes (LIGI *et al*., 2022), with contributions of detrital and biogenic material from the valley walls (CHAMOV *et al*., 2020).

Approximately 140 km west of the southern intersection of the transform with the ridge lies the Vema Transverse Ridge (VTR), a prominent topographic elevation extending parallel to the Vema Transform and rising more than 3 km above the predicted level of thermal contraction (BONATTI *et al*., 2005; LIGI *et al*., 2022). Recent studies suggest that the VTR represents the exposed edge of a flexed and uplifted oceanic lithospheric plate that, at some point, emerged above sea level. This area was subsequently eroded and covered by shallow-water carbonates, primarily during the Miocene and Pliocene, as it underwent subsidence (BONATTI *et al*., 2005; BONATTI *et al*., 1983; LIGI *et al*., 2022; PALMIOTTO *et al*., 2013).

The carbonates overlie a sequence of peridotites about 1 km thick, followed by a gabbro unit of variable thickness, a well-developed dike complex, and an upper layer of massive basalts. Together, these units comprise the Vema Lithospheric Section (VLS). The VTR marks the northern boundary of the 10°N axial segment, also known as the Eastern Mid-Atlantic Ridge (EMAR), whose development began approximately 40 million years ago (FABRETTI *et al*., 1998; LIGI *et al*., 2022).

The eastern end of the Vema is interpreted by a principal detachment zone (PDZF), which represents the beginning of the EMAR segment (BONATTI *et al*., 1994; EITTREIM & EWING, 1975), referred to in this work as the 10°N segment. In this segment, the crust maintained a constant thickness from 26 to 20 Ma, with a gradual thickening up to the present day (LIGI *et al*., 2022). Crustal thickness oscillations, with periods of 3 to 4 million years, have been attributed to secondary convection in the mantle beneath the ridge (LIGI *et al*., 2022). This mantle, rich in H_2O and of low viscosity, lies beneath a residual mantle depleted in H_2O and of high viscosity (BONATTI *et al*., 2003). This configuration may be related to changes in the geometry of tectonic plate boundaries, resulting in transpression or transtension regimes in the transform domain.

Since approximately million years ago, the degree of mantle melting beneath the MAR has increased, albeit in an oscillatory manner. Studies indicate that the asthenospheric mantle beneath the ridge, particularly near 11°N, shows a cooling gradient and/or a loss of fertility as it migrates from Iceland toward the equator (LIGI *et al*., 2022) (LIGI *et al*., 2022c). Waves of warm and fertile mantle, possibly originating from the Iceland and Azores plumes, have migrated southward, contributing to the increased melting observed in the region over the past 16 million years (BONATTI *et al*., 2003; LIGI *et al*., 2022).

Additionally, counterclockwise reorientations of the ridge axis and changes in the lithospheric spreading direction near the transform fault have been identified, combined with shifts in the position of the Euler rotation pole. These changes, occurring in plates older than 10 million years, culminated in the flexing and uplift of portions of the lithospheric plate.

Vertical movements along FZ may be related to several factors, including horizontal heat conduction across a fracture zone; viscodynamic forces; gravitational diapirism of serpentine; and horizontal compressive or extensional stresses(BONATTI, 1978)

3. Data and Methodology

3.1. Bathymetric Data

Multibeam bathymetry was collected by the Geological Survey of Brazil (SGB) as part of the Project for Prospecting and Exploration of Mineral Resources in the South and Equatorial Atlantic International Waters (PROCORDILHEIRA) (MOTA *et al*., 2021). The survey mapped an area of 13,550 km² between the Marathon and Vema fracture zones, with depths ranging from 1,636 m to 5,601 m. Bathymetric data was acquired using the Reson 7150-F system, operating at 12 kHz. The profiles crossed the ridge in an east-west direction, with a spacing of 6 to 7 km and lengths varying from 40 to 60 km (Fig. 4.2b). During the data collection, positioning, offsets, tides, and subsystems were integrated and corrected. The sound velocity in water was calculated from CTD/XBT profiles.

Post-processing was performed using CARIS HIPS & SIPS software, including calculations of Total Propagated Uncertainties (TPU) and the application of filters to remove outliers, minimizing edge effects. The bathymetric grid was generated with a resolution of 100 m/pixel using the CUBE algorithm (Combined Uncertainty and Bathymetry Estimator) (CALDER & MAYER, 2003) (Fig. 4.2).

Derived products from the bathymetric surface were generated in a GIS environment using the Spatial Analyst tool in ArcGIS, including bathymetric contours with 250 m intervals; slope maps calculated in degrees and classified according to IBGE (2007) as flat (0°-3°), gently undulating (3°-8°), undulating (8°-20°), strongly undulating (20°-45°), mountainous (45°-75°), and steep (>75°); roughness maps based on the Roughness Concentration Index (RCI) (SAMPAIO & AUGUSTIN, 2014), which measures the maximum elevation difference within a pixel's neighborhood, enabling terrain compartmentalization and the identification of geological structures; aspect maps indicating the preferential direction of slopes measured clockwise, with flat areas assigned a value of -1; backscatter maps generated with a resolution of 50 m using the SIPS Backscatter algorithm from CARIS HIPS & SIPS, with further processing in ArcGIS; and bathymetric profiles extracted perpendicular and orthogonal to the ridge axis, spaced at 1 km intervals. To enhance geological structures, relief shading with 45° altitude and 315° azimuth was applied, highlighting morphotectonic features.

Additionally, regional data from satellite altimetry and fracture zone traces were used, provided by the General Bathymetric Chart of the Oceans (GEBCO BATHYMETRIC COMPILATION GROUP 2022, 2022).

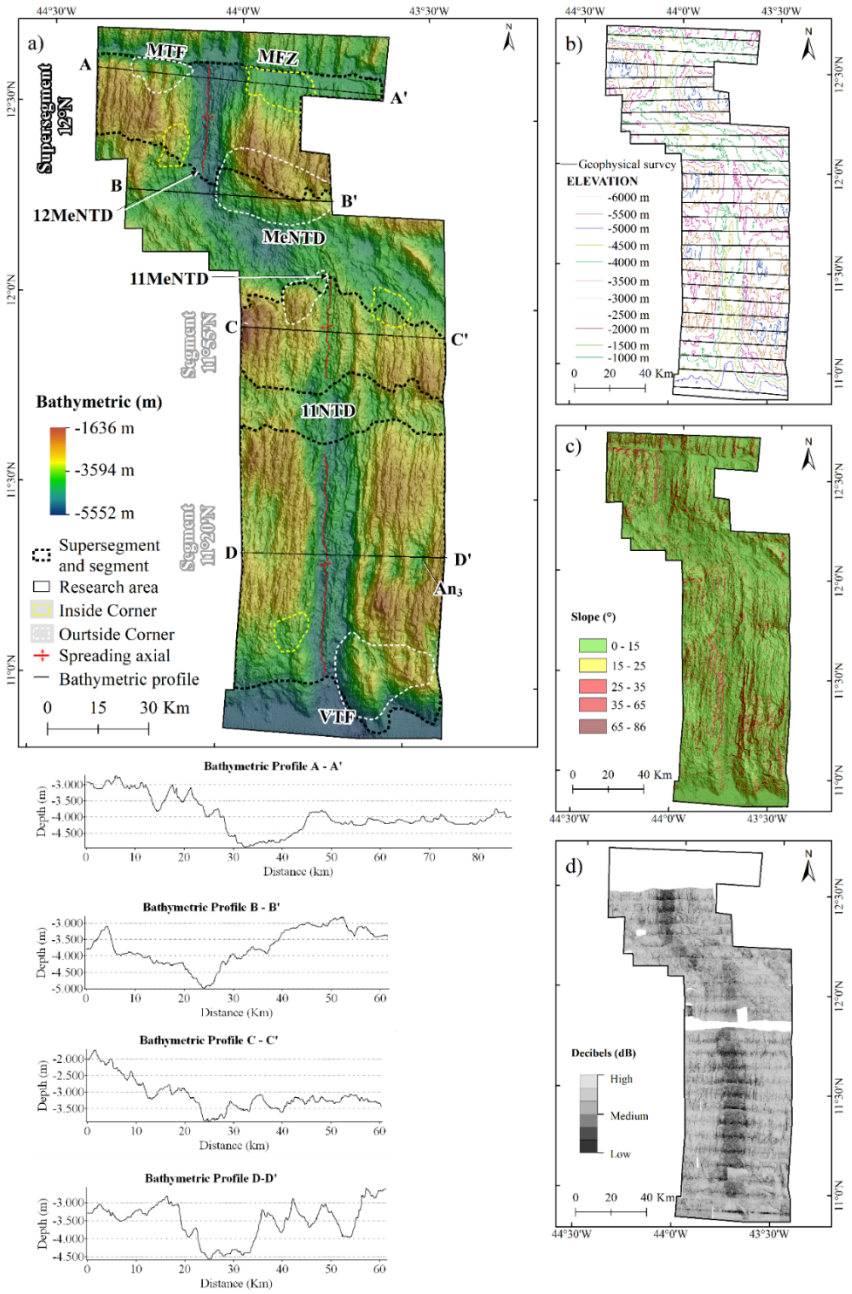

Figure 4.2 – (a) Bathymetric map with shaded relief: Supersegments and segments are represented by light gray dashed lines. The inside corner is indicated by withe dashed lines, while the outer corner is highlighted by dashed yellow lines. Continuous black lines represent the bathymetric profiles. The estimated axial ridge is indicated by red lines, and red arrows show the direction of plate movement. (b) Contourn map. Highlighting geophysical survey lines (black lines) spaced 6 to 7 km apart, with lengths ranging from 40 to 60 km. (c) Slope map: Classified into six categories – Flat (0-3%), Gently Undulating (3-8%), Undulating (8-20%), Strongly Undulating (20-36%), Mountainous (36-75%), and Steep (> 75%). (d) Backscatter map: Displays acoustic return intensity. Abbreviation: MTF – Marathon Transform Fault, MFZ – Marathon Fracture Zone, MeNTD – Mercurius Non-Transform Discontinuity, 11RNTD – 11°N Segment - Mercurius Non-Transform Discontinuity, and NVTF – Vema Ridge-Transform Intersection.

3.2. Gravity Data

For the gravimetric analysis, a regional grid was initially constructed using free-air gravity anomaly data (GEBCO BATHYMETRIC COMPILATION GROUP 2022, 2022), integrated with satellite altimetry data, as described by (MAIA; ARKANI-HAMED, 2002). This method calculates the gravitational effect of a constant-thickness layer with laterally variable densities. The calculations were performed in the Fourier Transform domain, adopting average densities of 2800 kg/m³ for the oceanic crust, 3300 kg/m³ for the upper mantle, and 1030 kg/m³ for seawater.

To calculate the Mantle Bouguer Anomaly (MBA), the effects of topography and the theoretical crust-mantle interface (Moho) were removed, assuming an average crustal thickness of 6 km. The gravitational effect of the theoretical Moho was added to the topography effect, resulting in the gravitational effect of the model. This effect was subtracted from the free-air anomalies, thus obtaining the MBA.

The effect of lithospheric cooling was modeled based on a half-space model dependent on lithospheric age, representing its thermal evolution. In this model, the lithosphere is assumed to cool and become denser as it moves away from the mid-ocean ridge axis. First, the base of the lithosphere was calculated, considering a density contrast between the asthenosphere and lithosphere of -60 kg/m³. The gravitational effect of this model was determined as described by (MAIA *et al*., 2011). Subsequently, the cooling effect was subtracted from the MBA to obtain the Residual Mantle Bouguer Anomaly (RMBA).

The RMBA was inverted to interpret variations in crustal thickness relative to the assumed 6 km model, with a density contrast of 500 kg/m³. The total crustal thickness was calculated by adding 6 km to the variations resulting from the inversion, following the method of (CHEN, 1992).

The RMBA reflects variations in crustal thickness and allows for detailed interpretations of tectonic structures and crustal formation processes. Low RMBA values indicate a thicker crust (up to 8 km) under the constant density model or the presence of less dense materials in the crust or upper mantle (CANNAT *et al*., 2006). High RMBA values indicate a thinner crust (as little as 0.5 km) and are associated with denser crustal or mantle materials (Fig. 4.3).

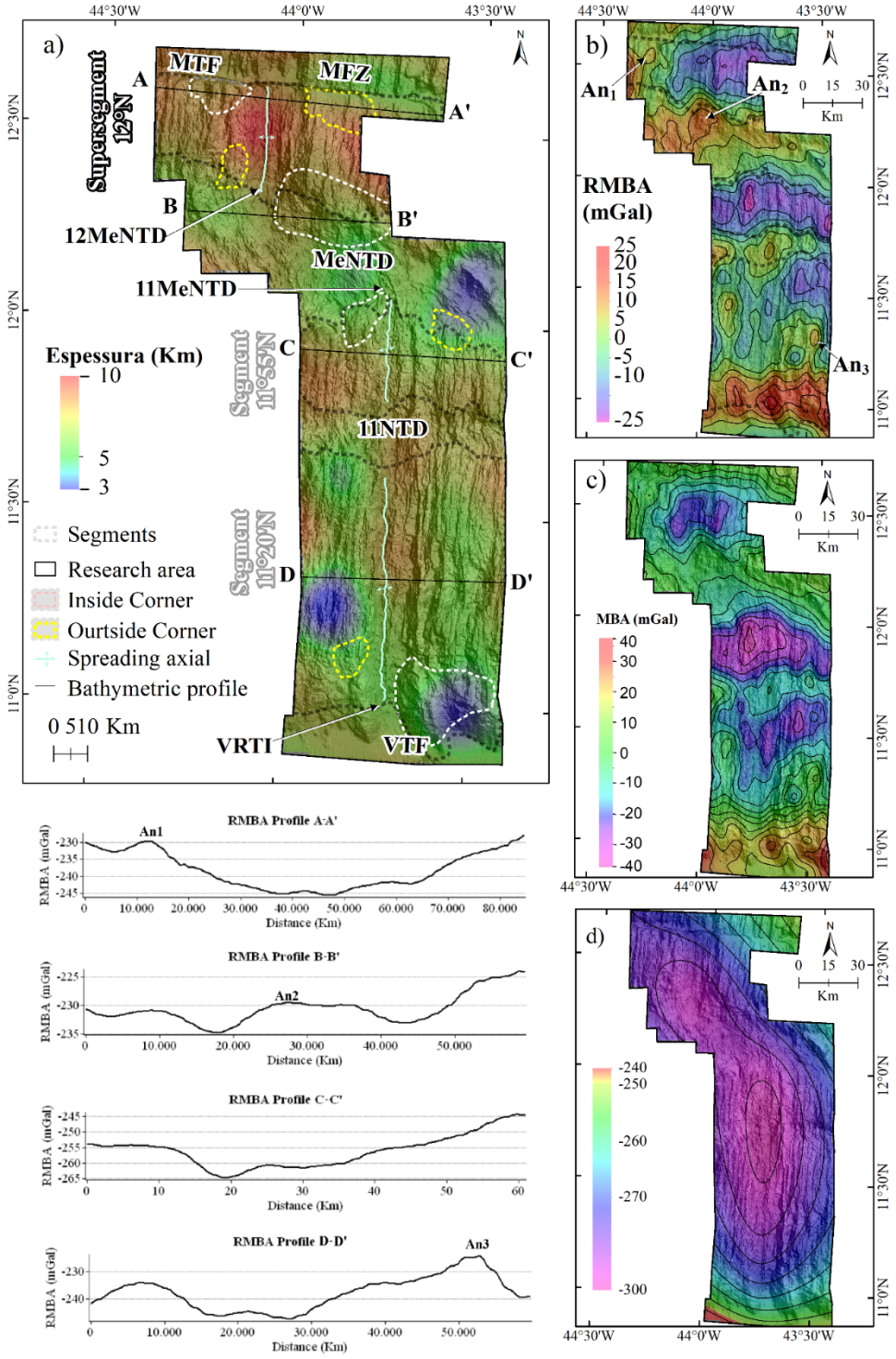

Figure 4.3 – (a) Crustal thickness map with supersegments and segments indicated by light gray dashed lines; the estimated axial ridge is represented by red lines, while red arrows indicate the direction of plate movement, and RMBA profiles are shown by black lines. (b) Residual Mantle Bouguer Anomaly (RMBA) map. (c) Mantle Bouguer Anomaly (MBA) map. (d) Map of the gravitational effect of lithospheric cooling, calculated from a crustal age model, with shaded relief overlaid on all maps. Abbreviations: MTF – Marathon Transform Fault, MFZ – Marathon Fracture Zone, MeNTD – Mercurius Non-Transform Discontinuity, 11NTD – 11°N Supersegment Non-Transform Discontinuity, VTF – Vema Transform Fault, and VRTI - Vema Ridge-Transform Intersection, and An1, An2, An3 – High RMBA Anomalies 1, 2, and 3.

3.3. Extraction of Morphoterctonic Features

Based on the bathymetric data and its derivatives, various structures were identified and delineated at different scales. The rift valley seafloor was identified as the deepest, narrowest, and most central portion of the ridge relief, as observed in the bathymetric profiles. This region is characterized by nearly linear and discontinuous escarpments of normal fault planes on both sides (BUCK *et al*., 2005). The valley floor corresponds to the area between the first major faults on each side of the axis, marked by basins or low-amplitude positive topographies, often elongated orthogonally to the spreading axis. These highs, with characteristic morphologies of extrusive volcanic accretion in submarine environments, were used to approximately delineate the axial volcanic ridge, considering the fissural volcanic peaks and the maximum local depths at the spreading centers. According to (SMALL, 1994), the axial valley can be determined by the presence of axial ridges (seamounts or hills) or the axial valley itself, which varies considerably between locations but maintains a consistent shape.

The neovolcanic zone was identified as the central region of the slow-spreading mid-ocean ridge, characterized by depths ranging from 1 to 2 km and widths between 20 and 30 km, bounded by normal faults on its flanks (BUCK *et al*., 2005). It is a narrow area that progressively diverges from the axial center (FOX; *et al*., 1991). The tectono-extensional terrains of mid-ocean ridges are marked by steep, linear escarpments that define rectangular depressions (grabens) and narrow, box-shaped canyons (FOX; *et al*., 1991).

Initially, evidence of abrupt changes in the contour lines derived from the bathymetric map was analyzed, indicating displacements in bathymetric patterns. The presence of escarpments, characterized as steep slopes with parallel strike linearity, was a key indicator. These escarpments can be either straight or sinuous and were highlighted by their asymmetry and clarity in profiles transverse to the ridge. Talus deposits were also used as indicators (MACDONALD & ATWATER, 1978). Additionally, the Slope Map was used to highlight escarpments with inclinations greater than 70°, following the IBGE (2007) criteria.

Seamounts were characterized as structures with predominantly planar geometry and symmetrical shapes in transverse profiles, exhibiting limited or no linearity. In some cases, collapsed or preserved summits were identified (YESSON *et al*., 2011).

Furthermore, according to (ESCARTÍN *et al*., 2008), smooth or gently inclined massifs, often abandoned, can be identified through striations or undulations on their surfaces, which are parallel to the ridge propagation direction.

4. Results

4.1. Segmentation of the ridge axis

The analysis of multibeam bathymetry and gravimetry along the Mid-Atlantic Ridge, between the Marathon and Vema transform faults, demonstrated the that region is divided into two main supersegments (first-order segments), centered at 12°N and 11°N, delimited by first-order discontinuities (TFs) (Figs. 4.1, 4.2 and 4.3). These discontinuities share common characteristics, such as significant offsets (>30 km) and marked morphological changes, primarily evidenced by deep nodal basins in their relief (Figs. 4.1d, 4.2 and 4.3). Additionally, theses spreading center discontinuities are located at local depth maxima. While the inner floor of the rift valley is shallower near the center of each supersegment and deepens towards the discontinuities (Figs. 4.1d, 4.2 and 4.3).

Although the supersegments are delimited by transform fault, the Mercurius discontinuity is classified in this study as a NTD. However, it is flanked by fossil traces off-axis that suggest the existence of a former transform fault. The 11°N supersegment has been subdivided into two smaller segments (second-order segments), centered at 11°55'N and 11°20'N (Fig. 4.1d), defined by NTDs. First-order discontinuities divide large morphotectonic domains, while NTDs allow the coexistence of adjacent spreading segments, characterized by variations in tectonic formation and evolution processes. These NTDs delimit smaller and distinct spreading segments that reflect different processes of tectonic formation and evolution.

In this study, TFs and FZs are treated separately, even though some approaches group both under the generic term "fracture zone." In the region of RTIs, we delineated a characteristic area known as the IC, located on the flank of the ridge where it intersects with the active portion of the TF.

4.2. Supersegment 12°N

The 12°N supersegment is bounded to the north by the MTF and the MFZ and to the south by the MeNTD (Fig. 4.1d). This supersegment spans approximately 32 km along the axial ridge, with depths ranging from 4,500 m to 5,000 m, flanked by subparallel fault scarps oriented toward the spreading axis. Abyssal hills on its flanks exhibit greater symmetry in the central region of the supersegment, progressively becoming more asymmetrical toward the discontinuities, as evidenced in bathymetric profiles (Fig. 4.4d). The rift valley floor is relatively narrow, about 4 km wide, but widens near the intersections, reaching a maximum width close to the MTF. In this area lies a nodal basin, with a maximum depth of approximately 5,070 m (Fig. 4.5). The floor of this basin is predominantly characterized by a continuous zone of high backscatter acoustic echo, covering an area of approximately 144 km² (Fig. 4.2d).

In the ridge flank terrain west of the 12°N supersegment, approximately 20 km from the spreading axis, a discontinuity about 1.8 km in length is identified (Fig. 4.5). This discontinuity separates two distinct tectonic terrains with varied ocean floor types (Fig. 4.5). East of the discontinuity, detachment faults dominate the IC terrain of the MRTI. The detachment surfaces lack corrugations or volcanic structures, being spatially restricted, with lengths, heights, and spacings of less than 4 km, 1 km, and 5 km, respectively (Fig. 4.5). Small relict nodal basins precede the detachment faults. Along these surfaces, small transfer faults are observed over 600 m from the initial rupture (Fig. 4.5). West of the discontinuity, the ocean floor is predominantly volcanic (abyssal hills), with gently sloping fault scarps oriented toward the spreading axis, spaced less than 2 km apart, and with amplitudes below 200 m. Between these two terrains lies a small extensional region extending, where fissural volcanism occurs at latitude 12°38.33'N (Figs. 4.4 and 4.5).

The OC terrain of the MRTI predominantly consists of volcanic terrains and extensional basins. The oceanic crust in this region exhibits relatively shallow topography compared to the IC region. The seafloor is characterized by abyssal hills that extend and curve in a “J-shape,” interrupted by extensional basins of various dimensions. Among these structures, isolated circular volcanic structures are also notable, present in the older portion of the plate.

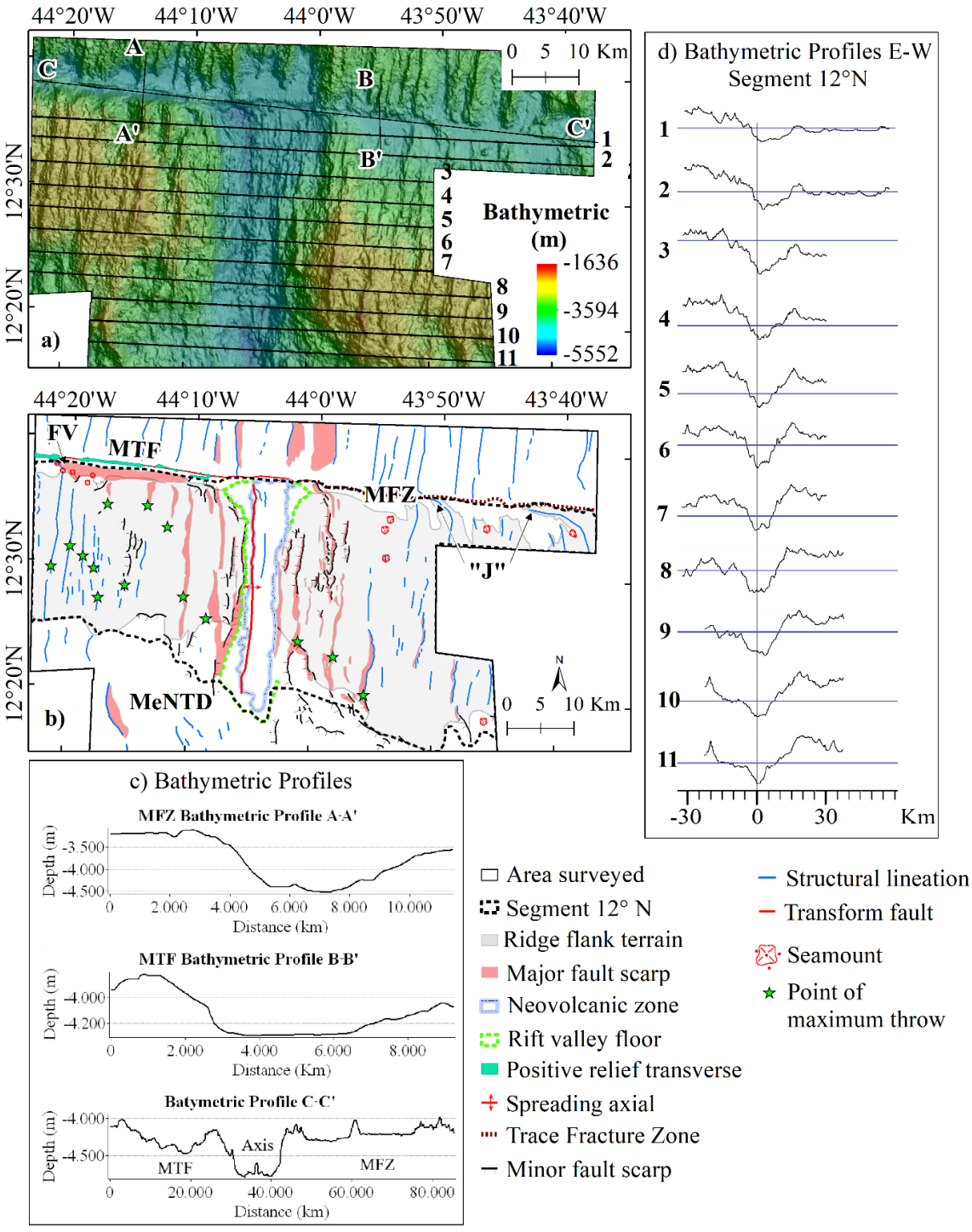

Figure 4.4 – (a) Bathymetric map with shaded relief underneath, showing the location of topographic profiles; (b) Interpretation map of 12°N supersegment of the Mid-Atlantic Ridge, with the green star represent the point of maximum throw. (c) Bathymetric profiles in the north-south direction: Profile A-A' crosses the Marathon Transform Fault (MTF), and profile B-B' traverses the MFZ. Profile C-C' run in the east-west direction, covering both the MTF and MFZ, and indicating the position of the "J-shaped" segments ("J"). (d) Bathymetric profiles oriented E-W, with their location show in (a). The blue lines on the profile indicate a depth of 4,000 m. Abbreviations: MTF – Marathon Transform Fault, MFZ – Marathon Fracture Zone, MeNTD – Mercurius Non-Transform Discontinuity, and FV – Probable Fissure Volcanism.

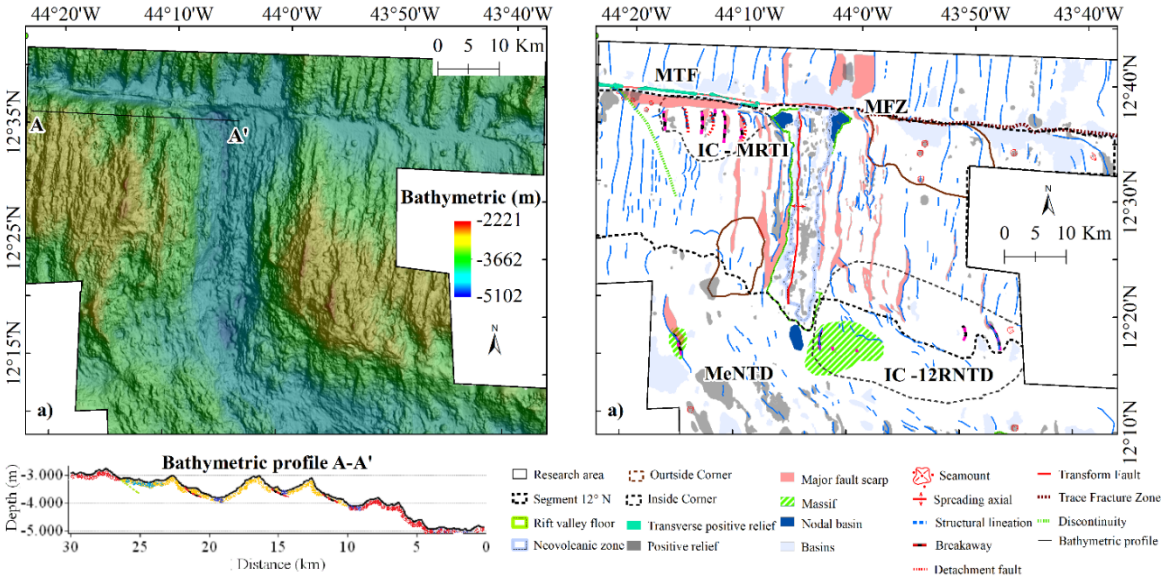

Figure 4.5 – Map of 12°N supersegment of the Mid-Atlantic Ridge, constructed using bathymetry, acoustic backscatter and gravimetric data. (a) Bathymetric map with shaded relief underneath. (b) Interpretation map. Abbreviations: MTF – Marathon Transform Fault, MFZ – Marathon Fracture Zone, MRTI – Marathon Ridge-transform Intersection, MeNTD – Mercurisus Non-Transform Discontinuity, 12RNTD – 12°N Segment - Mercurius Non-Transform Discontinuity, and IC – Inside Corner.

4.3. Supersegment 11°N

The 11°N supersegment, bounded to the north by the MeNTD and to the south by the VTF (Figs. 4.1 and 4.2), features an extensive axial ridge, interrupted near latitude 11°45'N by deep basins. Additionally, a shift in the orientation pattern of the lineations occurs, transitioning to a predominant NW-SE orientation, defining a NTD. Beyond bathymetric data, gravimetric analyses (see section 4.5) confirm the presence of this discontinuity, referred to in this work as the 11NTD. This discontinuity is narrow, approximately 12 km long, and divides the supersegment into two main subunits: the 11°20'N segment and the 11°55'N segment, each with distinct characteristics at their extremities, showing a gradual increase in depth (Fig. 4.6).

The 11°55'N segment, bounded to the north by the 11RNTD and to the south by the 11NTD, features an axial ridge approximately 32 km long, making it the shortest among the studied segments (Figs. 4.1 and 4.6). The axial valley is characterized by high roughness, with positive relief features formed by overlapping and aligned volcanic structures, as well as prominent and scattered volcanoes. The flanks are markedly asymmetric: the western flank exhibits higher altitudes and small terraces, while the

eastern flank is more regular. Approximately 12 km west of the ridge axis, a discontinuity is identified. In the first 12 km from the axial ridge, the floor is rougher, with less continuous ridges and reduced fault offsets. Beyond this distance, the ridges become more continuous, better spaced, and exhibit more significant fault throws (Fig. 4.6).

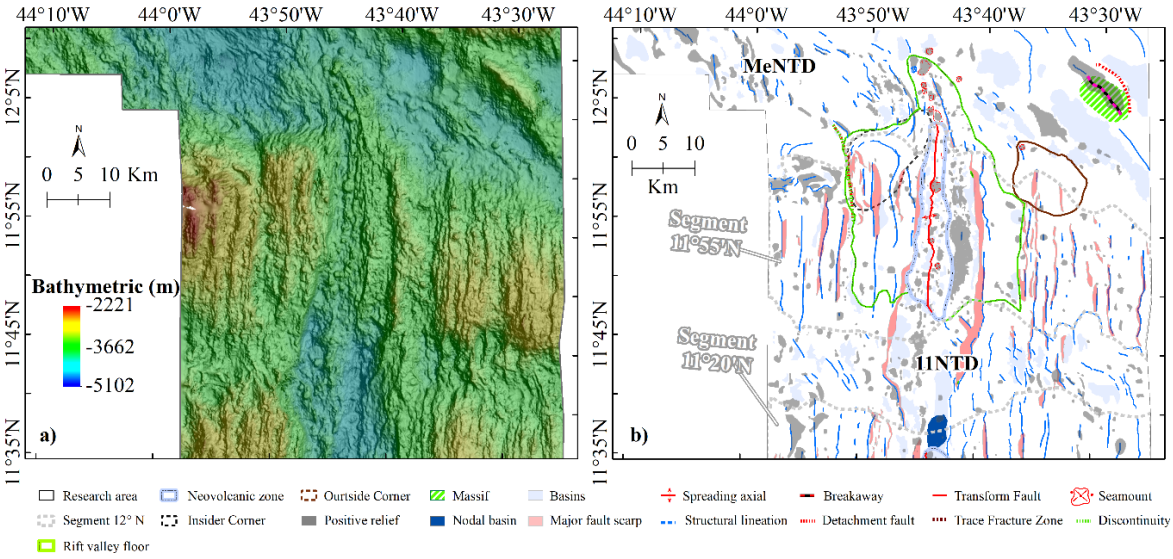

Figure 4.6 – Map of 11°55'N segment of the Mid-Atlantic Ridge based on bathymetry and gravimetric data. (a) Bathymetric map with shaded relief underneath. (b) Interpretation map. Abbreviations: MeNTD – Mercurisus Non-Transform Discontinuity, and 11RNTD – 11°N Segment - Mercurius Non-Transform Discontinuity.

The 11°20'N segment exhibits greater symmetry in its northern portion, which gradually decreases towards the discontinuities. The axial ridge, 69 km long, is both longer and deeper (5,000 to 4,400 m) compared to the axial ridge of the 11°55'N segment. The abyssal hills on both flanks are shorter and discontinuous, interrupted by significant extensional basins. The largest and most prominent of these basins are located on the eastern flank, near the intersection of the ridge with the IC-VRTI transform fault, where fault scarps exhibit the greatest displacements (Fig. 4.7).

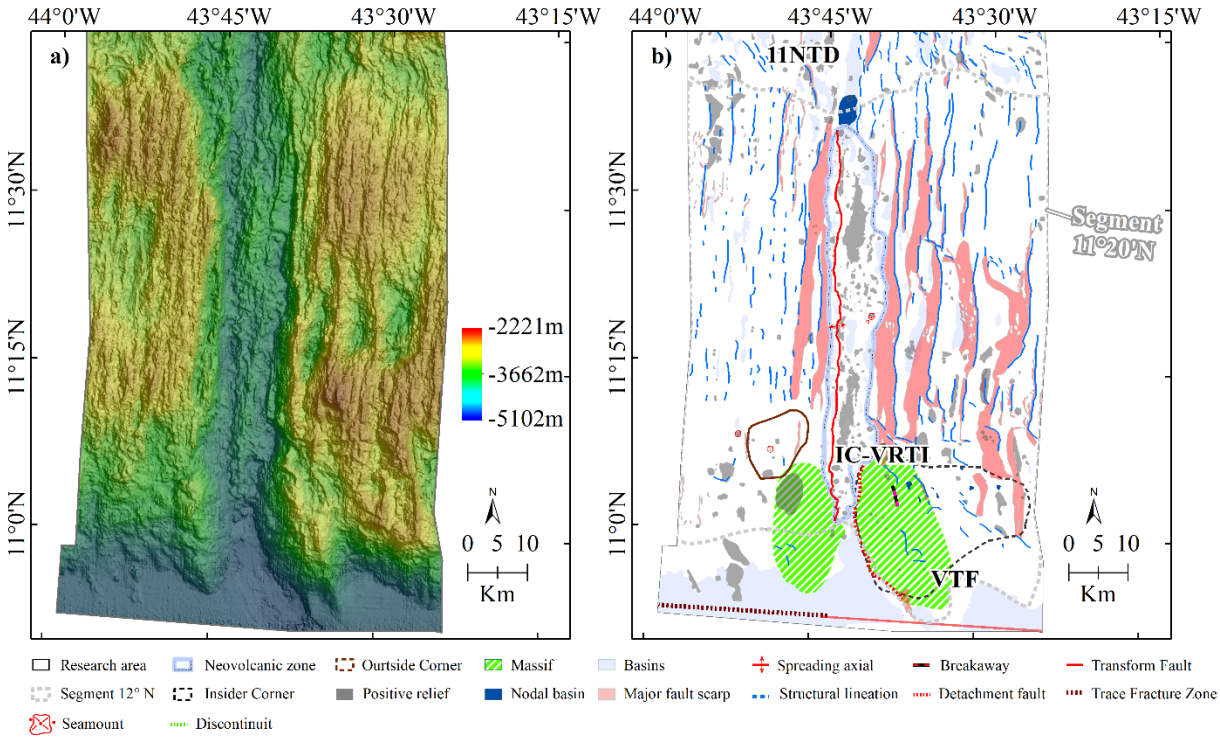

Figure 4.7 – Map of 11°20' segment of the Mid-Atlantic Ridge based on bathymetry and gravimetric data. (a) Bathymetric map with shaded relief underneath. (b) Interpretation map. Abbreviations: 11NTD – 11°N Supersegment Non-Transform Discontinuity, VRTI - Vema Ridge-Transform Intersection, VTF – Vema Transform Fault and IC – Inside Corner.

4.4. Discontinuities and intersection with ridge

4.4.1. Ridge-transform Intersection

The MTF offsets the MAR axis by approximately 80 km, of which 33 km of its eastern portion were analyzed in this study (Fig. 4.1b). The MTF valley gradually deepens toward the MRTI, being narrower (less than 6 km wide) and deeper (reaching up to 4,500 m) compared to the broader and relatively shallower MFZ valley, which reaches a depth of about 4,200 m (Fig. 4.2 and Bathymetric Profile A-A' in Fig.4. 4). Near latitude 12°38'N, circular structures, possibly associated with volcanism, are observed, aligned from the edge of the abyssal hills of the 12°N supersegment to the plate boundary (Fig. 4.4b).

The floor of the MTF valley is bounded by steep escarpments on both sides, with the northern flank exhibiting a smoother profile (Fig. 4.4, A-A' profile). This valley floor is interrupted by prominent, long, discontinuous, and narrow topographic highs oriented transversely to the axis (Fig. 4.4). In contrast, the floor of the MFZ valley is disrupted by

extensions of the abyssal hills of the 12°N supersegment, which delimit basins oriented roughly in the east-west direction.

Vema transform an offset of approximately 320 km (Figs. 4.1 and 4.9), represents one of the largest transforms in the Atlantic (BONATTI *et al*., 2005; FABRETTI *et al*., 1998; VAN ANDEL *et al*., 1971). About 30 km of this length where depths are deeper than 3,300 m. This linear depression has relatively smooth seabottom seafloor topography (Fig. 4.7).

The IC-VRTI region features elevated relief, predominantly composed of a detachment-controlle floor and an extensive massif in the IC, covering an area of approximately 314 km². In the OC of the VRTI, another structure resembling a massif can be identified, closely similar to the IC massif, with an area of about 196 km². At the top of the IC massif, small ridge segments are observed, highlighted by circular basins, along with the delineation of the "breakaway" (Fig. 4.7).

4.4.2. Ridge-Non-Transform Discontinuity

The MeNTD is an extensive transtensive discontinuity zone primarily characterized by the presence of faults preferentially NW-SE orientated, concentrated in the central valley floor, without a well-defined directional fault (Figs. 4.2 and 4.5). The regional satellite altimetry displays the alignment of this structure obliquely to spreading axis (Fig. 4.1), extending approximately 45 km in both directions, indicating the absence of a transform fault, which define a characteristic region of NTD.

The basin floor, with depths ranging from 2,221 to 5,101 m, extends for approximately 20 km and highlights a displacement of the ridge axis by about 40 km. Small basins emphasize the rotation and variations in fault orientation (Figs. 4.8). The IC of the 12RNTD exhibits high roughness, with the presence of a possible massif at the base of the southern escarpment, lacking volcanic characteristics and more resembling exhumed rocky caracteritic the Detachment-dominated terrains (Figs. 4.2 and 4.7).

On the other hand, the intersection region of the 11RNTD features volcanic cones spaced around a prominent linear topographic feature, which extends from the axial ridge and curves westward, ending in a basin located around latitude 12°9'N (Fig. 4.8b). The eastern portion of this area is marked by extensional basins and a prominent oblique topographic anomaly, situated around latitude 12°7'N, standing out from the surrounding

areas, with approximately 11 km in length. Overall, the extensional basins contrast with the western portion of the MeNTD, which presents a rougher and higher seafloor (Fig. 4.8).

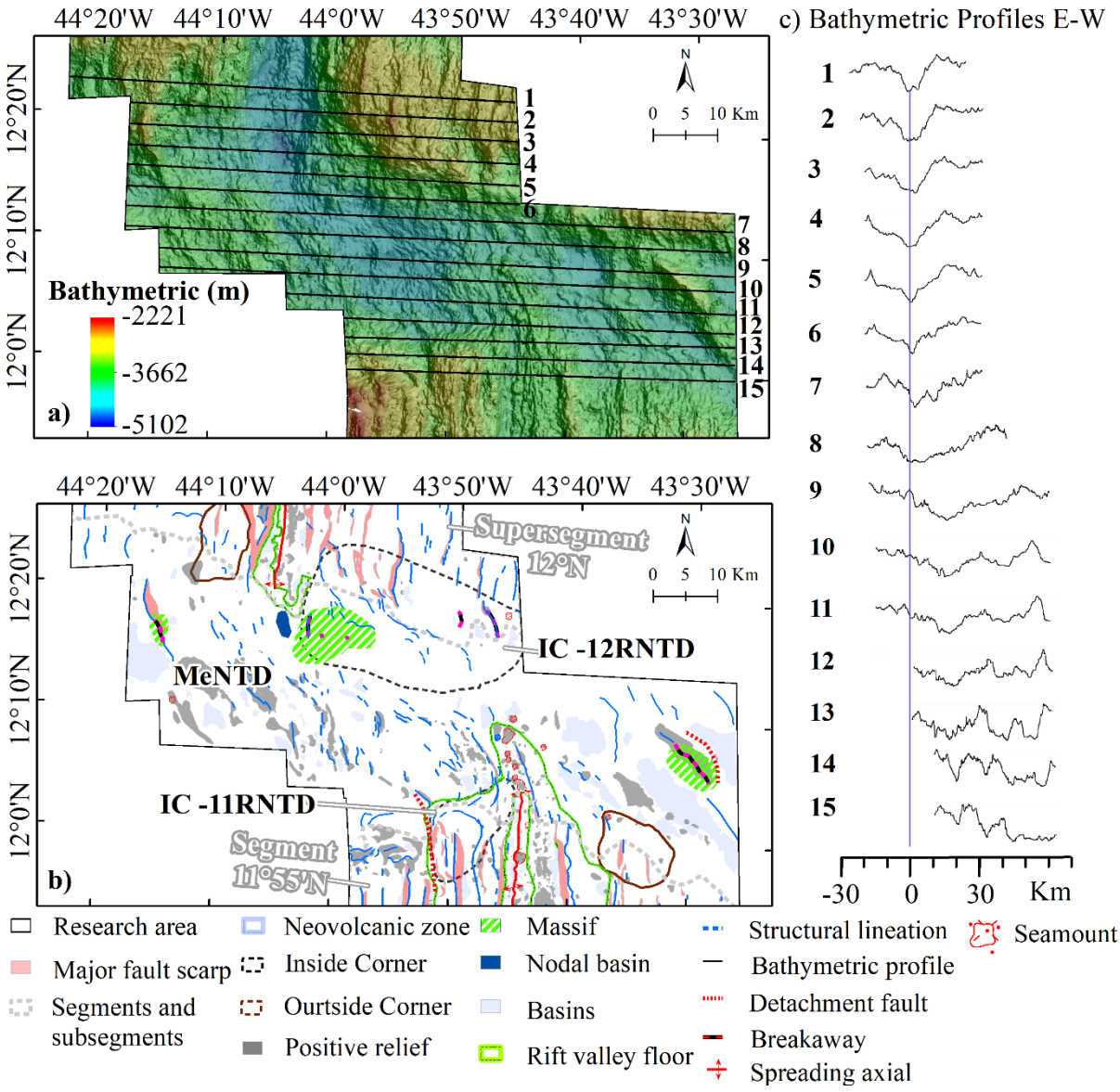

Figure 4.8 – (a) Bathymetric map with shaded relief underneath showing the location of topographic profiles, (b) Interpretation map of the MeNTD along the MAR, and (c) E-W oriented bathymetric profiles, with their locations indicated in (a). Blue lines on the profiles represent the 4,000 m depth contour. Abbreviations: MeNTD – Mercurius Non-Transform Discontinuity, 12RNTD – 12°N Supersegment - Mercurius Non-Transform Discontinuity, 11RNTD – 11°N Supersegment - Mercuius Non-Transform Discontinuity, and IC – Inside Corner.

4.5. Residual Mantle Bouguer Anomaly

The RMBA map shows maximum values of 25 mGal and minimum values of -25 mGal (Fig. 4.3b). In general, the lowest anomalies occur in the center and the eastern flank of the ridge supersegments, while the highest values are concentrated in the FZs, TFs, and NTDs.

The MTF and MFZ present moderate anomalies, ranging from 19 to -17 mGal, with the highest values located to the west of the spreading axis. In the MeNTD region, the values range from 13 to -15 mGal, being higher at the eastern and western extremities and lower along the rift valley axis.

The IC located at the 12RNTD and VTI intersections show abrupt transitions in RMBA values, with maxima reaching 19 mGal, particularly in the VTF.

The 12°N section reveals a heterogeneous distribution, ranging from -14 to -20 mGal. The lowest anomalies are located along the axis and eastern flank, while the values progressively increase toward the western flank. A notable rounded anomaly of approximately 7 mGal stands out southwest of the IC, near the MTF (An1 in Fig. 4.3b and profile A-A'). Another circular anomaly (An2 in Fig. 4.3b), with values close to 7 mGal, occurs to the west of the IC, at the northern boundary of the 12RNTD (Fig. 4.3d, profile B-B').

The 11°55'N segment exhibits the lowest gravity values, ranging from -1 to -22 mGal, with a low anomaly maximum on the western flank, approximately 8 km from the spreading axis (Fig. 4.3d, profile C-C'). The regions of MeNTD and 11NTD mark distinct boundaries, characterized by abrupt and well-defined gravity gradients.

In the 11°20'N subsegment, heterogeneity is observed, with the lowest values predominating in the center and eastern flank. These values gradually increase toward the south, where rounded anomalies with higher values (between 7 and 5 mGal) occur. An example is the An3 anomaly (Fig. 4.3, profile D-D').

5. Discussion

Overall, in our area, the ends of the supersegments have thinner crusts, while the central portion is thicker, with the 11°N supersegment, specifically the 11°45'N segment, having the thickest crust in the area. This correlates with two distinct types of terrains: a

volcanic terrain, indicative of melt-rich conditions in an older plate and lineated volcanic, and another detachment-dominated terrains, suggesting melt-poor or episodic conditions, the corrugated seafloor. This alternation between magmatic and tectonic phases, as discussed by (ESCARTÍN &CANNAT, 1999; HOWELL *et al*., 2019), suggests a variation in magmatic flux that contributes to the final configuration of crustal thickness. However, we observed that the crustal structure and the morpho-structural features at the RTIs and at RNTDs in our study area differ significantly. We therefore focus our study these areas, where the morphological and gravimetric features suggest contrasting tectonic processes.

The characteristics observed in the axial axis at the MRTI (Fig. 4.5) indicate a significant reduction in magmatic flux at its IC compared to the OC and the central segment of the ridge. This interpretation is based on the correlation between the reduced axial depth at the MRTI and the presence of nodal basins associated with spatially restricted detachment faults located at the IC of the MRTI (Figs. 4.4 and 4.5). These features reflect changes in tectonic regimes, where predominant extension along the axial axis is accompanied by shear stress near the MRTI, although the extensional component remains dominant. Nodal basins are documented as transition zones and areas of pressure relief between different faults, promoting structural accommodation in reduced magmatism environments. In these scenarios, tectonics play a predominant role, with detachment faults forming in response to lithospheric stress accumulation (CANN *et al*., 2015). This behavior is consistent with observations in other RTIs, such as those south of the Kane Fracture Zone (CANN *et al*., 2015; DANNOWSKI *et al*., 2018; KARSON & DICK, 1983) and the Fifteen-Twenty Fracture Zone (FUJIWARA *et al*., 2003; SMITH *et al*., 2008). These studies highlight the interaction between limited magmatism and extensional tectonics in the formation of detachment terrains (Fig. 4.9), reinforcing the idea that reduced magmatism is a determining factor in the morphology and evolution of these regions, characterized by detachment faults and elongated terrains. This region has gradually extended away from the FZs since its initiation and remains active today.

The works of BUCK (1988); TUCHOLKE *et al*. (1998) and TUCHOLKE *et al*. (1998) provide a solid theoretical foundation for understanding the formation of normal faults and their evolution into detachment faults. As newly formed oceanic crust moves away from the ridge axis, conductive cooling causes thermal contraction. This process is intensified along the cooled edges associated with TFs, accentuating crustal thinning in

these áreas (WILSON, 1965; SCLATER; FRANCBETEAU; FRANCHETEAU, 1970; COLLETTE, 1974; DAVIS; LISTER, 1974; SANDWELL, 1984). With stress accumulation, normal faults form, which, upon displacement, undergo flexural rotation, enabling mantle exhumation and the formation of megamullions (massifs) (MACLEOD *et al*., 2011). When these faults reach their maximum displacement, new faults form, initiating a continuous cycle of tectonic adjustment (TUCHOLKE *et al*. ; LIN; KLEINROCK, 1998). Recent studies GREVEMEYER *et al*. (2021); HOWELL *et al*. (2019); and MACLEOD *et al*. (2009) highlight that reduced magmatic supply prolongs the activity of detachment faults, allowing them to accommodate crustal extension for longer periods in a continuous cycle of formation, reactivation, and abandonment.

At the VRTI, the detachment-dominated terrains (Figs. 4.7 and 4.9) is more extensive and associated with a large massif, exhibiting characteristics markedly distinct from those observed at the MRTI. Gravity anomalies suggest the presence of a cooler lithosphere (Fig. 4.3), although the region shows a more prominent and magmatic axial ridge at the intersection, as well as volcanic structures located near the eastern flank of the massif. In contrast, at the MRTI, magmatism is intermittent and episodic, without significant massif exhumations or OCCs. This scenario underscores the relevance of magmatic availability, particularly in the exhumation of large massifs. The ZFV plays a critical role in conductive cooling, making the region more susceptible to faulting and contributing to instability in magmatic supply. The influence of the ZFV appears to extend up to approximately 40 km south of the 11°20’N segment, where depressions and detachment-dominated terrains were identified (Fig. 4.9) on both eastern and western flanks. This likely reduction in local magmatic input favored the development of more persistent and restricted faults, without massif exposure, similar to those observed at the MRTI, but not evolving into a NTD.

Another feature reinforcing the hypothesis of instability in magmatic flux is the morphological and gravimetric similarity between the IC and OC massifs at the VRTI. This similarity suggests the possible existence of a ridge jump in the intersection region, warranting further studies.

The 11RNTD stands out for intersecting the most magmatic supersegment of the ridge, specifically the 11°55’N segment. The robust magmatism in this segment, evidenced by a prominent axial ridge and larger volcanic cones, accommodates stress changes through a more persistent detachment fault, which spans the entire eastern flank

of the segment and moves a block of significant proportions. This scenario highlights the importance of magmatism in the tectonic sliding process associated with faults.

In RNTDs, deep basins predominate, and magmatic features are absent, indicating conditions of low magmatic supply with limited or nonexistent new oceanic crust formation. The obliquity observed in both the basins and the faults reflects changes in the stress field, where a shear component is introduced, but extension remains the predominant mechanism. At the IC of the 12RNTD, stress transfer is predominantly accommodated by an extensive detachment fault. The low magmatism favors the exhumation of deeper and altered rocks, culminating in the formation of a foothill massif. On the other hand, the 11NTD exhibits distinct characteristics, being narrower than the MeNTD and presenting less oblique oval basins, reflecting a shift in the tectonic and magmatic regime of the region.

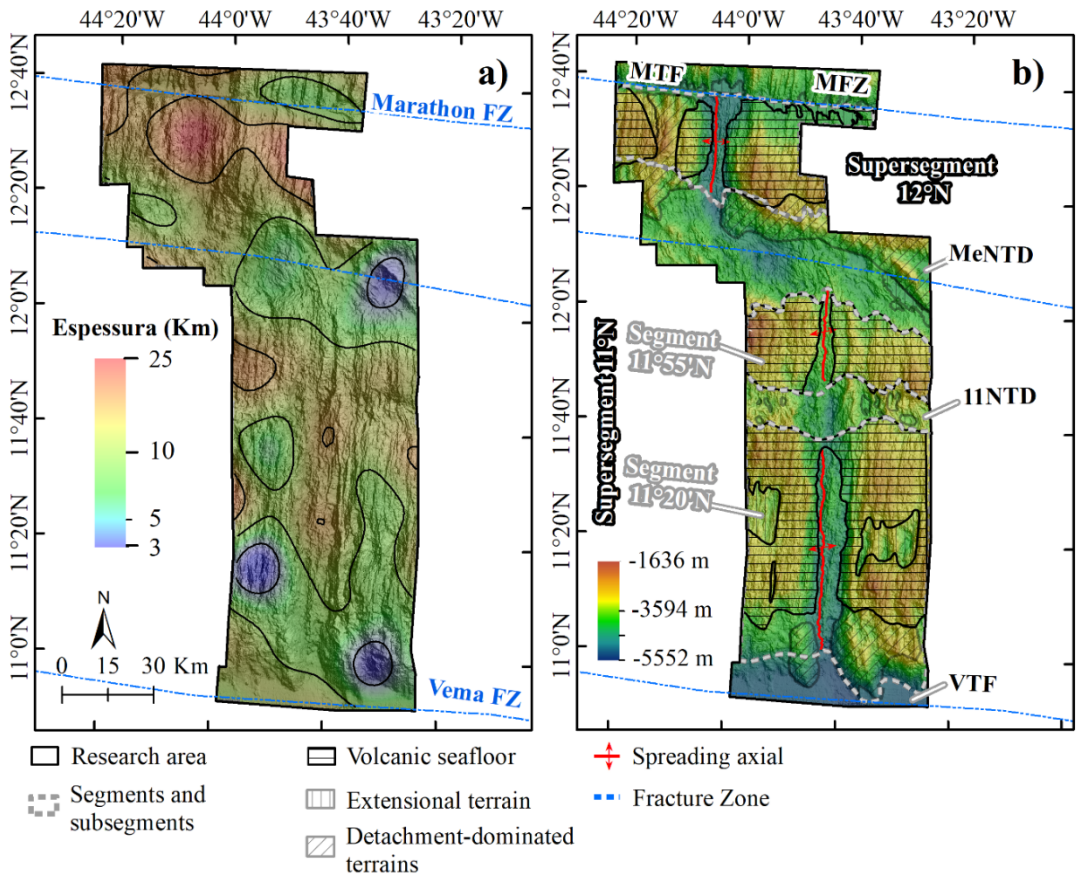

Figure 4.9 – Map the MAR between the Marathon and Vema transform faults. The specific study area is highlighted in the black polygon. a) Map of the gravitational effect of lithospheric cooling, calculated from a crustal age model, with shaded relief overlaid on all maps. b) Mapa bathymetric with division of supersegments and segments of the MAR axis (gray dotted line) and Type of seafloor" or "Seafloor type. Abbreviations: MTF – Marathon Transform Fault, MFZ – Marathon Fracture Zone, MeNTD – Mercurius Non-Transform Discontinuity, 11NTD – 11°N Supersegment Non-Transform Discontinuity, and VTF – Vema Transform Fault.

6. Conclusion

This study revealed an intrinsic relationship between the identified surface features and the internal processes of alternating tectonic and magmatic accommodation. How does the variation in crustal thickness and surface structures along the ridge axis, particularly in the 11°N and 12°N supersegments, relate to the rheology of the lithosphere and the behavior of magmatic flow? These variations occur in both transform and NTDs, influencing lateral changes in stress accumulation, the mechanical strength of the brittle lithosphere, and the fracture pattern.

The data indicate that the structural asymmetry observed in the 12ITR may be related to tectonic crustal thinning, primarily caused by the heterogeneity in magma supply beneath the ridge axis. This variation in magmatic supply promotes the formation of detachment faults, which accommodate a significant portion of plate extension.

The identified NTD is extensive and influences crustal rheology, possibly as a response to an axis adjustment due to a change in spreading direction, elevating the inside corner of the 12ºN supersegment at its intersection with the MeNTD. The 11ºN supersegment is the most magmatic and appears to be in the initial phase of detachment fault formation. In contrast, the VTF exhibits an intense and mature edge cooling effect, likely due to the reduction in magmatic flow, which favors hydrothermal circulation. The inside corner of the intersection presents long-lived detachment faults with a massif likely in the final stage of evolution.

The comparison between the 11ºN and 12ºN supersegments reveals the complexity of segmentation in mid-ocean ridges. To what extent is this segmentation controlled not only by variations in magmatic supply but also by the lithosphere's response to tectonic stresses and the dynamic behavior of mantle flow over time?

The observations of this study contribute to a deeper understanding of the tectonic and magmatic evolution of mid-ocean ridges, emphasizing the importance of integrated approaches to analyzing these complex structures. Further investigations, including geological sampling, seismicity analysis, and high-resolution geophysical studies, are necessary to validate the proposed hypotheses and refine the understanding of the formation mechanisms of these segments.

However, the causal relationship between magmatism and the development of detachment faults remains unclear. Additional studies that integrate geological sampling data, high-resolution seismic profiles, and detailed geophysical analyses are essential to

validate the hypotheses presented and refine the understanding of the mechanisms underlying the formation and evolution of these segments.

These contributions are fundamental for advancing the field of marine geology and enabling the sustainable exploration of resources in hydrothermal systems, providing a better understanding of the processes that shape slow-spreading ridges.

Declaration of Competing Interest

The authors declare that they have no known competing financial interests or personal relationships that could have appeared to influence the work reported in this paper.

Data availability

The foundational data supporting the conclusions of this study are readily accessible and can be found at: https://rigeo.sgb.gov.br/handle/doc/20437. In addition, other infringements will be made available upon request.

Acknowledgments

The authors express their gratitude to the Geological Survey of Brazil (SGB) for the indispensable technical, logistical, and financial support provided for the collection and processing of the data presented in this study. We extend special thanks to Dr. Oderson (SGB) for the insightful discussions that significantly contributed to the interpretation of the geophysical data. Finally, we extend our gratitude to the anonymous reviewers, whose suggestions and constructive critiques were essential for improving this manuscript, as well as to the editorial team of the journal for their care and attention dedicated to our work.

References

BEHN, M. D.; ITO, G. Magmatic and tectonic extension at mid-ocean ridges: 1. Controls on fault characteristics. Geochemistry, Geophysics, Geosystems, v. 9, n. 8, 2008.

BONATTI, E. Serpentinite protrusions in the oceanic crust. Earth and Planetary Science Letters, v. 32, n. 2, p. 107–113, out. 1976.

BONATTI, E. Vertical tectonism in oceanic fracture zones. Earth and Planetary Science Letters, v. 37, n. 3, p. 369–379, jan. 1978.

BONATTI, E. *et al*. Transform migration and vertical tectonics at the Romanche fracture zone, equatorial Atlantic. Journal of Geophysical Research: Solid Earth, v. 99, n. B11, p. 21779–21802, 10 nov. 1994.

BONATTI, E. *et al*. Mantle thermal pulses below the Mid-Atlantic Ridge and temporal variations in the formation of oceanic lithosphere. Nature, v. 423, n. 6939, p. 499–505, maio 2003.

BONATTI, E. *et al*. Flexural uplift of a lithospheric slab near the Vema transform (Central Atlantic): Timing and mechanisms. Earth and Planetary Science Letters, v. 240, n. 3–4, p. 642–655, 15 dez. 2005.

BONATTI, E.; SARTORI, R.; BOERSMA, A. Vertical crustal movements at the Vema Fracture Zone in the Atlantic: Evidence from dredged limestones. Tectonophysics, v. 91, n. 3–4, p. 213–232, jan. 1983.

BUCK, W. R. Flexural rotation of normal faults. Tectonics, v. 7, n. 5, p. 959–973, 26 out. 1988.

BUCK, W. R.; LAVIER, L. L.; POLIAKOV, A. N. B. B. Modes of faulting at mid-ocean ridges. Nature, v. 434, n. 7034, p. 719–723, 7 abr. 2005.

CALDER, B. R.; MAYER, L. A. Automatic processing of high-rate, high-density multibeam echosounder data. Geochemistry, Geophysics, Geosystems, v. 4, n. 6, jun. 2003.

CANALES, J. P. *et al*. Upper crustal structure and axial topography at intermediate spreading ridges: Seismic constraints from the southern Juan de Fuca Ridge. Journal of Geophysical Research: Solid Earth, v. 110, n. 12, p. 1–27, 2005.

CANNAT, M. *et al*. Modes of seafloor generation at a melt-poor ultraslow-spreading ridge. Geology, v. 34, n. 7, p. 605–608, jul. 2006.

CANN, J. R. *et al*. Tectonic evolution of 200 km of Mid-Atlantic Ridge over 10 million years: Interplay of volcanism and faulting. Geochemistry, Geophysics, Geosystems, v. 16, n. 7, p. 2303–2321, jul. 2015.

CARBOTTE, S. M.; MACDONALD, K. C. Comparison of seafloor tectonic fabric at intermediate, fast, and super fast spreading ridges: Influence of spreading rate, plate motions, and ridge segmentation on fault patterns. Journal of Geophysical Research: Solid Earth, v. 99, n. B7, p. 13609–13631, 10 jul. 1994.

CHAMOV, N. P.; SOKOLOV, S. YU.; MERENKOVA, S. I. Residual Sediments of the Vema Fracture Zone, Central Atlantic. Lithology and Mineral Resources, v. 55, n. 5, p. 338–344, 9 set. 2020.

CHEN, Y. J. Oceanic crustal thickness versus spreading rate. Geophysical Research Letters, v. 19, n. 8, p. 753–756, 1992.

CHEN, Y.; MORGAN, W. J. A nonlinear rheology model for mid-ocean ridge axis topography. Journal of Geophysical Research: Solid Earth, b. v. 95, n. B11, p. 17583–17604, 1990.

COLLETTE, B. J. Thermal contraction joints in a spreading seafloor as origin of fracture zones. Nature, v. 251, n. 5473, p. 299–300, set. 1974.

DANNOWSKI, A. *et al*. Enhanced Mantle Upwelling/Melting Caused Segment Propagation, Oceanic Core Complex Die Off, and the Death of a Transform Fault: The Mid-Atlantic Ridge at 21.5°N. Journal of Geophysical Research: Solid Earth, v. 123, n. 2, p. 941–956, 1 fev. 2018.

DAVIS, E. E.; LISTER, C. R. B. Fundamentals of ridge crest topography. Earth and Planetary Science Letters, v. 21, n. 4, p. 405–413, 1974.

DEMETS, C.; GORDON, R. G.; ARGUS, D. F. Geologically current plate motions. Geophysical Journal International, v. 181, n. 1, p. 1–80, 2010.

EITTREIM, S.; EWING, J. Vema fracture zone transform fault. Geology, v. 3, n. 10, p. 555, 1975.

ESCARTÍN, J. *et al*. Quantifying tectonic strain and magmatic accretion at a slow spreading ridge segment, Mid-Atlantic Ridge, 29°N. Journal of Geophysical Research: Solid Earth, v. 104, n. B5, p. 10421–10437, 10 maio 1999.

ESCARTÍN, J. *et al*. Central role of detachment faults in accretion of slow-spreading oceanic lithosphere. Nature, v. 455, n. 7214, p. 790–794, out. 2008.

ESCARTÍN, J. *et al*. Tectonic structure, evolution, and the nature of oceanic core complexes and their detachment fault zones (13°20′N and 13°30′N, Mid Atlantic Ridge). Geochemistry, Geophysics, Geosystems, v. 18, n. 4, p. 1451–1482, 8 abr. 2017.

ESCARTÍN, J.; CANNAT, M. Ultramafic exposures and the gravity signature of the lithosphere near the Fifteen-Twenty Fracture Zone (Mid-Atlantic Ridge, 14°–16.5°N). Earth and Planetary Science Letters, v. 171, n. 3, p. 411–424, set. 1999.

FABRETTI, P. *et al*. First results of cruise S19 (PRIMAR Project): petrological and structural investigations of the Vema Transverse Ridge (equatorial Atlantic)Russian Acad. Sci, Moscow Russia. Sergej Simonov-United Institutes of Geology, Geophysics and Mineralogy, Russian Acad. Sci. [s.l: s.n.].

FOX, P. J.; GRINDLAY, N. R.; MACDONALD, K. C. The Mid-atlantic Ridge (31°S–34°30′S): Temporal and spatial variations of accretionary processes. Marine Geophysical Researches, v. 13, n. 1, p. 1–20, fev. 1991.

FUJIWARA, T. *et al*. Crustal evolution of the mid-atlantic ridge near the fifteen-twenty fracture zone in the last 5 Ma. Geochemistry, Geophysics, Geosystems, v. 4, n. 3, mar. 2003.

GEBCO BATHYMETRIC COMPILATION GROUP 2022. The GEBCO_2022 Grid - a continuous terrain model of the global oceans and land.

GREVEMEYER, I. *et al*. Extensional tectonics and two-stage crustal accretion at oceanic transform faults. Nature, v. 591, n. 7850, p. 402–407, 18 mar. 2021.

HOWELL, S. M. *et al*. Magmatic and tectonic extension at the Chile Ridge: Evidence for mantle controls on ridge segmentation. Geochemistry, Geophysics, Geosystems, v. 17, n. 6, p. 2354–2373, 24 jun. 2016.

HOWELL, S. M. e*t al.* Seafloor expression of oceanic detachment faulting reflects gradients in mid-ocean ridge magma supply. Earth and Planetary Science Letters, v. 516, p. 176–189, jun. 2019.

IBGE. Manual Técnico de Pedologia 2a edição. [s.l: s.n.].

ITO, G.; BEHN, M. D. Magmatic and tectonic extension at mid-ocean ridges: 2. Origin of axial morphology. Geochemistry, Geophysics, Geosystems, v. 9, n. 9, p. 2008GC001970, 30 set. 2008.

KARSON, J. A.; DICK, H. J. B. Tectonics of ridge-transform intersections at the {Kane} fracture zone. Marine Geophysical Researches, v. 6, n. 1, p. 51–98, 1983.

LAGABRIELLE, Y. *et al*. Vema Fracture Zone (central Atlantic): Tectonic and magmatic evolution of the median ridge and the eastern ridge-Transform intersection domain. Journal of Geophysical Research: Solid Earth, v. 97, n. B12, p. 17331–17351, 10 nov. 1992.

LIGI, M. *et al*. Generation and evolution of the oceanic lithosphere in the North Atlantic. La Rivista del Nuovo Cimento, v. 45, n. 9, p. 587–659, 20 set. 2022.

LIN, J.; MORGAN, J. P. The spreading rate dependence of three-dimensional mid-ocean ridge gravity structure. Geophysical Research Letters, v. 19, n. 1, p. 13–16, 3 jan. 1992.

MACDONALD, K. C. *et al*. Volcanic growth faults and the origin of Pacific abyssal hills. Nature, v. 380, n. 6570, p. 125–129, 1996.

MACDONALD, K. C.; ATWATER, T. M. Evolution of rifted ocean ridges. Earth and Planetary Science Letters, v. 39, n. 3, p. 319–327, 1 maio 1978.

MACDONALD, KEN. C. Mid-ocean ridges: Fine scale tectonic, volcanic and hydrothermal processes within the plate boundary zone. Annual Review of Earth and Planetary Sciences, v. 10, p. 155, 1982.

MACLEOD, C. J. *et al*. Life cycle of oceanic core complexes. Earth and Planetary Science Letters, v. 287, n. 3–4, p. 333–344, 15 out. 2009.

MACLEOD, C. J. *et al*. Quantitative constraint on footwall rotations at the 1545N oceanic core complex, Mid-Atlantic Ridge: Implications for oceanic detachment fault processes. Geochemistry, Geophysics, Geosystems, v. 12, n. 5, p. 1–29, 2011.

MAIA, M. *et a*l. Building of the Amsterdam-Saint Paul plateau: A 10 Myr history of a ridge-hot spot interaction and variations in the strength of the hot spot source. Journal of Geophysical Research: Solid Earth, v. 116, set. 2011.

MAIA, M.; ARKANI-HAMED, J. The support mechanism of the young Foundation Seamounts inferred from bathymetry and gravity. Geophysical Journal International, v. 149, n. 1, p. 190–210, abr. 2002.

MORGAN, J. P. *et al*. The genesis of oceanic crust: Magma injection, hydrothermal circulation, and crustal flow. Journal of Geophysical Research: Solid Earth, a. v. 98, n. B4, p. 6283–6297, 10 abr. 1993.

MOTA, C. et al. Prospecção e exploração de sulfetos polimetálicos na cordilheira Mesoatlântica, oceano Atlântico Equatorial : relatório de etapa fase 1 : levantamento regional e caracterização batimétrica, geofísica e oceanográfica. [s.l: s.n.].

OLIVE, J.-A.; DUBLANCHET, P. Controls on the magmatic fraction of extension at mid-ocean ridges. Earth and Planetary Science Letters, v. 549, p. 116541, 2020.

OLIVE, J. A.; ESCARTÍN, J. Dependence of seismic coupling on normal fault style along the Northern Mid-Atlantic Ridge. Geochemistry, Geophysics, Geosystems, v. 17, n. 10, p. 4128–4152, 27 out. 2016.

PALMIOTTO, C. et al. Nonvolcanic tectonic islands in ancient and modern oceans. Geochemistry, Geophysics, Geosystems, v. 14, n. 10, p. 4698–4717, out. 2013.

PEIRCE, C. et al. Constraints on crustal structure of adjacent OCCs and segment boundaries at 13°N on the Mid-Atlantic Ridge. Geophysical Journal International, v. 217, n. 2, p. 988–1010, 1 maio 2019.

PEIRCE, C. et al. Magmatism versus serpentinization - Crustal structure along the 13°N segment at the Mid-Atlantic Ridge. Geophysical Journal International, v. 221, n. 2, p. 981–1001, 29 jan. 2020.

POCKALNY, R. A.; GENTE, P.; BUCK, R. Oceanic transverse ridges: A flexural response to fracture-zone-normal extension. Geology, v. 24, n. 1, p. 71–74, 1996.

SAMPAIO, T. V. M.; AUGUSTIN, C. H. R. R. Índice De Concentração Da Rugosidade: Uma Nova Proposta Metodológica Para O Mapeamento E Quantificação Da Dissecação Do Relevo Como Subsídio a Cartografia Geomorfológica. Revista Brasileira de Geomorfologia, v. 15, n. 1, 2014.

SANDWELL, D. T. Thermomechanical evolution of oceanic fracture zones. Journal of Geophysical Research: Solid Earth, v. 89, n. B13, p. 11401–11413, 1984.

SCLATER, J. G.; FRANCBETEAU, J.; FRANCHETEAU, J. The Implications of Terrestrial Heat Flow Observations on Current Tectonic and Geochemical Models of the Crust and Upper Mantle of the Earth. . 1970, p. 509–542.

SEMPÉRÉ, J.-C. et al. Segmentation and morphotectonic variations along a slow-spreading center: The Mid-Atlantic Ridge (24°00′ N– 30°40′ N). Marine Geophysical Researches, v. 15, n. 3, p. 153–200, ago. 1993.

SEVERINGHAUS, J. P.; MACDONALD, K. C. High inside corners at ridge-transform intersections. Marine Geophysical Researches, v. 9, n. 4, p. 353–367, 1988.

SHAW, W. J.; LIN, J. Models of ocean ridge lithospheric deformation: Dependence on crustal thickness, spreading rate, and segmentation. Journal of Geophysical Research: Solid Earth, v. 101, n. 8, p. 17977–17993, 10 ago. 1996.

SMALL, C. A global analysis of mid-ocean ridge axial topography. Geophysical Journal International, v. 116, n. 1, p. 64–84, jan. 1994.

SMITH, D. K. K. et al. Fault rotation and core complex formation: Significant processes in seafloor formation at slow-spreading mid-ocean ridges (Mid-Atlantic Ridge, 13°-15°N). Geochemistry, Geophysics, Geosystems, v. 9, n. 3, p. n/a-n/a, 5 mar. 2008.

TUCHOLKE, B. E.; LIN, J. A geological model for the structure of ridge segments in slow spreading ocean crust. Journal of Geophysical Research: Solid Earth, v. 99, 1994.

TUCHOLKE, B. E.; LIN, J.; KLEINROCK, M. C. Megamullions and mullion structure defining oceanic metamorphic core complexes on the {Mid}-{Atlantic} {Ridge}. Journal of Geophysical Research: Solid Earth, v. 103, n. B5, p. 9857–9866, 10 maio 1998.

VAN ANDEL, T. H.; VON HERZEN, R. P.; PHILLIPS, J. D. The Vema fracture zone and the tectonics of transverse shear zones in oceanic crustal plates. Marine Geophysical Researches, v. 1, n. 3, p. 261–283, set. 1971.

WILSON, J. A new class of faults and their bearing on continental drift. Nature, v. 207, n. 4995, p. 343–347, 1965.

YESSON, C. et al. The global distribution of seamounts based on 30 arc seconds bathymetry data. Deep-Sea Research Part I: Oceanographic Research Papers, v. 58, n. 4, p. 442–453, 2011.

YONGSHUN CHEN; MORGAN, W. J. Rift valley/no rift valley transition at mid-ocean ridges. Journal of Geophysical Research, v. 95, n. B11, 1990.

CAPÍTULO V
ARTIGO CIENTÍFICO

Non-transform discontinuities South of the Vema Transform fault: characteristics and tectonic implications

Este documento consiste em um artigo submetido à revista Brazilian Journal Geophysics.

Para garantir a conformidade com os critérios de originalidade informamos o código de submissão: GeoPhys-2025-0002.

5. ARTIGO CIENTÍFICO: NON-TRANSFORM DISCONTINUITIES SOUTH OF THE VEMA TRANSFORM FAULT: CHARACTERISTICS AND TECTONIC IMPLICATIONS

NON-TRANSFORM DISCONTINUITIES SOUTH OF THE VEMA TRANSFORM FAULT: CHARACTERISTICS AND TECTONIC IMPLICATIONS

ABSTRACT

This study examines the structures and morphologies of intersections in the Equatorial Mid-Atlantic Ridge (EMAR) between the Vema Transform Fault and 8°50'N using multibeam bathymetry, gravimetry, and seismicity data. Two supersegments and two non-transform discontinuities (NTDs), 10NTD and 9NTD, were characterized as tectonic transition zones influencing adjacent segment morphology and fault structures. The 9NTD exhibits intense seismic activity within the 9°10'N segment, with detachment faults and deep basins indicative of significant extensional accommodation, particularly in inside corners. Similar features, such as corrugated surfaces and ultramafic rock exhumation, are observed south of the Azores under low magma supply conditions. In contrast, the 10NTD shows greater symmetry, with lower-amplitude abyssal hills and shallower basins, likely influenced by variations in magma availability. Regions with low magma supply form asymmetric morphologies and oceanic core complexes (OCCs), while higher magma supply results in symmetrical features. NTDs also facilitate hydrothermal fluid circulation, promoting ultramafic rock serpentinization and hydrothermal vent formation. Inside corner uplift may reflect lithospheric flexure, as seen at the Vema Transform Fault. NTDs play a critical role in the tectonic and morphological evolution of adjacent supersegments by driving extensional faults, lithospheric thinning, and ultramafic massif exposure, shaping the region's tectonic configuration.

KEYWORDS: Oceanic ridges, second-order discontinuity and Vema Fracture Zone.

1. Introduction

Non-transform discontinuities (NTDs) are characterized by broad or gradual transitions between adjacent spreading segments where significant transform faulting is absent(GRÀCIA et al., 2000). They are often found at local highs along the axial depth profile, displaying oblique shearing and small-scale rift valley offsets, with offsets ranging from 15 to 30 km and age differences of 1 to 30 Ma (GRINDLAY et al., 1991; MACDONALD, 2001).

Although it is not entirely clear whether segmentation is primarily controlled by tectonic history or mantle upwelling, the presence of discontinuities is known to affect axial depth and ridge relief (SMALL, 1994). NTDs are commonly associated with off-axis discordances, possibly linked to variable conditions such as stress fields and rheology (SEMPÉRÉ et al., 1993). They are thought

to evolve from transform fault boundaries as a result of prolonged differential asymmetric spreading between adjacent ridge segments (GRINDLAY et al., 1991). GERYA (2012) suggests that the orthogonality observed between transform faults and spreading centers results from changes in thermal stresses within cooling oceanic plates. The orientation of these faults is influenced by plastic deformation at divergent plate margins, where differential cooling and spreading rates also impact the structural evolution of ridges.

Long-lived detachment faults, often associated with large-scale corrugations, are a common feature in slow-spreading ridges and low-magmatism environments, such as those associated with NDTs. Numerical models and lithospheric accretion studies suggest that these detachment faults form when magma supply is reduced, with approximately 30–50% of total extension being accommodated by magmatic accretion (LIGI et al., 2022). Oceanic Core Complexes (OCCs) mainly form under low-magmatism conditions, exhuming upper mantle and lower crustal rocks through detachment faults, forming corrugated terrains, and promoting hydrothermal activity (SMITH et al., 2008). In slow-spreading ridges, NTDs can act as conduits for hydrothermal fluid circulation and are associated with the exhumation of ultramafic rocks in OCCs (GRÀCIA et al., 2000).

Although comprehensive studies of NTDs have been conducted in other regions of the Mid-Atlantic Ridge, such as south of the Azores (38°N–34°N) and between 24°N and 30°N, where the exhumation of ultramafic rocks and occurrence of hydrothermal vents have been documented, there is a gap in understanding the behavior of NTDs in the EMAR, particularly south of the Vema Transform Fault. Most previous studies have focused on the relationship between transform faults and ridge segment formation. However, little is known about the impact of NTDs in regions with low magmatism, such as those between the Vema Fracture Zone and 8°50'N. Studies are lacking on how these NTDs influence morphology, fault distribution, and the formation of OCCs in slow-spreading ridge environments.

In studies south of the Azores (38°N–34°N) and between 24°N and 30°N (SPENCER et al., 1997) identified frequent occurrences of OCCs and hydrothermal vents associated with NTDs, suggesting that these discontinuities play a crucial role in the exhumation of deep rocks and the formation of asymmetric terrains in low-magmatism areas. It is understood that NTDs evolve from transform fault boundaries as a result of prolonged differential spreading between adjacent ridge segments.

This study, we explore how NTDs south of the Vema Transform Fault influence the morphology and tectonics of Mid-Atlantic Ridge segments in the equatorial region, specifically between the Vema Fracture Zone and 8°50'N (Figure 5.1). This research aims to understand the role of NTDs in shaping oceanic relief and exhuming deep-seated rocks. Our focus is on analyzing how

these structures affect segment morphology and promote the formation of OCC and asymmetric terrains in slow-spreading environments.

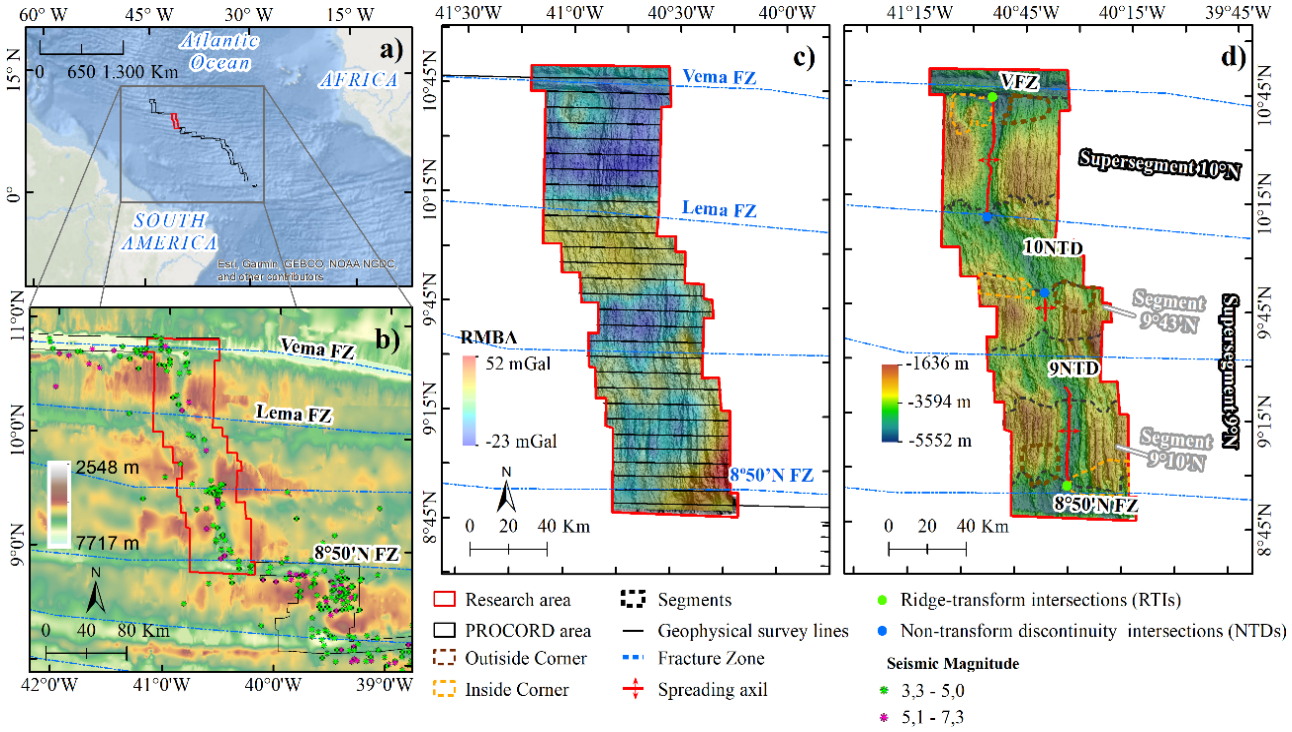

Figure 5.1 – Map showing the location of the study area. (a) Equatorial Atlantic Ocean and the Equatorial Margins of the South America and Africa, with the survey area of the Project for Prospecting and Exploration of Mineral Resources in the South Atlantic and International Equatorial region (PROCORD) outlined in a black polygon and specific study area highlighted in a red polygon. (b) Close-up of the specific study (red polygon) showing satellite altimetry, seismic and regional transform data sourced from (GEBCO BATHYMETRIC COMPILATION GROUP 2022, 2022). (c) Gravimetric map of the survey area (red polygon), with shaded relief of the specific study area, fracture zones (blue dotted lines), and geophysical survey lines (black lines) spaced 6-7 km apart, with lengths ranging from 40 to 60 km. d) Division of segments and subsegments of the EMAR axis on the bathymetric map with shaded relief, indicating inside and outside corners region. VFZ – Vema Fracture Zone, 10NTD – 10°N Non-Transform Discontinuity, 9NTD – 9°N Non-Transform Discontinuity, and 8°50'N FZ – 8°50'N Fracture Zone.

2. Study Area

This study is located in a portion of the Atlantic Ocean marked by a particularly unique tectonic history. The movement of the North American, South American, and African (NA-SA-AF) triple junction, combined with the opening of the Atlantic Ocean (e.g., (SMITH et al., 2008) and references therein), has shaped this region. Research suggests that the triple junction (NA-SA-AF) may have shifted from a position near 10°N to a region between 14°–16°N over a period between 72.5 and 35.5 Ma (SMITH et al. (2008) and references therein). Additionally, there are indications that movement may still be occurring between the NA and SA plates (SMITH et al., 2008).

2.1. Vema Fracture Zone

The Vema Fracture Zone is marked by a significant offset that displaces the Mid-Atlantic Ridge (MAR) by approximately 320 km in an E-W direction, between 10° and 11°N (BONATTI et al., 2005; FABRETTI et al., 1998; VAN ANDEL et al., 1971). The Vema transform valley exhibits strong asymmetry between its northern and southern portions (LIGI et al., 2022), with a width ranging from 15 to 22 km (Fabretti et al., 1997). The southern wall dips beneath the turbiditic deposits filling the valley, which reach a thickness of approximately 1 km (BONATTI et al., 2005; LIGI et al., 2022). These sediments, predominantly turbiditic in origin, were deposited during the Pleistocene as a result of complex sedimentary processes (e.g., LIGI et al., (2022), and references therein), with additional contributions of detrital and biogenic material from the valley walls (SKOLOTNEV et al., 2020).

Approximately 140 km west of the southern intersection of the transform with the ridge lies the Vema Transverse Ridge (VTR), a prominent topographic feature that runs parallel to the Vema Transform and rises more than 3 km above the predicted level of thermal contraction (BONATTI et al., 2005; LIGI et al., 2022).

Recent studies suggest that the VTR represents the exposed edge of a flexed and uplifted oceanic lithospheric plate, which at some point emerged above sea level. This area was subsequently eroded and covered by shallow-water carbonates, mainly during the Miocene and Pliocene, as it underwent subsidence (BONATTI et al., 2005; PALMIOTTO et al., 2013; LIGI et al., 2022). These carbonates overlie a sequence comprising peridotite (about 1 km thick), a variable-thickness gabbro unit, a well-developed sheeted dike complex, and an upper layer of massive basalts. Together, these units constitute the Vema Lithospheric Section (VLS). The VTR delineates the northern portion of the 10°N axial supersegment, also known as EMAR, which began developing approximately 40 million years ago(FABRETTI et al., 1998; LIGI et al., 2022). The eastern terminus of the active Vema Transform Fault is interpreted as being marked by a principal displacement zone (PDFZ), which represents the beginning of the EMAR segment (referred to in this work as the 10°N supersegment) (BONATTI et al., 1994; EITTREIM & EWING, 1975). In this segment, the crust maintained a constant thickness between 26 and 20 Ma, gradually increasing to the present day (LIGI et al., 2022). Crustal thickness oscillations with periods of 3 to 4 million years have been attributed to secondary mantle convection beneath the ridge (LIGI et al., 2022). This mantle, rich in H_2O and of low viscosity, is located beneath a residual mantle layer that is H_2O-poor and of high viscosity (BONATTI et al., 2003). Such a configuration may be related to changes in the geometry of plate boundaries, generating transpressional or transtensional regimes within the transform domain. This domain is covered by

sedimentary deposits composed of polymictic breccias, sandstones, and siltstones with basaltic, doleritic, and gabbroic clasts that underwent greenschist facies metamorphism before being disaggregated and deposited (LAGABRIELLE et al., 1992; LIGI et al., 2022).

Since approximately 16 million years ago, the degree of mantle melting beneath the Mid-Atlantic Ridge has increased, albeit with oscillations. Studies indicate that the asthenospheric mantle beneath the ridge, particularly near 11°N, exhibits a cooling gradient and/or fertility loss as it migrates southward from Iceland towards the equator. "Waves" of warm and fertile mantle, possibly originating from the Iceland and Azores plumes, have migrated southward, contributing to the increased melting observed in the region over the last 16 million years (BONATTI et al., 2003; LIGI et al., 2022).

Additionally, counterclockwise reorientations of the ridge axis and changes in the lithospheric spreading direction near the transform fault, combined with alterations in the position of the Euler rotation pole, have been identified. These changes, occurring in plates older than 10 million years, culminated in the flexure and uplift of a portion of the lithospheric plate.

2.1. Lema Fracture Zone

The Lema Fracture Zone delineates the southern boundary of the EMAR segment. According to (BONATTI et al., 2005), the Lema Fault Zone (Lema FZ) was reactivated due to the presence of a large, detachment-type normal fault located in the northern portion of this structure.

The southern edge of the flexed Vema plate intersects with the Lema escarpment, which is approximately 1 km high. This large detachment fault, associated with the reactivation of the Lema FZ, corresponds to an ancient transform offset of the Mid-Atlantic Ridge (MAR) axis. The Lema FZ functions as a decoupling structure, separating the flexed plate to the north from the "normal" lithosphere to the south. As a result, the inclined and flexed lithospheric plate extends approximately 300 km in an E-W direction and 80 km in a north-south direction.

3. Data and Methodology

3.1. Data Acquisition

As part of the PROCORD project, the Geological Survey of Brazil (SGB) conducted geophysical surveys in the EMAR, mapping an area of 13,550 km² between the Marathon and 18°50'N Fracture Zones. During these campaigns, bathymetric and gravimetric data were collected along acquisition profiles that traversed the ridge in an E-W direction, with spacings between 6 and 7 km and lengths ranging from 40 to 60 km. Additionally, regional satellite altimetry data, fracture zone traces, and seismicity information from the General Bathymetric Chart of the Oceans (GEBCO, 2022) were utilized (Figure 5.1).

3.1.1. Multibeam Bathymetry

Multibeam bathymetric data were collected using the Reson 7150-F dual-frequency echo sounder operating at 12 kHz. During acquisition, adjustments were made for positioning, offsets, tides, and sound velocity in water, utilizing continuous CTD/XBT profiles.

Processing was conducted using CARIS HIPS & SIPS software, where data were corrected for Total Propagated Uncertainty (TPU), extreme noise was removed, and edge artifacts were minimized. The final bathymetric surface was generated with a resolution of 100 m/pixel using the Combined Uncertainty and Bathymetry Estimator (CUBE) algorithm, which estimates multiple hypotheses for bathymetric values and their uncertainties, representing potential variations of the seafloor.

Derived sub-products from the bathymetric surface were generated in a GIS environment using ArcGIS's Spatial Analyst tool. A Bathymetric Contour Map was created with 250 m intervals, while a Slope Map was calculated in degrees and classified into intervals according to IBGE (2007): flat (0°-3°), gently undulating (3°-8°), undulating (8°-20°), strongly undulating (20°-45°), mountainous (45°-75°), and steep (>75°). The Rugosity Map was produced using the Rugosity Concentration Index (RCI) (SAMPAIO & AUGUSTIN, 2014), based on the maximum difference in the neighborhood of a pixel extracted from the digital terrain model, allowing relief compartmentalization, quantification, and identification of geological structures. The Aspect Map was generated to indicate the preferential direction of slopes, measured clockwise, with flat areas

assigned a value of -1. Additionally, a Backscatter Map was produced at a resolution of 50 m using the SIPS Backscatter algorithm in CARIS HIPS & SIPS software, with subsequent processing and refinement in ArcGIS. Finally, Bathymetric Profiles were extracted perpendicular and orthogonal to the ridge axis, spaced 1 km apart, providing detailed insights into the bathymetric relief. For a more detailed visualization of geological structures, hillshade was applied using illumination at 45° altitude and 315° azimuth, overlaid on all sub-products to enhance and emphasize morphotectonic features.

3.1.2. Gravity Field

For the gravimetric analysis, a regional grid was developed using free-air gravity anomaly data from the (GEBCO BATHYMETRIC COMPILATION GROUP 2022, 2022), integrated with satellite altimetry data, following the methodology described by MAIA & ARKANI-HAMED, 2002). This approach involves calculating the gravitational effect of a layer with constant thickness and laterally variable densities. The calculations were performed in the Fourier Transform domain, adopting average densities of 2800 kg/m³ for the oceanic crust, 3300 kg/m³ for MAIA & ARKANI-HAMED (2002) the upper mantle, and 1030 kg/m³ for seawater.

The Mantle Bouguer Anomaly (MBA) was calculated by removing the effects of topography and the theoretical crust-mantle interface (Moho), assuming an average crustal thickness of 6 km. The gravitational effect of the theoretical Moho was added to the topography effect to generate the model's gravitational effect, which was subsequently subtracted from the free-air anomalies, resulting in the MBA.

Lithospheric cooling was modeled using a half-space model dependent on lithospheric age, representing its thermal evolution. In this model, the lithosphere is considered to cool and gain higher density as it moves away from the mid-ocean ridge axis. Initially, the lithosphere's base was calculated, considering the density contrast between the asthenosphere and lithosphere of -60 kg/m³. The gravitational effect associated with this model was determined following MAIA et al. (2011). This effect was then subtracted from the MBA to obtain the Residual Mantle Bouguer Anomaly (RMBA).

The RMBA was inverted to interpret variations in crustal thickness relative to the assumed model of 6 km, considering a density contrast of 500 kg/m³. The total crustal thickness was determined by adding 6 km to the variations resulting from the inversion, according to the method of CHEN (1992).

The RMBA provides insights into crustal thickness variations and enables detailed interpretations of tectonic structures and crustal formation processes. Low RMBA values indicate a thicker crust (up to 8 km) in a constant density model or the presence of less dense materials in the crust or upper mantle (CANNAT et al., 2006). Conversely, high RMBA values are associated with thinner crusts (as thin as 0.5 km) and denser materials in the crust or upper mantle.

3.1.3. Seismicity

The seismicity data used in this study were obtained from the General Bathymetric Chart of the Oceans (GEBCO BATHYMETRIC COMPILATION GROUP 2022, 2022). The analysis covered a total of 72 seismic events recorded in the study area, with magnitudes ranging from 3.4 to 6.6.

4. Results

The study focused on the region between the active Vema transform fault and 8°48’N, which was divided into two supersegments, labeled 10ºN and 9°N (Figure 5.1).

4.1. Seismicity

The seismicity data reveal a total of 72 seismic events, with magnitudes ranging from 3.4 to 6.6. Most of these events are primarily concentrated along the rift valley floor and the inside corners of the segment-transform intersections (Figure 5.1).

In the 10°N supersegment, seismicity with magnitudes of up to 5.1 is recorded both on the rift valley floor and at the inside corner of the intersection with the transform fault and non-transform discontinuity, with the latter showing the highest values (> 5.1) (Figure 5.1 and 5.2a). The most intense seismic events (magnitude > 5) are observed at the end of the spreading axis of both supersegments. In contrast, three seismic events with magnitudes lower than 5 occur at the center of the non-transform discontinuity, in the central basin.

The 9°43'N segment shows no seismic activity. In contrast, the 9NTD represents the most seismically active area in the entire study region, with the highest concentration of earthquakes (24

events) exhibiting magnitudes ranging from 3.4 to 5.2, mainly concentrated in the eastern portion of the discontinuity floor, near the detachment faults.

Seismic data in the 9°10'N segment reveal a significant concentration of events on the eastern flank, with magnitudes ranging from 3.1 to 7.3. Most of these events occur mainly at the base of the eastern flank. In the 8°50'N Transform Zone, seismic activity is also concentrated, especially in the transform valley on the eastern portion.

4.2. Residual Mantle Bouguer Anomaly

The Residual Mantle Bouguer Anomaly (RMBA) reflects the morphotectonic compartmentalization of the studied area, with values ranging approximately from 52 to -23 mGal. This map highlights variations in the density and depth of mantle structures beneath the crust, indicating heterogeneity in the lithospheric mantle.

Fracture zones and inside corners (ICs) of ridge-transform intersections (RTIs) exhibit elevated RMBA values with a more homogeneous distribution. In contrast, NTD show slightly lower values, especially in the central portion of the 10NTD.

In the 10ºN and 9º43'N segments, a heterogeneous distribution of RMBA values is observed, with the lowest values primarily concentrated along the axial ridge. The 9º43'N segment stands out for presenting the most negative values, including a small negative anomaly (An1) in its outer corner, already under the influence of the 9NTD.

The 9ºN segment exhibits negative values that tend to concentrate over the axis and the eastern flank, gradually transitioning to more positive values towards the easternmost part of the area, reaching maximum values over the inner corner of the segment.

4.3. Vema Fracture Zone and supersegment 10°N

The northern segment, with a 57 km-long axis at 10°N latitude, extends from the VFZ in the north to approximately 10°12'N in the south. The terrain in this segment is predominantly composed of volcanic crust, with depths ranging from 2,000 m to 5,500 m, and ridges oriented parallel to the axial axis. The greatest depths occur on the rift valley floor, where a maximum depth of approximately 5,500 m is recorded at the intersection with the VT, over the nodal basin BN1 (Figure 5.2). This basin

highlights the contrast between the topography of the inside corner (IC) and outside corner (OC) at the intersection of the segment with the Vema Transform.

In contrast, the shallowest regions correspond to the northwestern and southeastern ends of the segment, reaching a maximum on the southeastern flank, around 2,000 m. Overall, the OC is shallower compared to the flank that constitutes the IC (Figure 5.2, Profiles EE' and GG'). However, the inside corner region at the intersection between the 10°N ridge segment and the Vema transform fault (ITR 10°20'N) presents a strip of anomalous crust, approximately 309 km² in area, running parallel to the transform fault and characterized by irregular topography.

The IC is bounded to the west b a fault scarp (Bf_1) approximately 13 km in length, located about 20 km from the xial axis and gently inclined toward the axis at an angle of less than 30°. Along the scarp, "raft"-like reliefs form small steps, while a basin (BN_1) of 33 km² separates this fault from another breakaway fault (Bf_2), which has a slightly lower angle. In the center of BN_1, there is a prominent rougher surface relief (R_1), with depths ranging from 3,200 to 4,200 m, rising less than 1 km above the seafloor (Figure 5.2, Profile EE'), similar to the pattern observed on the rift valley floor.

Bf2 is discontinuous, approximately 6 km in length, and marks a concave dome-shaped topography covering an area of about 50 km², located 10 km from the axial axis. On the dome's surface, a small corrugated area of 15 km² is observed, oriented perpendicular to the axial axis, while on the west-facing flank, a surface inclines in the opposite direction to the axial axis. The dome-shaped structure, near the spreading axis, is surrounded by regions with volcanic characteristics associated with R1 relief (Figure 5.2, Profiles EE' and BB').

The rift valley floor is bounded by normal fault scarps facing the spreading axis. The estimated axial axis, with a predominant N-S orientation, consists of prominent and rugged reliefs, extending approximately 54 km with depths ranging from 3,800 to 4,400 m, forming the neovolcanic zone, which is quite similar to the roughness of R1 relief. To the north, the elevated relief of the axial axis gradually transitions into a depression (BN2) with depths between 3,200 and 5,480 m; to the south, the relief transitions to NW-SE-oriented structures surrounded by basins with depths ranging from 3,700 to 4,800 m (Figure 5.2 and 3). A "hummock"-like structure, approximately 24 km² in size, is observed south of BN2, advancing toward the spreading axis (Figure 5.2).

The inactive portion of the VFZ comprises large basins interrupted by extensions of abyssal hills that extend to the plate boundary, where they appear to be cut by a prominent relief in the VFZ valley floor. These structures extend up to about 29 km from the axial axis, defining the OC region. In the older portion of the plate, small volcanic cones are observed. Beyond the OC boundary, the

abyssal hills curve westward, forming segments commonly described as "J-shaped," often associated with volcanic features (Figure 5.2).

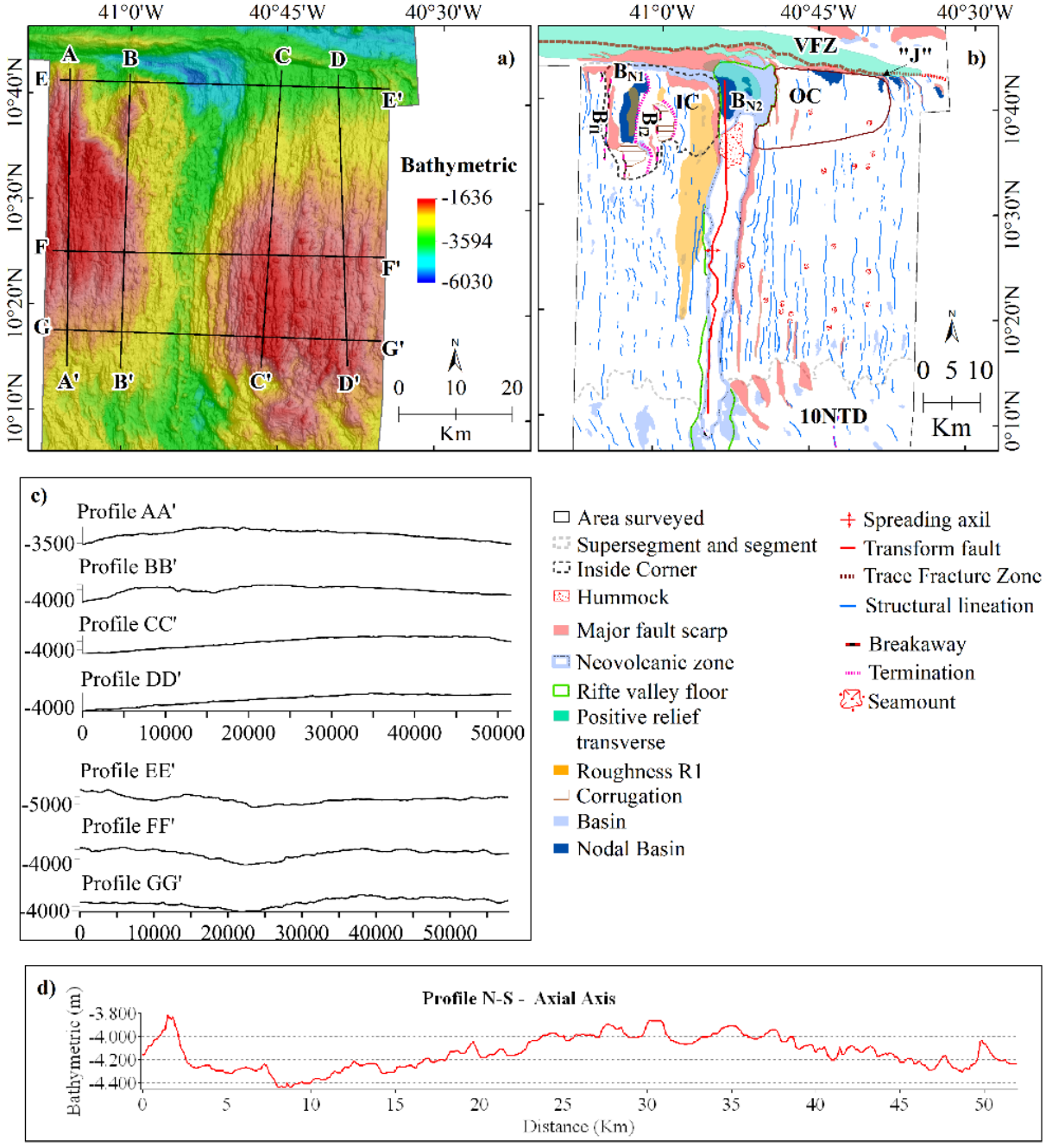

Figure 5.2 – Significant Structures Observed in the 10°N Segment with Bathymetric Profiles. (a) Shaded bathymetric map of the 10°N segment showing the locations of the topographic profiles. (b) Detailed map of the structures in the 10°N segment, including VFZ – Vema Fracture Zone, IC – Inside Corner, OC – Outside Corner, Bf1 and Bf2 – Breakaway Faults, BN1 and BN2 –Basins. (c) Bathymetric profiles AA', BB', CC', and DD' oriented N-S, and EE', FF', GG' oriented E-W, with locations shown in (a). (d) Bathymetric profile along the axial axis, represented by the red line, with location indicated in (a).

South of the 10°N segment, the eastern flank of the segment exhibits higher topography, with maximum depths of 2,000 m, accentuating the asymmetry observed at the segment's end, with this southern portion being the most prominent. The ridges in this segment are more continuous compared to the western flank, and scattered, isolated volcanoes are primarily observed at the segment's edges (Figure 5.2).

4.4. 10NTD

At approximately latitude 10°12'N, a second-order discontinuity, referred to as 10NTD, is observed. This discontinuity is characterized by an interruption in the axial ridge of the 10°N segment and a notable shift in the pattern of faults and basins, which adopt a sigmoidal shape predominantly oriented in a NW-SE direction. In this area, basins reach depths between 3,700 and 4,700 m, suggesting a lateral offset of the axial ridge by approximately 30 km. However, there is no clearly defined transform fault; instead, the region exhibits only discontinuous shear faults and small structures resembling hummocks (Figure 5.2). Additionally, two prominent massifs (M_1 and M_2), shallow and subequant, form discrete bathymetric highs isolated from the ridge flanks, identified at the base of the eastern flank of the 10°N segment. Generally, and also in reference to other areas, these types of structures will be referred to simply as 'massifs' (Figure 5.3).

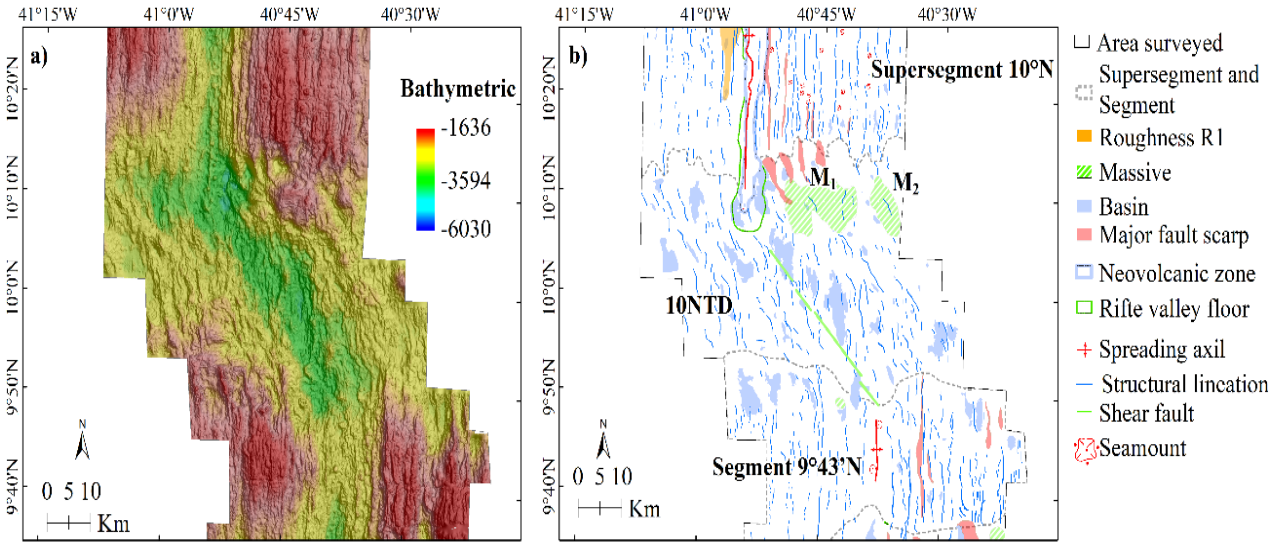

Figure 5.3 – Significant structures observed of the non-transform discontinuity 10°N. (a) Shaded bathymetric map of the 10°N non-transform discontinuity. (b) Detailed map of the structures in the 10°N non-transform discontinuity. 10NTD – 10°N Non-transform Discontinuity.

4.5. Segment 9°43'N

The 9°43'N ridge segment is located between two non-transform discontinuities (10NTD and 9NTD) and features an elevated, poorly defined axial crest, estimated to extend approximately 12 km. Rift valley floor depths within this segment range from 3,319 to 3,934 m. Its flanks are composed of relatively narrow and discontinuous ridges, displaying pronounced asymmetry. This asymmetry is highlighted by the presence of detachment faults on the eastern flank, approximately 25 km away from the spreading axis (Figure 5.4). At the intersection of this segment with the 10NTD, detachment

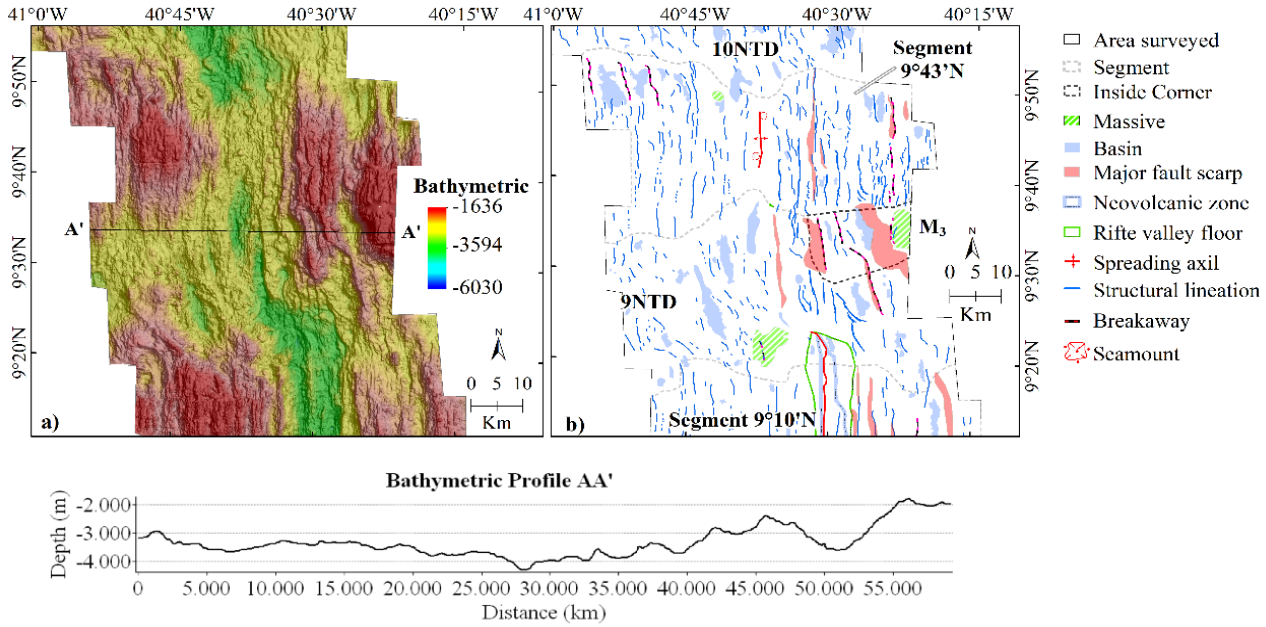

faults are observed with a spacing of less than 7 km, separated by basins (Figure 5.4).

Figure 5.4 – Significant structures observed of the 9NTD and segment 9°43'N. (a) Shaded bathymetric map of the 9NTD and segment 9°43'N showing the location of topographic profiles oriented AA'. (b) Detailed map of the structures on the 9NTD and segment 9°43'N. 10NTD – Discontinuity Non-transform 10°N.

4.6. 9NTD

The 9NTD is a small discontinuity characterized by a rugged and irregular seafloor, beginning around latitude 9°36'N. In this region, a shift is observed in the orientation of faults and the arrangement of basins, which adopt a predominant NW-SE orientation. At the inner corner of the 9°43'N segment with the 9NTD, there are detachment faults accompanied by longitudinal basins at the base (Figure 5.5) and the presence of a massif (M1) in the older portion. In the inner corner of the

9°10’N segment, another massif (M2) is identified, extending toward the center of the discontinuity (Figure 5.5).

4.7. Segment 9°10’N and 8°50’N FZ

In the 9°10’N segment, the abyssal hills exhibit low amplitudes and reduced spacing between crests, especially on the eastern flank, where broader linear basins are observed. Axial depths range from 3,900 to 4,800 m, interrupted to the south by a deep nodal basin located in the valley of the 8°50’N Fracture Zone, with depths varying between 5,000 and 6,000 m. The 8°50’N Fracture Zone is characterized by a narrow area composed of deep basins, interrupted to the south by an elevation with steep fault scarps reaching altitudes of up to 2 km.

The intersection between the axis of the 9°10’N segment and the 8°50’N is marked by a complex set of faults, including large scarps accompanied by basins with gentle dips facing opposite the axial direction. We have delineated breakaway areas and identified roughness, suggesting the presence of possibly altered deeper rocks.

The western portion of the discontinuity presents a deep basin with structures that appear to be extensions of the abyssal hills from segments adjacent to the 9NTD, although they suggest signatures of exhumed rocks (Figure 5).

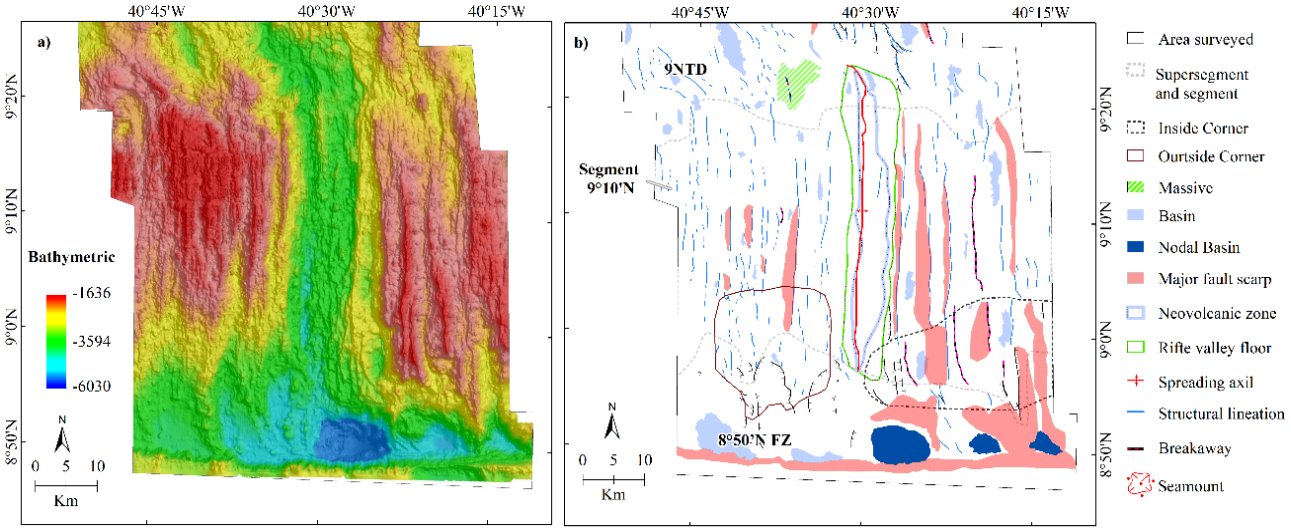

Figure 5.5 – Structures observed of the 8°50’N. (a) Shaded bathymetric map of the segment 8°50’N showing the location of topographic profiles oriented AA’. (b) Detailed map of the structures on the segment 8°50’N. 10NTD – Discontinuity Non-transform 10°N.

5. Discussion

The comparative analysis between the non-transform discontinuities 9NTD and 10NTD and their influence on the morphology of adjacent segments demonstrates that NTDs act as tectonic transition zones, enabling variations in relief and fault structures. The 9NTD delimits an area of intense seismic activity within the 9°10'N segment, with detachment faults and deep basins indicating significant extensional accommodation, particularly at the inside corner. Similar patterns were observed by CANNAT et al. (1999) in NTDs south of the Azores, where corrugated structures and exhumation surfaces were associated with low magma supply, which we believe is occurring in this segment.

In contrast, the 10NTD exhibits greater symmetry compared to the 9NTD, with abyssal hills of lower amplitudes and shallower basins. These differences may be related to variations in magma availability. Reduced magma supply tends to favor the formation of OCCs and asymmetric reliefs. OLIVE & ESCARTÍN (2016) support this hypothesis by suggesting that detachment faults prevail in regions with low magma supply, forming asymmetric morphologies, whereas areas with higher magma supply tend to develop more symmetric morphologies and regular abyssal hills.

Such regions may also enhance the alteration of these rocks, particularly serpentinization, through hydrothermal processes in NTDs, as these structures can facilitate hydrothermal fluid circulation in low-magma melting environments. This increases the likelihood that the studied area may be more favorable for the occurrence of hydrothermal vents, especially in regions where massifs have been identified, which are potentially exhumed ultramafic rocks.

The uplift observed in the inside corners of the segments may be associated with the flexural uplift of the lithosphere, as documented in studies on flexural uplift near the Vema Transform (BONATTI et al., 2005), where the occurrence of detachment faults is more active.

6. Conclusion

The analyzed exhibit tectonic and morphological characteristics that significantly influence the structural evolution of adjacent segments. Short, localized strike-slip faults with a predominant NW-SE orientation frequently develop within these discontinuities, resulting in the deformation and displacement of ultramafic massifs originally formed at the spreading axis.

Near the terminations of segments adjacent to NTDs, a reduction in magmatic structures is observed, indicating that these segments do not propagate into the discontinuities. This configuration, associated with oblique extension and lithospheric thinning within the NTDs, as evidenced by the mantle residual Bouguer anomaly pattern, appears to favor the formation of ultramafic massifs. For instance, the reduced size of the M5 massif may be explained by the higher magmatic activity of the 9°43'N axial segment, which is characterized by thicker crust.

The identified massifs, possibly originating at the spreading axis, show evidence of faulting and displacement away from the axis, suggesting that their evolution is linked to the development of localized strike-slip faults within the NTDs. Additionally, the uplift of these massifs can be attributed to the inside-corner mechanism, as observed at ridge-transform intersections. However, the evolution of these massifs seems to be closely tied to the dynamics of the discontinuities.

Previous studies confirm the association between ultramafic massifs and regions of maximum tectonic extension, such as inside corners near ridge-transform intersections (KARSON et al., 1987; TUCHOLKE; LIN, 1994), rift valley walls (CANNAT & CASEY, 1995), and off-axis oblique domains (CANNAT & CASEY, 1995). These massifs are often exposed in regions of low magmatic supply, as observed in other NTDs along the Mid-Atlantic Ridge.

Oblique extension within NTDs and the resulting lithospheric thinning facilitate the exposure of mantle-derived serpentinites and lower crustal rocks. Therefore, the formation and location of ultramafic massifs are directly associated with the evolution of the discontinuities, which act as transition zones between adjacent spreading centers, influencing regional tectonics and morphology.

ACKNOWLEDGMENTS

The authors express their gratitude to the Geological Survey of Brazil (SGB) for the crucial technical, logistical, and financial support that made it possible to collect and process the data presented in this work. Additionally, we extend our thanks to the anonymous reviewers, whose valuable suggestions and observations had a significant impact on improving this study, as well as to the journal's editorial team for their dedication and care throughout the review process.

REFERÊNCIAS

BEHN, M. D.; ITO, G. Magmatic and tectonic extension at mid-ocean ridges: 1. Controls on fault characteristics. *Geochemistry, Geophysics, Geosystems*, v. 9, n. 8, 2008.

BEHN, M. D.; LIN, J.; ZUBER, M. T. Mechanisms of normal fault development at mid-ocean ridges. *Journal of Geophysical Research: Solid Earth*, v. 107, n. B4, p. EPM 7--1--EPM 7--17, abr. 2002. . Acesso em: 16 jul. 2022.

BENEDIKTSDÓTTIR, Á. et al. Detailed tectonic evolution of the Reykjanes Ridge during the past 15 Ma. *Geochemistry, Geophysics, Geosystems*, v. 13, n. 2, p. 1–27, 2012.

BLACKMAN, D. K. et al. Origin of extensional core complexes: Evidence from the Mid-Atlantic Ridge at Atlantis fracture zone. *Journal of Geophysical Research: Solid Earth*, v. 103, n. 9, p. 21315–21333, 10 set. 1998. Disponível em: <https://onlinelibrary.wiley.com/doi/full/10.1029/98JB01756>. Acesso em: 16 jul. 2022.

BONATTI, E. Serpentinite protrusions in the oceanic crust. *Earth and Planetary Science Letters*, v. 32, n. 2, p. 107–113, out. 1976. Disponível em: <https://linkinghub.elsevier.com/retrieve/pii/0012821X76900480>.

BONATTI, E. Vertical tectonism in oceanic fracture zones. *Earth and Planetary Science Letters*, v. 37, n. 3, p. 369–379, jan. 1978. Disponível em: <https://linkinghub.elsevier.com/retrieve/pii/0012821X78900523>. Acesso em: 27 fev. 2024.

BONATTI, E. et al. Transform migration and vertical tectonics at the Romanche fracture zone, equatorial Atlantic. *Journal of Geophysical Research: Solid Earth*, v. 99, n. B11, p. 21779–21802, 10 nov. 1994. Disponível em: <https://agupubs.onlinelibrary.wiley.com/doi/10.1029/94JB01178>. Acesso em: 6 set. 2024.

BONATTI, E. et al. *Lower Cretaceous deposits trapped near the equatorial Mid-Atlantic RidgeNature*, 1996. .

BONATTI, E. et al. Mantle thermal pulses below the Mid-Atlantic Ridge and temporal variations in the formation of oceanic lithosphere. *Nature*, v. 423, n. 6939, p. 499–505, maio 2003. Disponível em: <www.nature.com/nature>.

BONATTI, E. et al. Flexural uplift of a lithospheric slab near the Vema transform (Central Atlantic): Timing and mechanisms. *Earth and Planetary Science Letters*, v. 240, n. 3–4, p. 642–655, 15 dez. 2005. Disponível em: <https://linkinghub.elsevier.com/retrieve/pii/S0012821X05006874>. Acesso em: 25 nov. 2024.

BONATTI, E.; SARTORI, R.; BOERSMA, A. Vertical crustal movements at the Vema Fracture Zone in the Atlantic: Evidence from dredged limestones. *Tectonophysics*, v. 91, n. 3–4, p. 213–232, jan. 1983. Disponível em: <https://linkinghub.elsevier.com/retrieve/pii/0040195183900422>. Acesso em: 30 ago. 2024.

BRASIL, M. do. *Diretoria de Hidrografia e NavegaçãoLimites Marítimos*, 2024. . Disponível em: <https://www.marinha.mil.br/dhn/?q=node/169.>. Acesso em: 9 dez. 2024.

BUCK, W. R. Flexural rotation of normal faults. *Tectonics*, v. 7, n. 5, p. 959–973, 26 out. 1988. Disponível em: <https://agupubs.onlinelibrary.wiley.com/doi/10.1029/TC007i005p00959>.

BUCK, W. R. et al. *Faulting and magmatism at mid-ocean ridges*. [s.l.] American Geophysical Union, 1998. v. 106

BUCK, W. R.; LAVIER, L. L.; POLIAKOV, A. N. B. B. Modes of faulting at mid-ocean ridges. *Nature*, v. 434, n. 7034, p. 719–723, 7 abr. 2005. Disponível em: <https://www.nature.com/articles/nature03358>.

CALDER, B. R.; MAYER, L. A. Automatic processing of high-rate, high-density multibeam echosounder data. *Geochemistry, Geophysics, Geosystems*, v. 4, n. 6, jun. 2003.

CANALES, J. P. et al. Upper crustal structure and axial topography at intermediate spreading ridges: Seismic constraints from the southern Juan de Fuca Ridge. *Journal of Geophysical Research: Solid Earth*, v. 110, n. 12, p. 1–27, 2005.

CANNAT, M. et al. Mid-Atlantic Ridge–Azores hotspot interactions: along-axis migration of a hotspot-derived event of enhanced magmatism 10 to 4 Ma ago. *Earth and Planetary Science Letters*, v. 173, n. 3, p. 257–269, nov. 1999. Disponível em: <https://linkinghub.elsevier.com/retrieve/pii/S0012821X99002344>.

CANNAT, M. et al. Modes of seafloor generation at a melt-poor ultraslow-spreading ridge. *Geology*, v. 34, n. 7, p. 605–608, jul. 2006.

CANNAT, M.; CASEY, J. F. An Ultramafic Lift at the Mid-Atlantic Ridge: Successive Stages of Magmatism in Serpentinized Peridotites from the 15°N Region. Em: [s.l: s.n.]p. 5–34.

Cannet al - 1997 - Corrugated slip surfaces formed at ridge-transform intersections on the Mid-Atlantic Ridge. [s.d.]

CANN, J. R. et al. Tectonic evolution of 200 km of Mid-Atlantic Ridge over 10 million years: Interplay of volcanism and faulting. *Geochemistry, Geophysics, Geosystems*, v. 16, n. 7, p. 2303–2321, jul. 2015. Disponível em: <http://doi.wiley.com/10.1002/2015GC005797>.

CARBOTTE, S. M.; MACDONALD, K. C. Comparison of seafloor tectonic fabric at intermediate, fast, and super fast spreading ridges: Influence of spreading rate, plate motions, and ridge segmentation on fault patterns. *Journal of Geophysical Research: Solid Earth*, v. 99, n. B7, p. 13609–13631, 10 jul. 1994. Disponível em: <https://agupubs.onlinelibrary.wiley.com/doi/10.1029/93JB02971>. Acesso em: 7 maio. 2024.

CHAMOV, N. P.; SOKOLOV, S. Yu.; MERENKOVA, S. I. Residual Sediments of the Vema Fracture Zone, Central Atlantic. *Lithology and Mineral Resources*, v. 55, n. 5, p. 338–344, 9 set. 2020. Disponível em: <https://link.springer.com/10.1134/S0024490220050028>. Acesso em: 31 ago. 2024.

CHEN, Y. J. Oceanic crustal thickness versus spreading rate. *Geophysical Research Letters*, v. 19, n. 8, p. 753–756, 1992. Disponível em: <https://agupubs.onlinelibrary.wiley.com/doi/10.1029/92GL00161>. Acesso em: 8 jun. 2024.

CHEN, Y.; MORGAN, W. J. A nonlinear rheology model for mid-ocean ridge axis topography. *Journal of Geophysical Research: Solid Earth*, b. v. 95, n. B11, p. 17583–17604, 1990. Disponível em: <https://agupubs.onlinelibrary.wiley.com/doi/10.1029/JB095iB11p17583>. Acesso em: 7 jun. 2024.

COLLETTE, B. J. Thermal contraction joints in a spreading seafloor as origin of fracture zones. *Nature*, v. 251, n. 5473, p. 299–300, set. 1974. Disponível em: <https://www.nature.com/articles/251299a0>.

DANNOWSKI, A. et al. Enhanced Mantle Upwelling/Melting Caused Segment Propagation, Oceanic Core Complex Die Off, and the Death of a Transform Fault: The Mid-Atlantic Ridge at 21.5°N. *Journal of Geophysical Research: Solid Earth*, v. 123, n. 2, p. 941–956, 1 fev. 2018.

DAVIS, E. E.; LISTER, C. R. B. Fundamentals of ridge crest topography. *Earth and Planetary Science Letters*, v. 21, n. 4, p. 405–413, 1974. Disponível em: <https://linkinghub.elsevier.com/retrieve/pii/0012821X74901800>. Acesso em: 15 maio. 2024.

DEMETS, C.; GORDON, R. G.; ARGUS, D. F. Geologically current plate motions. *Geophysical Journal International*, v. 181, n. 1, p. 1–80, 2010. Disponível em: <https://doi.org/10.1111/j.1365-246X.2009.04491.x>. Acesso em: 6 dez. 2024.

EITTREIM, S.; EWING, J. Vema fracture zone transform fault. *Geology*, v. 3, n. 10, p. 555, 1975. Disponível em: <https://pubs.geoscienceworld.org/geology/article/3/10/555-558/192119>. Acesso em: 28 fev. 2024.

ESCARTÍN, J. et al. Quantifying tectonic strain and magmatic accretion at a slow spreading ridge segment, Mid-Atlantic Ridge, 29°N. *Journal of Geophysical Research: Solid Earth*, v. 104, n. B5, p. 10421–10437, 10 maio 1999.

ESCARTÍN, J. et al. Central role of detachment faults in accretion of slow-spreading oceanic lithosphere. *Nature*, v. 455, n. 7214, p. 790–794, out. 2008. Disponível em: <https://www.nature.com/articles/nature07333>.

ESCARTÍN, J. et al. Tectonic structure, evolution, and the nature of oceanic core complexes and their detachment fault zones (13°20′N and 13°30′N, Mid Atlantic Ridge). *Geochemistry, Geophysics, Geosystems*, v. 18, n. 4, p. 1451–1482, 8 abr. 2017. Disponível em: <https://agupubs.onlinelibrary.wiley.com/doi/10.1002/2016GC006775>.

ESCARTÍN, J.; CANNAT, M. Ultramafic exposures and the gravity signature of the lithosphere near the Fifteen-Twenty Fracture Zone (Mid-Atlantic Ridge, 14°–16.5°N). *Earth and Planetary Science Letters*, v. 171, n. 3, p. 411–424, set. 1999. Disponível em: <www.elsevier.com/locate/epsl>.

ESCARTÍN, J.; SMITH, D. K.; CANNAT, M. Parallel bands of seismicity at the Mid-Atlantic Ridge, 12–14°N. *Geophysical Research Letters*, v. 30, n. 12, p. 2003GL017226, 20 jun. 2003. Disponível em: <https://agupubs.onlinelibrary.wiley.com/doi/10.1029/2003GL017226>. Acesso em: 15 mar. 2024.

ESTEP, J. et al. 70 million years of seafloor spreading and magmatism in the South Atlantic. *Earth and Planetary Science Letters*, v. 574, p. 117173, 2021.

FABRETTI, P. et al. *First results of cruise S19 (PRIMAR Project): petrological and structural investigations of the Vema Transverse Ridge (equatorial Atlantic)Russian Acad. Sci, Moscow Russia. Sergej Simonov-United Institutes of Geology, Geophysics and Mineralogy, Russian Acad. Sci*. [s.l: s.n.].

FOX, P. J.; GRINDLAY, N. R.; MACDONALD, K. C. The Mid-atlantic Ridge (31°S–34°30′S): Temporal and spatial variations of accretionary processes. *Marine Geophysical Researches*, v. 13, n. 1, p. 1–20, fev. 1991. Disponível em: <http://link.springer.com/10.1007/BF02428193>. Acesso em: 23 fev. 2024.

FUJIWARA, T. et al. Crustal evolution of the mid-atlantic ridge near the fifteen-twenty fracture zone in the last 5 Ma. *Geochemistry, Geophysics, Geosystems*, v. 4, n. 3, mar. 2003.

GEBCO BATHYMETRIC COMPILATION GROUP 2022. *The GEBCO_2022 Grid - a continuous terrain model of the global oceans and land*.

GERYA, T. Origin and models of oceanic transform faults. *Tectonophysics*, v. 522–523, p. 34–54, 2012. Disponível em: <http://dx.doi.org/10.1016/j.tecto.2011.07.006>.

GRÀCIA, E. et al. Non-transform offsets along the Mid-Atlantic Ridge south of the Azores (38°N-34°N): Ultramafic exposures and hosting of hydrothermal vents. *Earth and Planetary Science Letters*, v. 177, n. 1–2, p. 89–103, 15 abr. 2000.

GREVEMEYER, I. et al. Extensional tectonics and two-stage crustal accretion at oceanic transform faults. *Nature*, v. 591, n. 7850, p. 402–407, 18 mar. 2021.

GRINDLAY, N. R.; FOX, P. J.; MACDONALD, K. C. Second-order ridge axis discontinuities in the south Atlantic: Morphology, structure, and evolution. *Marine Geophysical Researches*, v. 13, n. 1, p. 21–49, fev. 1991. Disponível em: <http://link.springer.com/10.1007/BF02428194>.

HOWELL, S. M. et al. Magmatic and tectonic extension at the Chile Ridge: Evidence for mantle controls on ridge segmentation. *Geochemistry, Geophysics, Geosystems*, v. 17, n. 6, p. 2354–2373, 24 jun. 2016. Disponível em: <https://agupubs.onlinelibrary.wiley.com/doi/10.1002/2016GC006380>. Acesso em: 29 fev. 2024.

HOWELL, S. M. et al. Seafloor expression of oceanic detachment faulting reflects gradients in mid-ocean ridge magma supply. *Earth and Planetary Science Letters*, v. 516, p. 176–189, jun. 2019. Disponível em: <https://hal.science/hal-03016552>.

HU, H. et al. Prospective pyroxenite–peridotite mixed mantle source for the northern Carlsberg Ridge. *Lithos*, v. 436–437, n. November 2022, p. 106980, jan. 2023. Disponível em: <https://linkinghub.elsevier.com/retrieve/pii/S0024493722003899>.

IBGE. *Manual Técnico de Pedologia 2ª edição*. [s.l: s.n.]

ITO, G.; BEHN, M. D. Magmatic and tectonic extension at mid-ocean ridges: 2. Origin of axial morphology. *Geochemistry, Geophysics, Geosystems*, v. 9, n. 9, p. 2008GC001970, 30 set. 2008. Disponível em: <https://agupubs.onlinelibrary.wiley.com/doi/10.1029/2008GC001970>. Acesso em: 5 mar. 2024.

KARSON, J. A. et al. Along-axis variations in seafloor spreading in the MARK area. *Nature*, v. 328, n. 6132, p. 681–685, ago. 1987. Disponível em: <https://www.nature.com/articles/328681a0>.

KARSON, J. A.; DICK, H. J. B. Tectonics of ridge-transform intersections at the {Kane} fracture zone. *Marine Geophysical Researches*, v. 6, n. 1, p. 51–98, 1983. Disponível em: <http://link.springer.com/10.1007/BF00300398>. Acesso em: 13 out. 2024.

KEAREY, P.; KLEPEIS, K. A.; VINE, F. J. *Global tectonics*. [s.l.] John Wiley \& Sons, 2009.

KLEIN, E. M.; LANGMUIR, C. H. Global correlations of ocean ridge basalt chemistry with axial depth and crustal thickness. *Journal of Geophysical Research: Solid Earth*, v. 92, n. B8, p. 8089–8115, 1987. Disponível em: <https://agupubs.onlinelibrary.wiley.com/doi/10.1029/JB092iB08p08089>. Acesso em: 23 mar. 2024.

LAGABRIELLE, Y. et al. Vema Fracture Zone (central Atlantic): Tectonic and magmatic evolution of the median ridge and the eastern ridge-Transform intersection domain. *Journal of Geophysical Research: Solid Earth*, v. 97, n. B12, p. 17331–17351, 10 nov. 1992. Disponível em: <https://agupubs.onlinelibrary.wiley.com/doi/10.1029/92JB01086>. Acesso em: 10 set. 2024.

LIGI, M. et al. Generation and evolution of the oceanic lithosphere in the North Atlantic. *La Rivista del Nuovo Cimento*, v. 45, n. 9, p. 587–659, 20 set. 2022. Disponível em: <https://doi.org/10.1007/s40766-022-00035-0>.

LIN, J.; MORGAN, J. P. The spreading rate dependence of three-dimensional mid-ocean ridge gravity structure. *Geophysical Research Letters*, v. 19, n. 1, p. 13–16, 3 jan. 1992. Disponível em: <https://agupubs.onlinelibrary.wiley.com/doi/10.1029/91GL03041>.

MACDONALD, K. C. Crustal processes at spreading centers. *Reviews of Geophysics And Space Physics*, v. 21, n. 6, p. 1441–1454, 1983.

MACDONALD, K. C. et al. A new view of the mid-ocean ridge from the behaviour of ridge-axis discontinuities. *Nature*, v. 335, n. 6187, p. 217–225, 1988.

MACDONALD, K. C. et al. Volcanic growth faults and the origin of Pacific abyssal hills. *Nature*, v. 380, n. 6570, p. 125–129, 1996.

MACDONALD, K. C.; ATWATER, T. M. Evolution of rifted ocean ridges. *Earth and Planetary Science Letters*, v. 39, n. 3, p. 319–327, 1 maio 1978. . Acesso em: 20 mar. 2022.

MACDONALD, K. C. C. Mid-Ocean Ridge Tectonics, Volcanism, and Geomorphology. *Encyclopedia of Ocean Sciences*, v. 335, n. 6187, p. 852–866, 2001.

MACDONALD, K. C.; FOX, P. J. Overlapping spreading centres: New accretion geometry on the East Pacific Rise. *Nature*, v. 302, n. 5903, p. 55–58, 1983.

MACDONALD, K. C.; FOX, P. J. The axial summit graben and cross-sectional shape of the East Pacific Rise as indicators of axial magma chambers and recent volcanic eruptions. *Earth and Planetary Science Letters*, v. 88, n. 1–2, p. 119–131, 1988.

MACDONALD, Ken. C. Mid-ocean ridges: Fine scale tectonic, volcanic and hydrothermal processes within the plate boundary zone. *Annual Review of Earth and Planetary Sciences*, v. 10, p. 155, 1982.

MACLEOD, C. J. et al. Life cycle of oceanic core complexes. *Earth and Planetary Science Letters*, v. 287, n. 3–4, p. 333–344, 15 out. 2009. Disponível em: <https://linkinghub.elsevier.com/retrieve/pii/S0012821X09004877>. Acesso em: 20 maio. 2024.

MACLEOD, C. J. et al. Quantitative constraint on footwall rotations at the 1545N oceanic core complex, Mid-Atlantic Ridge: Implications for oceanic detachment fault processes. *Geochemistry, Geophysics, Geosystems*, v. 12, n. 5, p. 1–29, 2011.

MAIA, M. et al. Building of the Amsterdam-Saint Paul plateau: A 10 Myr history of a ridge-hot spot interaction and variations in the strength of the hot spot source. *Journal of Geophysical Research: Solid Earth*, v. 116, set. 2011.

MAIA, M.; ARKANI-HAMED, J. The support mechanism of the young Foundation Seamounts inferred from bathymetry and gravity. *Geophysical Journal International*, v. 149, n. 1, p. 190–210, abr. 2002. . Acesso em: 9 dez. 2024.

MCKENZIE, D.; BOWIN, C. The relationship between bathymetry and gravity in the Atlantic Ocean. *Journal of Geophysical Research*, v. 81, n. 11, p. 1903–1915, 10 abr. 1976. Disponível em: <http://doi.wiley.com/10.1029/JB081i011p01903>.

MORGAN, J. P. et al. The genesis of oceanic crust: Magma injection, hydrothermal circulation, and crustal flow. *Journal of Geophysical Research: Solid Earth*, a. v. 98, n. B4, p. 6283–6297, 10 abr. 1993. Disponível em: <http://doi.wiley.com/10.1029/92JB02650>. Acesso em: 26 nov. 2024.

MORRIS, A. et al. Footwall rotation in an oceanic core complex quantified using reoriented Integrated Ocean Drilling Program core samples. *Earth and Planetary Science Letters*, v. 287, n. 1–2, p. 217–228, set. 2009. Disponível em: <https://linkinghub.elsevier.com/retrieve/pii/S0012821X09004671>. Acesso em: 13 mar. 2024.

MOTA, C. et al. *Prospecção e exploração de sulfetos polimetálicos na cordilheira Mesoatlântica, oceano Atlântico Equatorial : relatório de etapa fase 1 : levantamento regional e caracterização batimétrica, geofísica e oceanográfica*. [s.l: s.n.]

OLIVE, J.-A.; DUBLANCHET, P. Controls on the magmatic fraction of extension at mid-ocean ridges. *Earth and Planetary Science Letters*, v. 549, p. 116541, 2020. Disponível em: <https://linkinghub.elsevier.com/retrieve/pii/S0012821X20304854>. Acesso em: 6 mar. 2024.

OLIVE, J. A.; ESCARTÍN, J. Dependence of seismic coupling on normal fault style along the Northern Mid-Atlantic Ridge. *Geochemistry, Geophysics, Geosystems*, v. 17, n. 10, p. 4128–4152, 27 out. 2016. Disponível em: <https://agupubs.onlinelibrary.wiley.com/doi/10.1002/2016GC006460>. Acesso em: 15 dez. 2024.

PALMIOTTO, C. et al. Nonvolcanic tectonic islands in ancient and modern oceans. *Geochemistry, Geophysics, Geosystems*, v. 14, n. 10, p. 4698–4717, out. 2013.

PEIRCE, C. et al. Constraints on crustal structure of adjacent OCCs and segment boundaries at 13°N on the Mid-Atlantic Ridge. *Geophysical Journal International*, v. 217, n. 2, p. 988–1010, 1 maio 2019. Disponível em: <https://academic.oup.com/gji/article/217/2/988/5307889>.

PEIRCE, C. et al. Magmatism versus serpentinization - Crustal structure along the 13°N segment at the Mid-Atlantic Ridge. *Geophysical Journal International*, v. 221, n. 2, p. 981–1001, 29 jan. 2020.

PERRAM, J.; MACDONALD, K. E. N. C. A One-Million-Year History of the 11ø45'N East Pacific Rise Discontinuity. v. 95, n. 90, 1990.

POCKALNY, R. A.; GENTE, P.; BUCK, R. Oceanic transverse ridges: A flexural response to fracture-zone-normal extension. *Geology*, v. 24, n. 1, p. 71–74, 1996.

POMEROL, C. et al. *Princípio de geologia: técnicas, modelos e teorias*. 14: Bookman, 2013.

PÜTHE, C.; GERYA, T. Dependence of mid-ocean ridge morphology on spreading rate in numerical 3-D models. *Gondwana Research*, v. 25, n. 1, p. 270–283, 2014. Disponível em: <http://dx.doi.org/10.1016/j.gr.2013.04.005>.

RUBIN, K. H. Mid-Ocean Ridge Magmatism and Volcanism. Em: *Encyclopedia of Marine Geosciences*. Dordrecht: Springer Netherlands, 2014. p. 1–21.

SAMPAIO, T. V. M.; AUGUSTIN, C. H. R. R. Índice De Concentração Da Rugosidade: Uma Nova Proposta Metodológica Para O Mapeamento E Quantificação Da Dissecação Do Relevo Como Subsídio a Cartografia Geomorfológica. *Revista Brasileira de Geomorfologia*, v. 15, n. 1, 2014.

SANDWELL, D. T. Thermomechanical evolution of oceanic fracture zones. *Journal of Geophysical Research: Solid Earth*, v. 89, n. B13, p. 11401–11413, 1984. Disponível em: <https://agupubs.onlinelibrary.wiley.com/doi/10.1029/JB089iB13p11401>. Acesso em: 8 abr. 2024.

SCLATER, J. G.; FRANCBETEAU, J.; FRANCHETEAU, J. The Implications of Terrestrial Heat Flow Observations on Current Tectonic and Geochemical Models of the Crust and Upper Mantle of the Earth. . 1970, p. 509–542.

SELLA, G. F.; DIXON, T. H.; MAO, A. REVEL: A model for Recent plate velocities from space geodesy. *Journal of Geophysical Research: Solid Earth*, v. 107, n. B4, p. ETG 11--1--ETG 11--30, 27 abr. 2002. Disponível em: <https://agupubs.onlinelibrary.wiley.com/doi/10.1029/2000JB000033>. Acesso em: 6 dez. 2024.

SEMPÉRÉ, J.-C. et al. Segmentation and morphotectonic variations along a slow-spreading center: The Mid-Atlantic Ridge (24°00′ N– 30°40′ N). *Marine Geophysical Researches*, v. 15, n. 3, p. 153–200, ago. 1993. Disponível em: <https://www.wellesu.com/10.1007/bf01204232>. Acesso em: 29 nov. 2024.

SEVERINGHAUS, J. P.; MACDONALD, K. C. High inside corners at ridge-transform intersections. *Marine Geophysical Researches*, v. 9, n. 4, p. 353–367, 1988. Disponível em: <http://link.springer.com/10.1007/BF00315005>.

SHAW, W. J.; LIN, J. Models of ocean ridge lithospheric deformation: Dependence on crustal thickness, spreading rate, and segmentation. *Journal of Geophysical Research: Solid Earth*, v. 101, n. 8, p. 17977–17993, 10 ago. 1996.

SKOLOTNEV, S. G. et al. Large-scale structure of the doldrums multi-fault transform system (7-8ºn equatorial atlantic): Preliminary results from the 45th expedition of the R/V A.N. strakhov. *Ofioliti*, v. 45, n. 1, p. 25–41, 2020.

SMALL, C. A global analysis of mid-ocean ridge axial topography. *Geophysical Journal International*, v. 116, n. 1, p. 64–84, jan. 1994. Disponível em: <https://academic.oup.com/gji/article-lookup/doi/10.1111/j.1365-246X.1994.tb02128.x>.

SMITH, D. K.; CANN, J. R.; ESCARTÍN, J. Widespread active detachment faulting and core complex formation near 13°N on the Mid-Atlantic Ridge. *Nature*, v. 442, n. 7101, p. 440–443, 27 jul. 2006.

SMITH, D. K. K. et al. Fault rotation and core complex formation: Significant processes in seafloor formation at slow-spreading mid-ocean ridges (Mid-Atlantic Ridge, 13°-15°N). *Geochemistry, Geophysics, Geosystems*, v. 9, n. 3, p. n/a-n/a, 5 mar. 2008. Disponível em: <https://agupubs.onlinelibrary.wiley.com/doi/10.1029/2007GC001699>.

SOHN, R. A. et al. Explosive volcanism on the ultraslow-spreading Gakkel ridge, Arctic Ocean. *Nature*, v. 453, n. 7199, p. 1236–1238, 2008.

SOUZA, K. G. SOUZA, K.G.; PEREIRA, C.V. 2007. Minerais do Fundo do Mar. Avanços e Retrocessos das Negociações Internacionais da Convenção das Nações Unidas sobre o Direito do Mar. In: Estudos do Mar: importância econômica, política e estratégica dos recursos minerais. p. 1–274, 2007.

SPENCER, S. et al. Structure and stability of non-transform discontinuities on the Mid-Atlantic Ridge between 24 N and 30 N. *Marine Geophysical Researches*, v. 19, n. 4, p. 339–362, 1997.

THAMMINIDI, M. *Physical Geography*. [s.l: s.n.]

TUCHOLKE, B. E.; LIN, J. A geological model for the structure of ridge segments in slow spreading ocean crust. *Journal of Geophysical Research: Solid Earth*, v. 99, 1994. Disponível em: <https://core.ac.uk/reader/10127150>. Acesso em: 25 nov. 2024.

TUCHOLKE, B. E.; LIN, J.; KLEINROCK, M. C. Megamullions and mullion structure defining oceanic metamorphic core complexes on the {Mid}-{Atlantic} {Ridge}. *Journal of Geophysical Research: Solid Earth*, v. 103, n. B5, p. 9857–9866, 10 maio 1998. Disponível em: <https://agupubs.onlinelibrary.wiley.com/doi/10.1029/98JB00167>. Acesso em: 25 nov. 2024.

VAN ANDEL, T. H.; VON HERZEN, R. P.; PHILLIPS, J. D. The Vema fracture zone and the tectonics of transverse shear zones in oceanic crustal plates. *Marine Geophysical Researches*, v. 1, n. 3, p. 261–283, set. 1971. Disponível em: <http://link.springer.com/10.1007/BF00338257>. Acesso em: 25 nov. 2024.

WILSON, J. A new class of faults and their bearing on continental drift. *Nature*, v. 207, n. 4995, p. 343–347, 1965.

YESSON, C. et al. The global distribution of seamounts based on 30 arc seconds bathymetry data. *Deep-Sea Research Part I: Oceanographic Research Papers*, v. 58, n. 4, p. 442–453, 2011. Disponível em: <http://dx.doi.org/10.1016/j.dsr.2011.02.004>.

YONGSHUN CHEN; MORGAN, W. J. Rift valley/no rift valley transition at mid-ocean ridges. *Journal of Geophysical Research*, v. 95, n. B11, 1990.

CAPÍTULO VI
CONSIDERAÇÕES FINAIS

6. CONSIDERAÇÕES FINAIS

Os dois estudos que compõem esta tese investigam diferentes aspectos dessas interações no segmento localizado entre as zonas de fratura Marathon e Vema. O primeiro estudo (The magmatic and tectonic role on spreading styles at ridge-transform intersection between Marathon and Vema Transform faults) aborda a influência dos processos tectônicos e magmáticos na segmentação da dorsal oceânica. O segundo estudo (Non-transform discontinuities south of the Vema Transform Fault: Characteristics and Tectonic Implications) concentra-se na caracterização das NTDs ao sul da Transformante Vema, destacando como essas feições influenciam a morfologia do fundo oceânico e a formação de falhas da região.

Este capítulo integrativo tem como objetivo contextualizar os achados desses dois estudos dentro de um panorama mais amplo da evolução estrutural e magmática da DMA, destacando suas conexões e implicações para a geotectônica de dorsais meso-oceânicas de espalhamento lento.

6.1. Segmentação e Influência das Transformantes na Morfotectônica da DMA

A DMA apresenta uma configuração morfotectônica influenciada pela interação entre falhas transformantes, NTDs e falhas de descolamento. Essas estruturas desempenham um papel fundamental na segmentação do assoalho oceânico e na evolução crustal, deslocando o eixo da dorsal e influenciam a distribuição do magma e o desenvolvimento e reativação de falhas. O estudo sobre o papel tectônico e magmático na propagação da dorsal destaca que as RTIs da Marathon e da Vema exibem diferenças significativas na morfologia crustal.

- O segmento 11°N, subdividido em 11°55'N e 11°20'N, apresenta uma maior atividade magmática na parte norte, resultando em um fundo oceânico mais irregular e elevado. À medida que a disponibilidade de magma diminui, a influência tectônica se torna dominante, favorecendo o desenvolvimento de falhas de descolamento e OCCs.

- No segmento 12°N, a menor taxa de suprimento magmático favorece o desenvolvimento de falhas de descolamento mais maduras, refletindo um regime tectônico predominante.

- A Transformante Vema é caracterizada por contribuir para o resfriamento litosférico, promover exumação de rochas ultramáficas e a formação de massivos oceânicos ao longo do seu canto interno.

- A Transformante Marathon, em contrapartida, exibe feições tectônicas menos evoluídas, sem evidências expressivas de corrugações associadas a falhas de descolamento.

Esses resultados reforçam a ideia de que a segmentação da DMA não é apenas um reflexo das falhas transformantes, mas sim de uma interação complexa entre processos tectônicos, magmatismo e variações na espessura crustal.

6.2. O Papel das Descontinuidades Não Transformantes na Evolução Morfotectônica

As NTDs representam limites de segmentos onde a transição ocorre sem a presença de falhas transformantes bem definidas, caracterizadas principalmente pela mudança do eixo axial.

- Foram identificadas duas NTDs principais: 9NTD e 10NTD, atuando como zonas de transição entre os segmentos adjacentes.

- A 9NTD é caracterizada por intensa atividade sísmica e falhas de descolamento bem desenvolvidas, refletindo um regime tectônico de acomodação extensional.

- A 10NTD, por outro lado, apresenta uma morfologia mais simétrica, com colinas abissais de menor amplitude e bacias mais rasas, sugerindo uma influência maior do magmatismo na sua configuração estrutural.

As NTDs aprecem funcionar como zonas de afinamento litosférico, promovendo a exposição de rochas ultramáficas e facilitando a circulação de fluidos hidrotermais. Isso favorece a serpentinização do manto, processos diápiros, e a formação de possíveis fontes hidrotermais associadas a maciços oceânicos.

A relação entre suprimento magmático e desenvolvimento tectônico nas NTDs corrobora estudos prévios que indicam que segmentos com baixo suprimento magmático

tendem a apresentar morfologias assimétricas, enquanto segmentos com maior suprimento magmático resultam em feições mais simétricas.

6.3. Integração dos Resultados e Implicações Geodinâmicas

Os resultados desta tese fornecem uma visão abrangente da interação entre tectonismo e magmatismo na segmentação da DMA entre as Transformantes Marathon e Vema. Alguns tópicos importantes podem ser destacados:

- Segmentação Complexa: A região estudada apresenta uma segmentação que vai além da influência das falhas transformantes, sendo fortemente impactada por NTDs e variações no suprimento magmático.

- Formação de OCCs e maciços: As falhas de descolamento observadas nas NTDs indicam a formação e exumação de OCCs e Maciços, reforçando o papel dessas estruturas na exposição de rochas ultramáficas e na evolução litosférica.

- Evolução Morfotectônica Controlada pelo Magmatismo: A variabilidade na espessura crustal e no suprimento magmático influencia diretamente a segmentação e a morfologia dos segmentos estudados, impactando desde a geração de falhas até a configuração do relevo submarino. Sendo importante a presença de magma na evolução de falhas de descolamento mais pronunciadas.

6.4. Conclusão

A presente tese contribui significativamente para o entendimento de como o magmatismo e o tectonismo controlam a morfologia e a estruturação de segmentos da DMA situados entre as Transformantes Marathon e Vema. Os métodos empregados mostraram-se bastante eficientes nessa primeira análise regional, fornecendo uma base robusta para investigações futuras.

De modo a expandir essa abordagem e aprofundar a compreensão dos processa atuantes na DMA, estudos futuros deverão incorporar téctincas mais detalhadas, como veículos autônomos subaquáticos (AUV), gravímetros e magmetômetos rebocados

próximo ao fundo, além de amostragem geológicas e oceanográficas. Esses métdos permitirão a caracterização mais precisa das estruturas tectônbicas e feições associadas aos processos hidrotermais. Em particular, as regiões onde foram identificadas falhas de descolmaneto associadas a DNT demostraram-se mais propensas à ocorrência de processos hidrotermais e exumação de rochas do manto. Desta forma, em uma primeira análise, inidicamos essas áreas como prioritárias para avaliação do potencial mineral, sendo recomendadas como alvos para mapeasdas detalhados em investigações futuras.

CAPÍTULO VII
REFERÊNCIAS BIBLIOGRÁFICAS

7. REFERÊNCIAS BIBLIOGRÁFICAS

BEHN, M. D.; ITO, G. Magmatic and tectonic extension at mid-ocean ridges: 1. Controls on fault characteristics. *Geochemistry, Geophysics, Geosystems*, v. 9, n. 8, 2008.

BEHN, M. D.; LIN, J.; ZUBER, M. T. Mechanisms of normal fault development at mid-ocean ridges. *Journal of Geophysical Research: Solid Earth*, v. 107, n. B4, p. EPM 7--1--EPM 7--17, abr. 2002. . Acesso em: 16 jul. 2022.

BENEDIKTSDÓTTIR, Á. et al. Detailed tectonic evolution of the Reykjanes Ridge during the past 15 Ma. *Geochemistry, Geophysics, Geosystems*, v. 13, n. 2, p. 1–27, 2012.

BLACKMAN, D. K. et al. Origin of extensional core complexes: Evidence from the Mid-Atlantic Ridge at Atlantis fracture zone. *Journal of Geophysical Research: Solid Earth*, v. 103, n. 9, p. 21315–21333, 10 set. 1998. Disponível em: <https://onlinelibrary.wiley.com/doi/full/10.1029/98JB01756>. Acesso em: 16 jul. 2022.

BONATTI, E. Serpentinite protrusions in the oceanic crust. *Earth and Planetary Science Letters*, v. 32, n. 2, p. 107–113, out. 1976. Disponível em: <https://linkinghub.elsevier.com/retrieve/pii/0012821X76900480>.

BONATTI, E. Vertical tectonism in oceanic fracture zones. *Earth and Planetary Science Letters*, v. 37, n. 3, p. 369–379, jan. 1978. Disponível em: <https://linkinghub.elsevier.com/retrieve/pii/0012821X78900523>. Acesso em: 27 fev. 2024.

BONATTI, E. et al. Transform migration and vertical tectonics at the Romanche fracture zone, equatorial Atlantic. *Journal of Geophysical Research: Solid Earth*, v. 99, n. B11, p. 21779–21802, 10 nov. 1994. Disponível em: <https://agupubs.onlinelibrary.wiley.com/doi/10.1029/94JB01178>. Acesso em: 6 set. 2024.

BONATTI, E. et al. *Lower Cretaceous deposits trapped near the equatorial Mid-Atlantic RidgeNature*, 1996. .

BONATTI, E. et al. Mantle thermal pulses below the Mid-Atlantic Ridge and temporal variations in the formation of oceanic lithosphere. *Nature*, v. 423, n. 6939, p. 499–505, maio 2003. Disponível em: <www.nature.com/nature>.

BONATTI, E. et al. Flexural uplift of a lithospheric slab near the Vema transform (Central Atlantic): Timing and mechanisms. *Earth and Planetary Science Letters*, v. 240, n. 3–4, p. 642–655, 15 dez. 2005. Disponível em: <https://linkinghub.elsevier.com/retrieve/pii/S0012821X05006874>. Acesso em: 25 nov. 2024.

BONATTI, E.; SARTORI, R.; BOERSMA, A. Vertical crustal movements at the Vema Fracture Zone in the Atlantic: Evidence from dredged limestones. *Tectonophysics*, v. 91, n. 3–4, p. 213–232, jan. 1983. Disponível em: <https://linkinghub.elsevier.com/retrieve/pii/0040195183900422>. Acesso em: 30 ago. 2024.

BRASIL, M. do. *Diretoria de Hidrografia e NavegaçãoLimites Marítimos*, 2024. . Disponível em: <https://www.marinha.mil.br/dhn/?q=node/169.>. Acesso em: 9 dez. 2024.

BUCK, W. R. Flexural rotation of normal faults. *Tectonics*, v. 7, n. 5, p. 959–973, 26 out. 1988. Disponível em: <https://agupubs.onlinelibrary.wiley.com/doi/10.1029/TC007i005p00959>.

BUCK, W. R. et al. *Faulting and magmatism at mid-ocean ridges*. [s.l.] American Geophysical Union, 1998. v. 106

BUCK, W. R.; LAVIER, L. L.; POLIAKOV, A. N. B. B. Modes of faulting at mid-ocean ridges. *Nature*, v. 434, n. 7034, p. 719–723, 7 abr. 2005. Disponível em: <https://www.nature.com/articles/nature03358>.

CALDER, B. R.; MAYER, L. A. Automatic processing of high-rate, high-density multibeam echosounder data. *Geochemistry, Geophysics, Geosystems*, v. 4, n. 6, jun. 2003.

CANALES, J. P. et al. Upper crustal structure and axial topography at intermediate spreading ridges: Seismic constraints from the southern Juan de Fuca Ridge. *Journal of Geophysical Research: Solid Earth*, v. 110, n. 12, p. 1–27, 2005.

CANNAT, M. et al. Mid-Atlantic Ridge–Azores hotspot interactions: along-axis migration of a hotspot-derived event of enhanced magmatism 10 to 4 Ma ago. *Earth and Planetary Science Letters*, v. 173, n. 3, p. 257–269, nov. 1999. Disponível em: <https://linkinghub.elsevier.com/retrieve/pii/S0012821X99002344>.

CANNAT, M. et al. Modes of seafloor generation at a melt-poor ultraslow-spreading ridge. *Geology*, v. 34, n. 7, p. 605–608, jul. 2006.

CANNAT, M.; CASEY, J. F. An Ultramafic Lift at the Mid-Atlantic Ridge: Successive Stages of Magmatism in Serpentinized Peridotites from the 15°N Region. Em: [s.l: s.n.]p. 5–34.

Cannet al - 1997 - Corrugated slip surfaces formed at ridge-transform intersections on the Mid-Atlantic Ridge. [s.d.]

CANN, J. R. et al. Tectonic evolution of 200 km of Mid-Atlantic Ridge over 10 million years: Interplay of volcanism and faulting. *Geochemistry, Geophysics, Geosystems*, v. 16, n. 7, p. 2303–2321, jul. 2015. Disponível em: <http://doi.wiley.com/10.1002/2015GC005797>.

CARBOTTE, S. M.; MACDONALD, K. C. Comparison of seafloor tectonic fabric at intermediate, fast, and super fast spreading ridges: Influence of spreading rate, plate motions, and ridge segmentation on fault patterns. *Journal of Geophysical Research: Solid Earth*, v. 99, n. B7, p. 13609–13631, 10 jul. 1994. Disponível em: <https://agupubs.onlinelibrary.wiley.com/doi/10.1029/93JB02971>. Acesso em: 7 maio. 2024.

CHAMOV, N. P.; SOKOLOV, S. Yu.; MERENKOVA, S. I. Residual Sediments of the Vema Fracture Zone, Central Atlantic. *Lithology and Mineral Resources*, v. 55, n. 5, p. 338–344, 9 set. 2020. Disponível em: <https://link.springer.com/10.1134/S0024490220050028>. Acesso em: 31 ago. 2024.

CHEN, Y. J. Oceanic crustal thickness versus spreading rate. *Geophysical Research Letters*, v. 19, n. 8, p. 753–756, 1992. Disponível em: <https://agupubs.onlinelibrary.wiley.com/doi/10.1029/92GL00161>. Acesso em: 8 jun. 2024.

CHEN, Y.; MORGAN, W. J. A nonlinear rheology model for mid-ocean ridge axis topography. *Journal of Geophysical Research: Solid Earth*, b. v. 95, n. B11, p. 17583–17604, 1990. Disponível em: <https://agupubs.onlinelibrary.wiley.com/doi/10.1029/JB095iB11p17583>. Acesso em: 7 jun. 2024.

COLLETTE, B. J. Thermal contraction joints in a spreading seafloor as origin of fracture zones. *Nature*, v. 251, n. 5473, p. 299–300, set. 1974. Disponível em: <https://www.nature.com/articles/251299a0>.

DANNOWSKI, A. et al. Enhanced Mantle Upwelling/Melting Caused Segment Propagation, Oceanic Core Complex Die Off, and the Death of a Transform Fault: The Mid-Atlantic Ridge at 21.5°N. *Journal of Geophysical Research: Solid Earth*, v. 123, n. 2, p. 941–956, 1 fev. 2018.

DAVIS, E. E.; LISTER, C. R. B. Fundamentals of ridge crest topography. *Earth and Planetary Science Letters*, v. 21, n. 4, p. 405–413, 1974. Disponível em: <https://linkinghub.elsevier.com/retrieve/pii/0012821X74901800>. Acesso em: 15 maio. 2024.

DEMETS, C.; GORDON, R. G.; ARGUS, D. F. Geologically current plate motions. *Geophysical Journal International*, v. 181, n. 1, p. 1–80, 2010. Disponível em: <https://doi.org/10.1111/j.1365-246X.2009.04491.x>. Acesso em: 6 dez. 2024.

EITTREIM, S.; EWING, J. Vema fracture zone transform fault. *Geology*, v. 3, n. 10, p. 555, 1975. Disponível em: <https://pubs.geoscienceworld.org/geology/article/3/10/555-558/192119>. Acesso em: 28 fev. 2024.

ESCARTÍN, J. et al. Quantifying tectonic strain and magmatic accretion at a slow spreading ridge segment, Mid-Atlantic Ridge, 29°N. *Journal of Geophysical Research: Solid Earth*, v. 104, n. B5, p. 10421–10437, 10 maio 1999.

ESCARTÍN, J. et al. Central role of detachment faults in accretion of slow-spreading oceanic lithosphere. *Nature*, v. 455, n. 7214, p. 790–794, out. 2008. Disponível em: <https://www.nature.com/articles/nature07333>.

ESCARTÍN, J. et al. Tectonic structure, evolution, and the nature of oceanic core complexes and their detachment fault zones (13°20′N and 13°30′N, Mid Atlantic Ridge). *Geochemistry, Geophysics, Geosystems*, v. 18, n. 4, p. 1451–1482, 8 abr. 2017. Disponível em: <https://agupubs.onlinelibrary.wiley.com/doi/10.1002/2016GC006775>.

ESCARTÍN, J.; CANNAT, M. Ultramafic exposures and the gravity signature of the lithosphere near the Fifteen-Twenty Fracture Zone (Mid-Atlantic Ridge, 14°–16.5°N). *Earth and Planetary Science Letters*, v. 171, n. 3, p. 411–424, set. 1999. Disponível em: <www.elsevier.com/locate/epsl>.

ESCARTÍN, J.; SMITH, D. K.; CANNAT, M. Parallel bands of seismicity at the Mid-Atlantic Ridge, 12–14°N. *Geophysical Research Letters*, v. 30, n. 12, p. 2003GL017226, 20 jun. 2003. Disponível em: <https://agupubs.onlinelibrary.wiley.com/doi/10.1029/2003GL017226>. Acesso em: 15 mar. 2024.

ESTEP, J. et al. 70 million years of seafloor spreading and magmatism in the South Atlantic. *Earth and Planetary Science Letters*, v. 574, p. 117173, 2021.

FABRETTI, P. et al. *First results of cruise S19 (PRIMAR Project): petrological and structural investigations of the Vema Transverse Ridge (equatorial Atlantic)Russian Acad. Sci, Moscow Russia. Sergej Simonov-United Institutes of Geology, Geophysics and Mineralogy, Russian Acad. Sci*. [s.l: s.n.].

FOX, P. J.; GRINDLAY, N. R.; MACDONALD, K. C. The Mid-atlantic Ridge (31°S–34°30′S): Temporal and spatial variations of accretionary processes. *Marine Geophysical Researches*, v. 13, n. 1, p. 1–20, fev. 1991. Disponível em: <http://link.springer.com/10.1007/BF02428193>. Acesso em: 23 fev. 2024.

FUJIWARA, T. et al. Crustal evolution of the mid-atlantic ridge near the fifteen-twenty fracture zone in the last 5 Ma. *Geochemistry, Geophysics, Geosystems*, v. 4, n. 3, mar. 2003.

GEBCO BATHYMETRIC COMPILATION GROUP 2022. *The GEBCO_2022 Grid - a continuous terrain model of the global oceans and land*.

GERYA, T. Origin and models of oceanic transform faults. *Tectonophysics*, v. 522–523, p. 34–54, 2012. Disponível em: <http://dx.doi.org/10.1016/j.tecto.2011.07.006>.

GRÀCIA, E. et al. Non-transform offsets along the Mid-Atlantic Ridge south of the Azores (38°N-34°N): Ultramafic exposures and hosting of hydrothermal vents. *Earth and Planetary Science Letters*, v. 177, n. 1–2, p. 89–103, 15 abr. 2000.

GREVEMEYER, I. et al. Extensional tectonics and two-stage crustal accretion at oceanic transform faults. *Nature*, v. 591, n. 7850, p. 402–407, 18 mar. 2021.

GRINDLAY, N. R.; FOX, P. J.; MACDONALD, K. C. Second-order ridge axis discontinuities in the south Atlantic: Morphology, structure, and evolution. *Marine Geophysical Researches*, v. 13, n. 1, p. 21–49, fev. 1991. Disponível em: <http://link.springer.com/10.1007/BF02428194>.

HOWELL, S. M. et al. Magmatic and tectonic extension at the Chile Ridge: Evidence for mantle controls on ridge segmentation. *Geochemistry, Geophysics, Geosystems*, v. 17, n. 6, p. 2354–2373, 24 jun. 2016. Disponível em: <https://agupubs.onlinelibrary.wiley.com/doi/10.1002/2016GC006380>. Acesso em: 29 fev. 2024.

HOWELL, S. M. et al. Seafloor expression of oceanic detachment faulting reflects gradients in mid-ocean ridge magma supply. *Earth and Planetary Science Letters*, v. 516, p. 176–189, jun. 2019. Disponível em: <https://hal.science/hal-03016552>.

HU, H. et al. Prospective pyroxenite–peridotite mixed mantle source for the northern Carlsberg Ridge. *Lithos*, v. 436–437, n. November 2022, p. 106980, jan. 2023. Disponível em: <https://linkinghub.elsevier.com/retrieve/pii/S0024493722003899>.

IBGE. *Manual Técnico de Pedologia 2ª edição*. [s.l: s.n.]

ITO, G.; BEHN, M. D. Magmatic and tectonic extension at mid-ocean ridges: 2. Origin of axial morphology. *Geochemistry, Geophysics, Geosystems*, v. 9, n. 9, p. 2008GC001970, 30 set. 2008. Disponível em: <https://agupubs.onlinelibrary.wiley.com/doi/10.1029/2008GC001970>. Acesso em: 5 mar. 2024.

KARSON, J. A. et al. Along-axis variations in seafloor spreading in the MARK area. *Nature*, v. 328, n. 6132, p. 681–685, ago. 1987. Disponível em: <https://www.nature.com/articles/328681a0>.

KARSON, J. A.; DICK, H. J. B. Tectonics of ridge-transform intersections at the {Kane} fracture zone. *Marine Geophysical Researches*, v. 6, n. 1, p. 51–98, 1983. Disponível em: <http://link.springer.com/10.1007/BF00300398>. Acesso em: 13 out. 2024.

KEAREY, P.; KLEPEIS, K. A.; VINE, F. J. *Global tectonics*. [s.l.] John Wiley \& Sons, 2009.

KLEIN, E. M.; LANGMUIR, C. H. Global correlations of ocean ridge basalt chemistry with axial depth and crustal thickness. *Journal of Geophysical Research: Solid Earth*, v. 92, n. B8, p. 8089–8115, 1987. Disponível em: <https://agupubs.onlinelibrary.wiley.com/doi/10.1029/JB092iB08p08089>. Acesso em: 23 mar. 2024.

LAGABRIELLE, Y. et al. Vema Fracture Zone (central Atlantic): Tectonic and magmatic evolution of the median ridge and the eastern ridge-Transform intersection domain. *Journal of Geophysical Research: Solid Earth*, v. 97, n. B12, p. 17331–17351, 10 nov. 1992. Disponível em: <https://agupubs.onlinelibrary.wiley.com/doi/10.1029/92JB01086>. Acesso em: 10 set. 2024.

LIGI, M. et al. Generation and evolution of the oceanic lithosphere in the North Atlantic. *La Rivista del Nuovo Cimento*, v. 45, n. 9, p. 587–659, 20 set. 2022. Disponível em: <https://doi.org/10.1007/s40766-022-00035-0>.

LIN, J.; MORGAN, J. P. The spreading rate dependence of three-dimensional mid-ocean ridge gravity structure. *Geophysical Research Letters*, v. 19, n. 1, p. 13–16, 3 jan. 1992. Disponível em: <https://agupubs.onlinelibrary.wiley.com/doi/10.1029/91GL03041>.

MACDONALD, K. C. Crustal processes at spreading centers. *Reviews of Geophysics And Space Physics*, v. 21, n. 6, p. 1441–1454, 1983.

MACDONALD, K. C. et al. A new view of the mid-ocean ridge from the behaviour of ridge-axis discontinuities. *Nature*, v. 335, n. 6187, p. 217–225, 1988.

MACDONALD, K. C. et al. Volcanic growth faults and the origin of Pacific abyssal hills. *Nature*, v. 380, n. 6570, p. 125–129, 1996.

MACDONALD, K. C.; ATWATER, T. M. Evolution of rifted ocean ridges. *Earth and Planetary Science Letters*, v. 39, n. 3, p. 319–327, 1 maio 1978. . Acesso em: 20 mar. 2022.

MACDONALD, K. C. C. Mid-Ocean Ridge Tectonics, Volcanism, and Geomorphology. *Encyclopedia of Ocean Sciences*, v. 335, n. 6187, p. 852–866, 2001.

MACDONALD, K. C.; FOX, P. J. Overlapping spreading centres: New accretion geometry on the East Pacific Rise. *Nature*, v. 302, n. 5903, p. 55–58, 1983.

MACDONALD, K. C.; FOX, P. J. The axial summit graben and cross-sectional shape of the East Pacific Rise as indicators of axial magma chambers and recent volcanic eruptions. *Earth and Planetary Science Letters*, v. 88, n. 1–2, p. 119–131, 1988.

MACDONALD, Ken. C. Mid-ocean ridges: Fine scale tectonic, volcanic and hydrothermal processes within the plate boundary zone. *Annual Review of Earth and Planetary Sciences*, v. 10, p. 155, 1982.

MACLEOD, C. J. et al. Life cycle of oceanic core complexes. *Earth and Planetary Science Letters*, v. 287, n. 3–4, p. 333–344, 15 out. 2009. Disponível em: <https://linkinghub.elsevier.com/retrieve/pii/S0012821X09004877>. Acesso em: 20 maio. 2024.

MACLEOD, C. J. et al. Quantitative constraint on footwall rotations at the 1545N oceanic core complex, Mid-Atlantic Ridge: Implications for oceanic detachment fault processes. *Geochemistry, Geophysics, Geosystems*, v. 12, n. 5, p. 1–29, 2011.

MAIA, M. et al. Building of the Amsterdam-Saint Paul plateau: A 10 Myr history of a ridge-hot spot interaction and variations in the strength of the hot spot source. *Journal of Geophysical Research: Solid Earth*, v. 116, set. 2011.

MAIA, M.; ARKANI-HAMED, J. The support mechanism of the young Foundation Seamounts inferred from bathymetry and gravity. *Geophysical Journal International*, v. 149, n. 1, p. 190–210, abr. 2002. . Acesso em: 9 dez. 2024.

MCKENZIE, D.; BOWIN, C. The relationship between bathymetry and gravity in the Atlantic Ocean. *Journal of Geophysical Research*, v. 81, n. 11, p. 1903–1915, 10 abr. 1976. Disponível em: <http://doi.wiley.com/10.1029/JB081i011p01903>.

MORGAN, J. P. et al. The genesis of oceanic crust: Magma injection, hydrothermal circulation, and crustal flow. *Journal of Geophysical Research: Solid Earth*, a. v. 98, n. B4, p. 6283–6297, 10 abr. 1993. Disponível em: <http://doi.wiley.com/10.1029/92JB02650>. Acesso em: 26 nov. 2024.

MORRIS, A. et al. Footwall rotation in an oceanic core complex quantified using reoriented Integrated Ocean Drilling Program core samples. *Earth and Planetary Science Letters*, v. 287, n. 1–2, p. 217–228,

set. 2009. Disponível em: <https://linkinghub.elsevier.com/retrieve/pii/S0012821X09004671>. Acesso em: 13 mar. 2024.

MOTA, C. et al. *Prospecção e exploração de sulfetos polimetálicos na cordilheira Mesoatlântica, oceano Atlântico Equatorial : relatório de etapa fase 1 : levantamento regional e caracterização batimétrica, geofísica e oceanográfica*. [s.l: s.n.]

OLIVE, J.-A.; DUBLANCHET, P. Controls on the magmatic fraction of extension at mid-ocean ridges. *Earth and Planetary Science Letters*, v. 549, p. 116541, 2020. Disponível em: <https://linkinghub.elsevier.com/retrieve/pii/S0012821X20304854>. Acesso em: 6 mar. 2024.

OLIVE, J. A.; ESCARTÍN, J. Dependence of seismic coupling on normal fault style along the Northern Mid-Atlantic Ridge. *Geochemistry, Geophysics, Geosystems*, v. 17, n. 10, p. 4128–4152, 27 out. 2016. Disponível em: <https://agupubs.onlinelibrary.wiley.com/doi/10.1002/2016GC006460>. Acesso em: 15 dez. 2024.

PALMIOTTO, C. et al. Nonvolcanic tectonic islands in ancient and modern oceans. *Geochemistry, Geophysics, Geosystems*, v. 14, n. 10, p. 4698–4717, out. 2013.

PEIRCE, C. et al. Constraints on crustal structure of adjacent OCCs and segment boundaries at 13°N on the Mid-Atlantic Ridge. *Geophysical Journal International*, v. 217, n. 2, p. 988–1010, 1 maio 2019. Disponível em: <https://academic.oup.com/gji/article/217/2/988/5307889>.

PEIRCE, C. et al. Magmatism versus serpentinization - Crustal structure along the 13°N segment at the Mid-Atlantic Ridge. *Geophysical Journal International*, v. 221, n. 2, p. 981–1001, 29 jan. 2020.

PERRAM, J.; MACDONALD, K. E. N. C. A One-Million-Year History of the 11ø45'N East Pacific Rise Discontinuity. v. 95, n. 90, 1990.

POCKALNY, R. A.; GENTE, P.; BUCK, R. Oceanic transverse ridges: A flexural response to fracture-zone-normal extension. *Geology*, v. 24, n. 1, p. 71–74, 1996.

POMEROL, C. et al. *Princípio de geologia: técnicas, modelos e teorias*. 14: Bookman, 2013.

PÜTHE, C.; GERYA, T. Dependence of mid-ocean ridge morphology on spreading rate in numerical 3-D models. *Gondwana Research*, v. 25, n. 1, p. 270–283, 2014. Disponível em: <http://dx.doi.org/10.1016/j.gr.2013.04.005>.

RUBIN, K. H. Mid-Ocean Ridge Magmatism and Volcanism. Em: *Encyclopedia of Marine Geosciences*. Dordrecht: Springer Netherlands, 2014. p. 1–21.

SAMPAIO, T. V. M.; AUGUSTIN, C. H. R. R. Índice De Concentração Da Rugosidade: Uma Nova Proposta Metodológica Para O Mapeamento E Quantificação Da Dissecação Do Relevo Como Subsídio a Cartografia Geomorfológica. *Revista Brasileira de Geomorfologia*, v. 15, n. 1, 2014.

SANDWELL, D. T. Thermomechanical evolution of oceanic fracture zones. *Journal of Geophysical Research: Solid Earth*, v. 89, n. B13, p. 11401–11413, 1984. Disponível em: <https://agupubs.onlinelibrary.wiley.com/doi/10.1029/JB089iB13p11401>. Acesso em: 8 abr. 2024.

SCLATER, J. G.; FRANCBETEAU, J.; FRANCHETEAU, J. The Implications of Terrestrial Heat Flow Observations on Current Tectonic and Geochemical Models of the Crust and Upper Mantle of the Earth. . 1970, p. 509–542.

SELLA, G. F.; DIXON, T. H.; MAO, A. REVEL: A model for Recent plate velocities from space geodesy. *Journal of Geophysical Research: Solid Earth*, v. 107, n. B4, p. ETG 11--1--ETG 11--30, 27 abr. 2002. Disponível em: <https://agupubs.onlinelibrary.wiley.com/doi/10.1029/2000JB000033>. Acesso em: 6 dez. 2024.

SEMPÉRÉ, J.-C. et al. Segmentation and morphotectonic variations along a slow-spreading center: The Mid-Atlantic Ridge (24°00′ N– 30°40′ N). *Marine Geophysical Researches*, v. 15, n. 3, p. 153–200, ago. 1993. Disponível em: <https://www.wellesu.com/10.1007/bf01204232>. Acesso em: 29 nov. 2024.

SEVERINGHAUS, J. P.; MACDONALD, K. C. High inside corners at ridge-transform intersections. *Marine Geophysical Researches*, v. 9, n. 4, p. 353–367, 1988. Disponível em: <http://link.springer.com/10.1007/BF00315005>.

SHAW, W. J.; LIN, J. Models of ocean ridge lithospheric deformation: Dependence on crustal thickness, spreading rate, and segmentation. *Journal of Geophysical Research: Solid Earth*, v. 101, n. 8, p. 17977–17993, 10 ago. 1996.

SKOLOTNEV, S. G. et al. Large-scale structure of the doldrums multi-fault transform system (7-8ºn equatorial atlantic): Preliminary results from the 45th expedition of the R/V A.N. strakhov. *Ofioliti*, v. 45, n. 1, p. 25–41, 2020.

SMALL, C. A global analysis of mid-ocean ridge axial topography. *Geophysical Journal International*, v. 116, n. 1, p. 64–84, jan. 1994. Disponível em: <https://academic.oup.com/gji/article-lookup/doi/10.1111/j.1365-246X.1994.tb02128.x>.

SMITH, D. K.; CANN, J. R.; ESCARTÍN, J. Widespread active detachment faulting and core complex formation near 13°N on the Mid-Atlantic Ridge. *Nature*, v. 442, n. 7101, p. 440–443, 27 jul. 2006.

SMITH, D. K. K. et al. Fault rotation and core complex formation: Significant processes in seafloor formation at slow-spreading mid-ocean ridges (Mid-Atlantic Ridge, 13°-15°N). *Geochemistry, Geophysics, Geosystems*, v. 9, n. 3, p. n/a-n/a, 5 mar. 2008. Disponível em: <https://agupubs.onlinelibrary.wiley.com/doi/10.1029/2007GC001699>.

SOHN, R. A. et al. Explosive volcanism on the ultraslow-spreading Gakkel ridge, Arctic Ocean. *Nature*, v. 453, n. 7199, p. 1236–1238, 2008.

SOUZA, K. G. SOUZA, K.G.; PEREIRA, C.V. 2007. Minerais do Fundo do Mar. Avanços e Retrocessos das Negociações Internacionais da Convenção das Nações Unidas sobre o Direito do Mar. In: Estudos do Mar: importância econômica, política e estratégica dos recursos minerais. p. 1–274, 2007.

SPENCER, S. et al. Structure and stability of non-transform discontinuities on the Mid-Atlantic Ridge between 24 N and 30 N. *Marine Geophysical Researches*, v. 19, n. 4, p. 339–362, 1997.

THAMMINIDI, M. *Physical Geography*. [s.l: s.n.]

TUCHOLKE, B. E.; LIN, J. A geological model for the structure of ridge segments in slow spreading ocean crust. *Journal of Geophysical Research: Solid Earth*, v. 99, 1994. Disponível em: <https://core.ac.uk/reader/10127150>. Acesso em: 25 nov. 2024.

TUCHOLKE, B. E.; LIN, J.; KLEINROCK, M. C. Megamullions and mullion structure defining oceanic metamorphic core complexes on the {Mid}-{Atlantic} {Ridge}. *Journal of Geophysical Research: Solid Earth*, v. 103, n. B5, p. 9857–9866, 10 maio 1998. Disponível em: <https://agupubs.onlinelibrary.wiley.com/doi/10.1029/98JB00167>. Acesso em: 25 nov. 2024.

VAN ANDEL, T. H.; VON HERZEN, R. P.; PHILLIPS, J. D. The Vema fracture zone and the tectonics of transverse shear zones in oceanic crustal plates. *Marine Geophysical Researches*, v. 1, n. 3, p. 261–283, set. 1971. Disponível em: <http://link.springer.com/10.1007/BF00338257>. Acesso em: 25 nov. 2024.

WILSON, J. A new class of faults and their bearing on continental drift. *Nature*, v. 207, n. 4995, p. 343–347, 1965.

YESSON, C. et al. The global distribution of seamounts based on 30 arc seconds bathymetry data. *Deep-Sea Research Part I: Oceanographic Research Papers*, v. 58, n. 4, p. 442–453, 2011. Disponível em: <http://dx.doi.org/10.1016/j.dsr.2011.02.004>.

YONGSHUN CHEN; MORGAN, W. J. Rift valley/no rift valley transition at mid-ocean ridges. *Journal of Geophysical Research*, v. 95, n. B11, 1990.